UNIVERSITÉ DU QUÉBEC À MONTRÉAL

LES ACTINIDES DANS LES SÉDIMENTS QUATERNAIRES DE L'OCÉAN ARCTIQUE

THÈSE
PRÉSENTÉE
COMME EXIGENCE PARTIELLE
DU DOCTORAT EN SCIENCES DE L'ENVIRONNEMENT

PAR
CHRISTELLE NOT

NOVEMBRE 2010

AVANT-PROPOS

Cette thèse est construite sous forme de trois articles scientifiques, rédigés en anglais, formant chacun un chapitre. Pour cette raison, les titres et figures de chaque chapitre ne sont pas numérotés selon le *Guide de présentation des mémoires et thèses*; plutôt la numérotation de chacune des publications a été conservée. De plus, les formats des références pour chacun des chapitres suivent les critères propres à chacune des revues de publication.

Ma contribution aux publications qui constituent le corps de cette thèse couvre d'abord la quasi-totalité du domaine analytique. Dans les chapitres I, II et III, j'ai en effet réalisé l'ensemble des analyses des divers isotopes utilisés: ^{210}Pb, ^{137}Cs, ^{226}Ra, ^{230}Th, ^{232}Th, ^{234}U et ^{238}U. Les autres analyses, géochimiques et/ou minéralogiques, ont cependant été réalisées en collaboration avec les équipes de géochimie et micropaléontologie du GEOTOP. J'ai colligé l'ensemble des données obtenues. J'ai également réalisé le travail interprétatif et j'ai rédigé les manuscrits, aux fins de publication, sous la supervision et les conseils de mon directeur de recherche, Monsieur Claude Hillaire-Marcel. Les coauteurs de l'article qui constitue le chapitre I ont participé à mes recherches en fournissant les échantillons et en discutant l'interprétation des résultats.

L'article du chapitre I a été publié en 2008 dans le *Journal canadien des sciences de la Terre* (vol 45, doi : 10.1139/E08-047) et ayant pour titre *^{210}Pb-^{226}Ra-^{230}Th systematiccs in very low sedimentation rate sediments from the Mendeleev Ridge (Arctic Ocean)* avec pour coauteurs Claude Hillaire-Marcel, Bassam Ghaleb, Leonid Polyak et Dennis Darby. Il porte sur l'utilisation des radio-isotopes de courte période comme traceurs des vitesses de sédimentation et de mélange sous diverses dynamiques sédimentaires. Il met cependant l'accent sur le comportement du ^{210}Pb et de ses ascendants dans les milieux de très faible flux sédimentaire.

Le deuxieme chapitre *Time constraints from ^{230}Th and ^{231}Pa data in late Quaternary, lw sedimentation rate sequences from the Arctic Ocean : an example from the northern Mendeleev Ridge* a été publié dans la revue *Quaternary Science Reviews, en 2010 (vol 29,* doi:10.1016/j.quascirev.2010.06.042) ; il a été rédigé en collaboration avec mon directeur de thèse, Claude Hillaire-Marcel. Il expose l'utilisation des ^{230}Th et ^{231}Pa comme outils chronostratigraphiques dans les mêmes milieux de faible vitesse de sédimentation, où les

outils chronostratigraphiques courants font défaut ou livrent des résultats contradictoires. Les enregistrements sédimentaires choisis se situent au centre de l'océan Arctique sur la ride de Mendeleiv.

Le troisième chapitre est un article soumis à la revue *Geology*, intitulé *Sedimentological evidence from Lomonosov ridge for a western Arctic trigger of the Younger Dryas*". Écrit lui aussi en collaboration avec mon directeur de thèse sur la base de données sédimentologique et géochimique (notamment flux de ^{230}Th), il éclaire le mode de mise en place d'une unité sédimentologique exceptionnelle liée au drainage du Lac Agassiz vers l'Arctique lors de l'événement du Dryas récent. La version originale de ce manuscrit était déjà en voie de soumission lors de la parution d'un article récent sur le sujet (Murton et al 2010). Par suite, nous avons dû le modifier légèrement, dans la mesure où nous ne pouvions plus arguer de l'originalité de la découverte, mais, simplement d'une "évidence" complémentaire, via le milieu marin, de cet événement régional.

REMERCIEMENTS

Dans un premier temps, je souhaiterais remercier trois hommes qui ont contribué chacun à leur façon à fairede cette thèse ce qu'elle est:

- Mon directeur de recherche, Monsieur Claude Hillaire-Marcel, de m'avoir apporté une aide précieuse tout au long de mon doctorat. Nos rencontres ont sans aucun doute ont contribué à développer mon esprit scientifique. Je voudrais aussi le remercier pour son soutien aussi bien sur le plan théorique que matériel. De plus, je voudrais le remercier de m'avoir offert la chance de rencontrer des chercheurs qui m'ont eux aussi permis d'évoluer à travers mes séjours dans différents laboratoires (UBC, IPGP, WHOI) et les missions océanographiques auxquelles j'ai participé au cours de mon doctorat.
- Monsieur Bassam Ghaleb, à qui je dois toutes mes connaissances techniques sur l'analyse des radio-isotopes. Bassam a toujours été présent pour discuter de mes différents travaux. De plus, Bassam m'a permis d'acquérir des compétences dans des domaines variés à travers ces discussions. Bassam, je voudrais te remercier pour ta confiance et de ton aide inconditionnelle, travailler à tes côtés sera toujours un plaisir.
- Monsieur Benoît Thibodeau, qui mieux que personne sait ce qu'a été cette thèse. Merci Benoît d'avoir toujours été présent et à mon écoute. Durant ces quatre années, tu m'as toujours supportée dans les bons et les mauvais moments avec toujours le ton juste. Je suis fière de notre «collaboration»

Dans un second temps, je voudrais remercier l'ensemble des gens qui sont passés au GEOTOP. Chacun à sa façon, de la plus discrète, à travers un sourire, ou de façon plus importante m'a permis de faire cette thèse dans un cadre agréable. Merci particulièrement à Josée, Maryse, Julie, Agnieska. De plus cette thèse n'aurait pas été la même sans la présence et le soutien de Sandrine, Chantal, Jenny, Emilie, Audrey, Angela, Olivia, Christian, Jean-Baptiste, Matthieu, André et Greg.

Finalement, je voudrais bien sûr remercier ma famille; mes parents, mon frère, Julie, Danielle, Jean-Jacques et tous mes amis en France qui, malgré la distance, m'ont toujours encouragée et ont été présents pour moi.

Merci à vous tous de votre support, vous êtes responsable de ces belles années.

TABLE DES MATIÈRES

LISTE DES FIGURES

LISTE DES TABLEAUX

RÉSUMÉ

Le rôle de l'océan Arctique dans le climat global est important. Les apports d'eau douce sont essentiels au maintien de la couche de faible salinité à la surface de l'océan qui permet la formation de la glace de mer. Les variations du budget d'eau douce influencent donc l'étendue du couvert de glace. Les variations du couvert de glace modifient l'albédo, le budget énergétique et les conditions de salinité et de température des masses d'eaux superficielles qui, à leur tour, influencent le climat global. Dans le contexte des changements climatiques actuels, il est indispensable de reconstituer l'histoire climatique de l'océan Arctique, en particulier au cours des cycles glaciaires-interglaciaires récents, afin de comprendre sa variabilité naturelle. L'étude paléoclimatique de l'océan Arctique a été entreprise dès les années 60 sur la base d'analyses des enregistrements sédimentaires livrés par des carottes de forage. Les sédiments situés sur les plateaux continentaux (30% de la surface de l'océan Arctique) sont caractérisés par des hauts taux de sédimentation qui permettent des études paléoclimatiques de haute résolution. Les bassins profonds et les rides connaissent des taux de sédimentation beaucoup plus faibles autorisant des études sur une plus grande échelle de temps. Ce sont de tels enregistrements qui ont été utilisés dans la présente thèse dont l'objectif principal consistait à établir des éléments de chronologie de la sédimentation grâce à l'étude des actinides.

Le premier chapitre concerne le comportement des isotopes à courte période dans les sédiments de sub-surface de l'océan Arctique en relation avec les larges gradients de vitesse de sédimentation. L'étude a été focalisée sur le ^{210}Pb, analysé dans neuf carottages courts (multicores) représentant des environnements différents (plateau, ride, etc.) afin de déterminer les conditions de son utilisation éventuelle aux fins de détermination des vitesses de sédimentation récentes. Deux multicores provenant de la ride de Mendeleiv ont été étudiés en détail et ont permis de mettre en évidence les particularités du comportement des actinides ascendants dans les environnements caractérisés par de très faibles taux de sédimentation. On a pu démontrer que sous de telles conditions, le profil de ^{210}Pb était rapidement contrôlé par son ascendant, le ^{226}Ra, lui même contrôlé par le ^{230}Th ascendant. De plus, les budgets de ^{210}Pb estimés dans ces deux multicores indiquent que le ^{210}Pb du sédiment correspond à la somme des sources atmosphériques et de la colonne d'eau, à une profondeur de ~1600 m. Par contre, un déficit s'observe dans la colonne sédimentaire, plus bas, à ~2500 m de profondeur. Il permet de conclure à un transport latéral du ^{210}Pb ou à une capacité limitée d'adsorption particulaire, au delà de 1600 m de profondeur.

Le deuxième chapitre présente une étude sédimentologique, minéralogique et géochimique détaillée des deux multicores utilisés dans le chapitre I. Les outils stratigraphiques courants (^{14}C, ^{18}O) s'avèrent peu concluants dans un tel contexte sédimentologique. Nous avons donc utilisé le ^{230}Th et le ^{231}Pa pour établir des éléments de chronostratigraphie. Deux régimes distincts ont été observés, l'un correspondant aux périodes glaciaires où la sédimentation est caractérisée exclusivement par les apports sédimentaires des glaces flottantes (Ice Rafted Debris, IRD), l'autre correspondant aux périodes interglaciaires et déglaciations, marquées par des flux sédimentaires plus élevés et des apports plus fins issus de l'archipel de l'Arctique Canadien, et un contenu micro-faunistique (foraminifères) peu abondant. En se basant sur les

caractéristiques géochimiques et sédimentaires des deux régimes et les éléments de chronologie issus des données ^{230}Th et ^{231}Pa, on a mis en évidence la présence d'un transport latéral en ^{230}Th et ^{231}Pa dans les sédiments glaciaires.

Le troisième chapitre présente des données géochimiques et sédimentologiques provenant de la ride Lomonossov. Cette ride, au centre de l'océan Arctique, est marquée par des vitesses de sédimentation plus élevées. La séquence sédimentaire examinée correspond ainsi aux derniers 25 000 ans. Un événement sédimentaire ponctuel, daté à ~ 12 000 ans (chronologie ^{14}C calibrée), rend compte d'une source sédimentaire de l'Arctique Canadien. Cet événement correspondrait au Dryas récent (Younger Dryas-YD). Cette observation est l'une des premières observations d'origine marine de la débacle du Lac Agassiz vers le nord, proposée par divers auteurs.

Mots clés: Océan Arctique; Paléocéanographie; Quaternaire; Actinides

ABSTRACT

The Arctic Ocean has an important role in the global climate. Freshwater is necessary to maintain low salinity surface water, which allows the sea ice formation. Thus, variations in freshwater budget influence the extend of the sea ice cover, which in turn modify the albedo, the energetic budget and salinity/temperature conditions of the surface water inducing feedback on Earth's climate. In the context of the actual climatic changes it is necessary to reconstruct the climatic history of the Arctic Ocean in order to estimate its natural variability. The first paleoceanographic studies of the Arctic Ocean started in 60's on sediment cores retrieved from the surroundings of the Arctic. Arctic shelves, which correspond to more than 30% of the Arctic Ocean surface are characterized by high sedimentation rates, allowing high resolution paleoclimatic studies. However deep basins and ridges are characterized by lower sedimentation rate allowing long time paleoclimatic studies. This study focus on ridge sediment cores used for the establishment of time constrain based on U-series isotopes.

The first chapter discuss the behaviour of short half-life isotopes in sub-surface sediment from different environments characterized by distinct sedimentation rates. The study focus on ^{210}Pb measured in nine short sediment cores in order to estimate recent sedimentation rates. Two short cores from the Mendeleev were studied in detail and allowed to show the particular behaviour of U-series isotopes in very low sedimentation rate environment. Under these conditions ^{210}Pb profile is rapidly controlled by its parent the ^{226}Ra it-shelf controlled by its parent the ^{230}Th. In addition, ^{210}Pb budget estimation indicated that the ^{210}Pb measured in the sediment corresponded to the sum of ^{210}Pb atmospheric and water column sources at 1600 m of water depth. However deeper, a deficit of ^{210}Pb was observed indicating a lateral transport of ^{210}Pb.

The second chapter present detailed sedimentological, mineralogical and geochemical data of the two cores used in the chapter 1. In such sedimentological context, we shown that traditional stratigraphic tools could not allow the establishment of unquestionable chronostratigraphy. Then we used ^{230}Th and ^{231}Pa isotopes for time constrain estimates. Two sedimentary regimes were observed, one corresponding to glacial period characterized by Ice Rafted Debris sediment, and the second regime, the interglacial period regime was characterized higher sediment flux composed by fine sediment from the Canadian Arctic Archipelago or Mackenzie area and some foraminifera content. Based on geochemical and sedimentological data from the two regimes and ^{230}Th-^{231}Pa time constrains, a lateral transport of these isotopes was observed.

The third chapter presented geochemical and sedimentological data coming from a sediment core located on the Lomonosov Ridge. The sediment core studied represented the last 25 ka. A sedimentary event, dated at ~12 ka, characterized by fine sediment coming from the Mackenzie basin with high particle reactive U-series isotopes (^{230}Th) content was observed. This sedimentary layer seems to be a marine record of the Lake Agassiz outflow responsible of the Younger Dryas.

Keywords: Arctic Ocean; Paleoceanography; Quaternary; U-series isotopes

INTRODUCTION

Malgré des efforts importants de la communauté scientifique pour l'amélioration de la compréhension du système climatique global, certaines composantes de ce système sont encore peu connues. Le rôle de l'océan Arctique dans le climat mondial ainsi que son influence sur la circulation thermohaline générale en sont des exemples. La difficulté pour bien comprendre le rôle de l'océan Arctique dans le système climatique global réside non seulement dans la complexité et la multitude des interactions qui y ont lieu, mais aussi dans la difficulté d'accès, qui a limité les recherches afférentes pendant des décennies. Plusieurs grandes campagnes océanographiques ont cependant pu être organisées, au cours de la dernière décennie en particulier. Nous savons ainsi maintenant que l'Arctique joue un rôle important sur la circulation océanique par l'exportation d'eau douce vers l'océan Atlantique par le détroit de Fram et les archipels de l'arctique canadien (Carmack et al., 2000 ; Peterson et al., 2006 ; Saenko et al., 2003 ; Serreze et al., 2006). Nous savons également que la sensibilité du climat Arctique est due à certaines de ses caractéristiques, tels le couvert de glace et sa forte saisonnalité. Celles-ci ont une influence en ce qui a trait, par exemple, au ruissellement sur les continents bordiers, à la formation de glace de mer et, naturellement, à l'intensité du rayonnement solaire reçu (Serreze and Francis, 2006 ; Stein et al., 2008). De fortes interactions avec les variations du climat découlent des caractéristiques de l'océan Arctique. Ainsi, le flux d'eau douce est-il responsable du maintien d'une couche de faible salinité au centre de l'océan Arctique qui, lui-même, contribue à la forte stratification de la masse d'eau de surface. Des changements des apports d'eau douce vont donc avoir des répercussions sur l'étendue et l'épaisseur du couvert de glace de mer. Ces variations du couvert de glace de mer entraînent à leur tour des changements dans l'albédo et donc influencent directement le bilan radiatif et la température de la masse d'eau superficielle, par suite les processus biologiques (White et al., 2007 ; Winton, 2006). Les changements des apports d'eau douce se répercutent dans l'Atlantique Nord et peuvent exercer une influence sur la formation des eaux océaniques profondes.

La compréhension du rôle de l'océan Arctique, et de celui des océans en général, nécessite une connaissance de la variabilité naturelle des conditions climatiques et hydrographiques,

ainsi que et des forçages qui les régissent. Or notre compréhension de la variabilité naturelle de l'Arctique est imparfaite, principalement à cause du manque de données. Les variations climatiques des derniers siècles sur le continent européen sont accessibles grâce aux enregistrements instrumentaux; or dans le cas de l'océan Arctique, ces enregistrements couvrent moins d'un siècle, période insuffisante pour tenter d'estimer la variabilité naturelle du système. Les études paléoclimatiques sont basées sur des enregistrements sédimentaires lacustres ou marins ou encore sur les forages des calottes glaciaires. Cependant, ici encore, les conditions de travail difficile de l'océan Arctique, tel le couvert de glace de mer, ont retardé les campagnes de carottage et de forage. Avant les années 90, les données provenaient essentiellement des expéditions basées sur les 'drifting ice-islands' comme T-3 (Clark et al., 1980) et CESAR (Canadian Expedition to Study Alpha Ridge; Jackson et al., 1985). Dans les années suivantes, les progrès technologiques et logistiques ont permis d'échantillonner de plus en plus loin vers le centre de l'océan Arctique, et de carotter des séquences sédimentaires plus épaisses, permettant d'obtenir des carottes couvrant des périodes temporelles. Ainsi, sauf quelques exceptions (quatre carottes provenant de la ride Alpha; Stein, 2008), l'ensemble des enregistrements sédimentaires obtenus au cours des différentes campagnes océanographiques (e.g. Polarstern/Oden Expedition en 1991, the Polar Sea Expedition en 1993, the HOTRAX expedition en 2005) couvrent la période temporelle située entre la fin du Pliocène et le Quaternaire (Darby et al., 2005; Futterer, 1992; Grantz et al., 1998). En 2004, un premier forage IODP (International Ocean Drilling Program; Arctic Coring Expedition, ACEX) a été réalisé sur la ride de Lomonossov. Situé près du pôle Nord, il est le premier enregistrement sédimentaire arctique couvrant une grande partie du Cénozoïque (Backman and Moran, 2008; Poirier and Hillaire-Marcel, 2009).

L'établissement d'une chronologie des enregistrements sédimentaires arctiques constitue une autre difficulté. Les outils traditionnels de chronostratigraphie marine, tels que l'usage des isotopes de l'oxygène des foraminifères, s'avèrent inadequates. La faible productivité biologique, la faible diversité des espèces et la faible préservation des microfossiles limitent leur utilisation à des fins biostratigraphiques. De plus, après van Donk et Mathieu (1969) divers auteurs ont relevé un décalage des teneurs en ^{18}O des foraminifères arctiques lié à la distillation de saumures isotopiquement "légères" lors de la formation de la glace de mer

(e.g., Spielhagen and Erlenkeuser, 1994, Bauch et al., 1997, Hillaire-Marcel and de Vernal, 2008). En outre, si la datation par le ^{14}C de tels foraminifères reste possible, d'autres limitations en réduisent l'usage. L'une, par exemple, correspond à la limite d'utilisation des données ^{14}C sur carbonates marins à six demi-vies environ (i.e., 30 à 40 ka); une autre est liée à la correction requise pour tenir compte de l'âge apparent des eaux de l'océan Arctique encore très mal estimé (Ostlund et al., 1987, McNeely et al., 2006). Dans cette optique, des outils non traditionnels doivent être développés pour circonscrire temporellement les enregistrements sédimentaires. Les taux de racémisation des acides aminés en sont un exemple, les isotopes du béryllium, un autre. Cependant, des études récentes (Kaufman et al., 2008, Sellen et al., 2008, Polyak et al., 2009) indiquent d'importantes différences entre les vitesses de sédimentation calculées ou les chronostratigraphies établies (jusqu'à plus d'un ordre de grandeur) entre ces approches et démontrent l'importance de combiner plusieurs méthodes pour réussir à établir au mieux les interprétations chronostratigraphiques. Cette thèse s'inscrit dans cette optique et vise à examiner les possibilités d'utilisation des actinides à cette fin.

Les actinides présentent un double intérêt. Ils constituent des traceurs des processus sédimentaires et permettent de fixer une dimension temporelle. Les actinides présentent une large gamme d'isotopes et éléments radioactifs dont les périodes couvrent une large gamme de temps; on dispose ainsi de chronomètres pour déterminer la cinétique de nombreux processus marins. De plus, les différences de comportement chimique entre plusieurs des éléments concernés (U, Th, Pa, Ra, Rn, Pb), génèrent des déséquilibres radioactifs dans les différentes phases du milieu marin: eau de mer, particules en suspension, sédiment, qui fournissent des informations spécifiques sur divers processus sédimentaires: advection et focalisation sédimentaire, flux benthiques et mélange sédimentaire (e.g., Henderson and Anderson, 2003 ; Ivanovich and Harmon, 1992). Les caractéristiques de chacun des isotopes et éléments utilisés ici sont détaillées dans le tableau 1.

Isotope	Demi-vie (a)	Comportement	Utilisation
Famille ^{238}U			
^{238}U	4,46 x 10^{9}	Soluble	U autigène vs. détritique, effets diagenétiques...
^{234}U	2,45 x 10^{5}	Soluble	U autigène, lessivage continental, diagenèse...
^{230}Th	7,57 x 10^{4}	Insoluble	Flux sédimentaire (sédimentation vs export), Chronostratigraphie 0-300 ka
^{226}Ra	1,60 x 10^{3}	Soluble	Flux benthiques
^{210}Pb	2,26 x 10^{1}	Insoluble	Taux de sédimentation et mélange sédimentaire
Famille ^{235}U			
^{235}U	2,34 x 10^{7}	Soluble	
^{231}Pa	3,25 x 10^{4}	Insoluble	Flux sédimentaires (sédimentation vs export), Chronostratigraphie (0-150 ka)
Famille ^{232}Th			
^{232}Th	1,40 x 10^{10}	Insoluble	Apports terrigènes
Retombées nucléaires			
^{137}Cs	3,07 x 10^{1}	Soluble	Mélange sédimentaire

Tableau 1 : Inventaire des isotopes/éléments utilisés (voir Bourdon et al., 2003, Henderson and Anderson, 2003, pour plus de détails)

Aux fins de notre étude, nous avons eu accès aux carottes sédimentaires provenant de la mission océanographique HOTRAX (Healy-Oden Trans Arctic Expedition), qui a eu lieu à l'été 2005. Au cours de cette mission, à travers l'océan Arctique de l'Alaska jusqu'à la Norvège, différents environnements (plateau, ride, bassin profond) ont été échantillonnés, grâce à des carottages courts (multi-cores) et longs (piston cores). Le parcours suivi lors de l'expédition est présenté sur la figure 1.

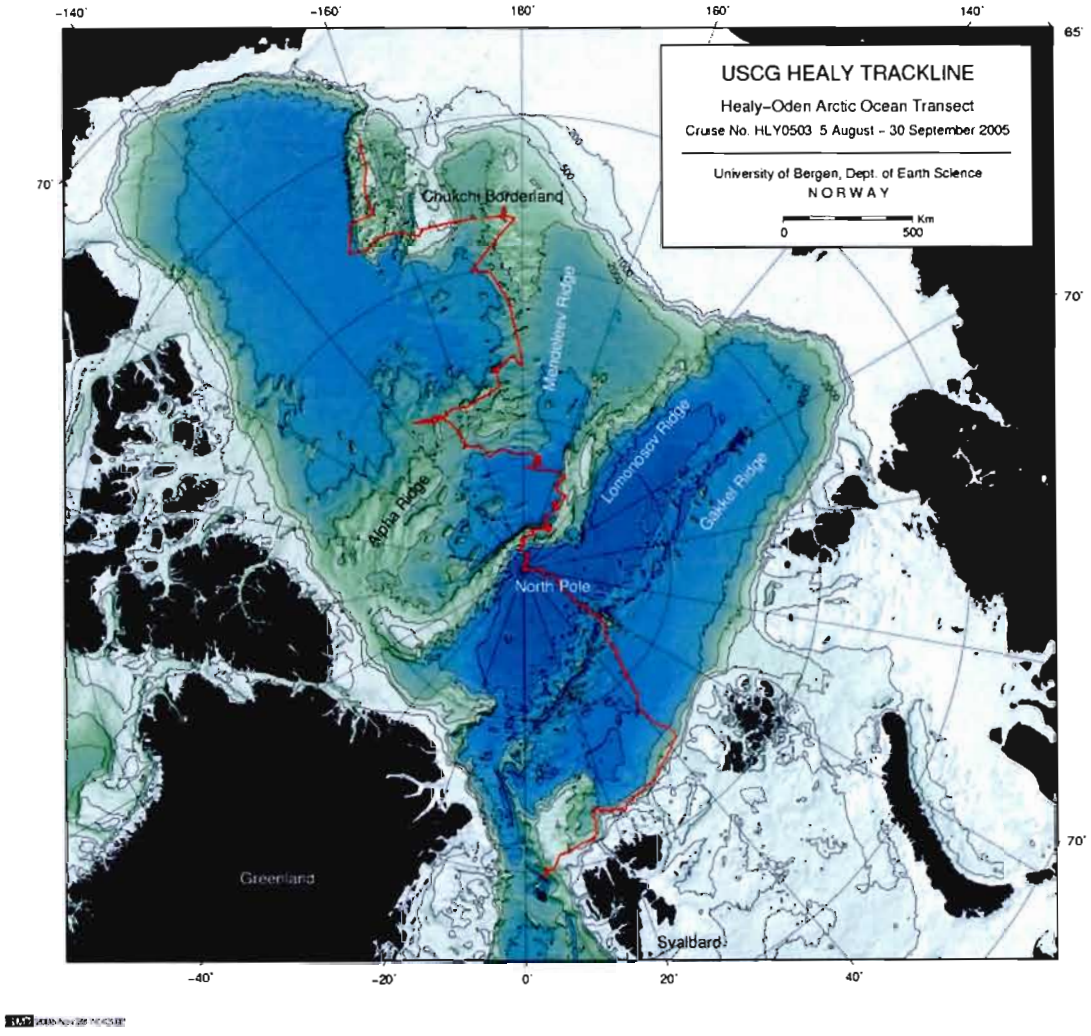

Figure 1 : Parcours de l'expédition océanographique HOTRAX 2005.

La thèse s'articule autour de deux volets, l'un, méthodologique, concernant l'utilisation des actinides en tant que traceurs ou outils chronostratigraphiques et l'autre, plus thématique, portant sur certains changements environnementaux mis en évidence grâce à la combinaison des données provenant de l'étude des actinides et des données sédimentologiques. Plus spécifiquement, les objectifs sont les suivants:

1. Combiner les données sur les radio-isotopes à courtes périodes, tels que le ^{137}Cs et le ^{210}Pb, afin d'apporter de l'information sur la vitesse de sédimentation et les processus de mélange dans les sédiments de sub-surface. Dans cette optique, différents contextes hydrographiques

et sédimentologiques ont été examinés, afin de comprendre le comportement spécifique de ces radio-isotopes.

2. Fixer des éléments de chronologie dans les enregistrements sédimentaires en utilisant des radio-isotopes tels que ^{230}Th et ^{231}Pa.

3. Combiner les informations obtenues grâce aux radio-isotopes (U-Th) et les données minéralogiques afin de déterminer les signatures spécifiques des sources sédimentaires et les mécanismes responsables de tels apports.

Il serait cependant erroné de voir, dans la présente thèse, un essai de contribution à une meilleure compréhension de la dynamique sédimentaire ou de la paléocéanographie quaternaire de l'océan Arctique. L'objectif primordial a toujours été d'examiner dans quelle mesure les actinides et isotopes à courte période pouvaient donner lieu à des applications, tant en matière de chronologie que de géochimie sédimentaire, dans un tel contexte particulier. Comme le démontreront les divers chapitres de la thèse, ces éléments et isotopes apportent en effet des informations originales et exclusives. Il n'en reste pas moins que tout effort de reconstitution de la dynamique sédimentaire ou de la paléocéanographie de cet océan requiert la confrontotation de données issues d'une large gamme d'approches, sédimentologique, géochimique, micropaléontologique, etc. La présente étude démontre que les déséquilibres radioactifs dans les familles U-Th, en particulier, sont un outil performant qui mérite une plus large utilisation dans les études multidisciplinaires en cours à propos du rôle de l'Arctique dans le système global océan-climat.

CHAPITRE 1

^{210}Pb-^{226}Ra-^{230}Th SYSTEMATICS IN VERY LOW SEDIMENTATION RATE FROM THE MENDELEEV RIDGE (ARCTIC OCEAN)

Christelle Not[1], Claude Hillaire-Marcel[1], Bassam Ghaleb[1], Leonid Polyak[2] and Dennis Darby[3]

[1]GEOTOP, Université du Québec à Montréal, C. P. 8888, Montréal, QC, H3C 3P8, Canada
[2]Byrd Polar Research Center, Ohio State University, Columbus, OH 43210, USA
[3]Old Dominion University, Norfolk, VA 23529, USA

Article publié en 2008 dans la revue Canadian Journal of Earth Sciences, 45: 1207-1219, doi: 10.1139/E08-047

Resumé

Le comportement des isotopes des séries de l'uranium dans les sédiments de sub-surface de l'océan Arctique est étudié en se basant sur les mesures de radionucléides naturels (^{210}Pb, ^{226}Ra, ^{230}Th) et de quelques analyses de ^{137}Cs anthropique dans des carottes prélevées durant l'expédition HOTRAX « Healy-Oden Trans-Arctic Expedition ». Deux carottes de la ride Mendeleev, représentant deux environnements bathymétriques distincts, sont analysées plus en détail afin d'évaluer le potentiel de datation de tels radionucléides à des sites caractérisés par de très faibles taux de sédimentation (~3 mm ka^{-1}). Les sédiments comprennent des proportions variables de carbonates à grain fin, d'argiles et de débris transportés par les glaces, et ils montrent des excès de ^{210}Pb (^{210}Pb$_{xs}$), par rapport au contenu parent de ^{226}Ra, jusqu'à ~1 cm sous le sommet de la carotte. Cette distribution du ^{210}Pb$_{xs}$ est due au mélange, à faible profondeur, par des organismes benthiques et (ou) la diffusion à partir de l'interface sédiment–eau; la profondeur du mélange est aussi indiquée par les activités de ^{137}Cs. De ~1 à 7 cm de profondeur dans la carotte, les activités ^{210}Pb suivent de près les activités du ^{226}Ra. Plus bas dans la carotte, les activités du ^{226}Ra sont contrôlées par des excès variables du ^{230}Th (^{230}Th$_{xs}$) parent, qui découle de son piégeage dans la colonne d'eau sus-jacente. La diffusion du ^{226}Ra vers la colonne d'eau est observée dans les ~7 cm supérieurs de sédiments sous le plancher océanique (avec un flux d'environ 0,043 dpm cm^{-2} an^{-1}) et plus profondément dans les sédiments au niveau des pics de ^{230}Th$_{xs}$, mais avec des flux moindres. Les deux carottes montrent des profils de ^{210}Pb identiques malgré leur différence bathymétrique d'un (1) km. Cela suggère un scavenging négligeable du ^{230}Th et du ^{210}Pb à des profondeurs d'eau inférieures à 1,6 km, qui correspond à la bathymétrie de la carotte la moins profonde. Dans des milieux où les taux de sédimentation sont très faibles et la pluie verticale de particules constitue la principale source de sédiment, les estimations du ^{210}Pb$_{xs}$ réel exigent une connaissance précise de la fraction soutenue par le ^{226}Ra, laquelle est contrôlée par le ^{230}Th$_{xs}$, la diffusion du Ra et donc par les taux de sédimentation et la porosité.

Abstract

U-series isotope behaviour in subsurface sediment of the Arctic Ocean is investigated based on high resolution measurements of natural radionuclides (^{210}Pb, ^{226}Ra, ^{230}Th) and a few analyses of anthropogenic ^{137}Cs in cores collected during the 2005 Healy-Oden Trans-Arctic Expedition (HOTRAX). Cores from the Mendeleev Ridge, representing distinct bathymetric settings, are analyzed in more detail as a means to assess the dating potential of such radionuclides at sites characterized by very low sedimentation rates (~3 mm ka^{-1}). The sediment consists of variable proportions of fine-grained carbonates, clays, and ice-rafted debris and shows excesses in ^{210}Pb (^{210}Pb$_{xs}$) over parent ^{226}Ra content, down to ~1 cm below core top. This ^{210}Pb$_{xs}$ distribution is due to shallow mixing by benthic organisms and (or) diffusion from the sediment–water interface, as also indicated by ^{137}Cs activities. From ~1 to 7 cm downcore, ^{210}Pb activities closely follow ^{226}Ra activities. Below 7 cm downcore, ^{226}Ra activities are controlled by variable excesses in parent ^{230}Th (^{230}Th$_{xs}$) resulting from its scavenging in the overlying water column. ^{226}Ra diffusion is observed towards the water column occuring from the upper ~7 cm of sediment below the seafloor (with a flux of ~0.043 disintegrations per minute (dpm) cm^{-2} a^{-1}) and deeper in the sediment below ^{230}Th$_{xs}$ peaks but with lesser fluxes. Both cores show identical ^{210}Pb profiles despite their 1 km bathymetric difference. This suggests negligible ^{230}Th and ^{210}Pb scavenging below water depths of ~1.6 km, i.e., the bathymetry of the shallower core. In such settings where sedimentation rates are very low and vertical particle rain is the major sediment source, estimates of the actual ^{210}Pb$_{xs}$ require precise knowledge of the ^{226}Ra-supported fraction, which is controlled by ^{230}Th$_{xs}$, Ra diffusion, and thus sedimentation rates and porosity.

1.1. Introduction

The Holocene interval in the central Arctic Ocean ridges is relatively well documented by radiocarbon chronologies (Darby et al. 1997; Polyak et al. 2004), suggesting in particular low mean sedimentation rates (0.3–1.5 cm ka^{-1} and much less in the last glacial except during deglaciation events). However, information on these rates in the most recent past, i.e., within the last few thousand years (Dyke et al. 1996), is rare and often disputable. In a similar fashion, chronostratigraphies of Pleistocene sediments beyond ^{14}C time control (>40 ka) are still poorly constrained (Backman et al. 2004). During glacial periods, exemplified by the last glaciation, deposition rates display a large variability, reaching up to tens of cm ka^{-1} during episodes of massive iceberg discharge but decreasing occasionally to very low values or even to hiatuses of up to several thousand years, particularly during the last glacial maximum in the Amerasian Basin (Darby et al. 2006). This drop in deposition rates, coupled with an absence of faunal remnants, indicates that a very thick or perennially snow-covered pack-ice existed during the last glacial maxima, suppressing both biological productivity and lithic deposition. Most late Cenozoic sedimentary records from the Arctic Ocean's interior yield unconstrained age models leading to contrasting paleoceanographic interpretations depending upon the stratigraphic approaches used (Poore et al. 1994; Jakobsson et al. 2000, 2001). In this context, investigations on the behaviour of U series and short-lived isotopes, particularly on ^{210}Pb, can help document sedimentation rates, as well as benthic mixing processes.

In the ocean, ^{210}Pb originates from the decay of ^{226}Ra dissolved in the water column and from the decay of its gaseous daughter, ^{222}Rn, in the atmosphere. In the first case, ^{226}Ra diffuses from the sediments, thus maintaining a more or less steady-state ^{226}Ra concentration in the water column. This makes the production rate of ^{210}Pb in the water column predictable (Cochran 1992). The residence time of ^{210}Pb with respect to scavenging is brief at the ocean's surface (on the order of 1 year), whereas it reaches 30–100 years in the deeper ocean (Cochran et al. 1990). Since intermediate decay products between ^{222}Rn and ^{210}Pb depict short half-lives by comparison with the average residence time of aerosols, it is usually assumed that essentially all atoms of ^{222}Rn are transformed into ^{210}Pb in the atmosphere. This atmospheric ^{210}Pb is then scavenged by precipitation and dry fallout. On a global scale, ^{210}Pb

delivery from the atmosphere to the ocean surface is known to be latitude dependent (Turekian et al. 1977).

In the Arctic Ocean, investigations on the behavior of natural (^{210}Pb, ^{226}Ra, ^{7}Be) and anthropogenic (^{137}Cs, ^{239}Pu, ^{240}Pu) radionuclides, in coastal and shelf regions in particular, provide information on sea-ice transit time, sea-ice interactions with surface seawater, and surface sediment (Baskaran and Naidu 1995; Baskaran et al. 1996, 2000; Baskaran 2005). A few studies have also addressed natural radionuclide behavior in the water column (Smith and Ellis 1995) and helped document shelf–basin interactions (Smith et al. 2003) as well as infaunal benthos ecology (Clough et al. 1997; Smith et al. 2003). In addition to the high scavenging efficiency, ^{210}Pb deficits measured in the Arctic Ocean suggest that additional processes, such as "boundary scavenging", contribute to the removal of ^{210}Pb (Smith et al. 2003). To understand ^{210}Pb behavior in the Arctic environment, a thorough investigation of ^{210}Pb parent isotopes (^{222}Rn, ^{226}Ra) is necessary. The relatively low concentrations of ^{222}Rn in northern latitudes suggest that the atmospheric flux of its longer lived decay product, ^{210}Pb, may also be reduced in this environment (Weiss and Naidu 1986). Permafrost can suppress exhalation of gaseous ^{222}Rn, the ^{210}Pb parent from soils, resulting in a lower ^{210}Pb input to Arctic sediment (Hermanson 1990). In addition, radon loss from the ocean surface is about two orders of magnitude lower than from soils (Baskaran and Naidu 1995).

Despite the importance of the Arctic Ocean sedimentary archives with respect to the understanding of ocean–climate dynamics, investigations on the behaviour of such isotopes in sediments from deep Arctic basins and ridges are scarce, essentially due to the lack of records available for such studies. Recent major coring expeditions such as the 2005 Healy-Oden Trans-Arctic Expedition (HOTRAX) yielded a new and important series of sedimentary records from such sites (Darby et al. 2005*b*; Moran et al. 2006; Stein 2007). We conducted a systematic study of the distributions of short-lived and U-series radionuclides in several of the HOTRAX cores to help constrain sedimentation rates and the stratigraphy of core-top sediments. This study focuses on core HLY0503-11 raised from a depth of 2570 m on the Mendeleev Ridge (Fig. 1), for which analyses of both short-lived (^{210}Pb, ^{137}Cs) and parent isotope (^{226}Ra, ^{230}Th) were performed. In this particular setting (i.e., far from slope processes and deep current influence), vertical fluxes from the overlying water column are dominant.

We demonstrate that both the low sedimentary fluxes and dominant vertical particulate rain result in a downcore ^{210}Pb distribution essentially controlled by the behaviour of parent ^{226}Ra and ^{230}Th, independently of bathymetry of the site below a given water depth.

1.2. Materials and methods

1.2.1. Core location

Sediment multicores (MC) were collected in the summer of 2005 during the HOTRAX expedition (Darby et al. 2005*a*). In this study, we present ^{210}Pb measurements on nine of these cores selected along the trans-Arctic route of the coring vessel US Coast Guard Cutter (USCGC) *Healy* (Fig. 1). They represent various settings with respect to the bathymetry and ice-cover (from shelf to deep basin or ridge; from perennial-ice margin to permanent ice cover; Table 1). Special attention is paid to two cores from the northern Mendeleev Ridge, collected ~22 nautical miles apart, representing two distinct bathymetric domains (~1600 and ~2600 m, respectively), in which exhaustive geochemical investigations were carried out (HLY0503-11MC and HLY0503-12MC, henceforth cores MC-11 and MC-12, respectively; Table 1; Fig. 1). The Mendeleev Ridge extends from the East Siberian shelf to where it joins the Alpha Ridge (Fig. 1). The Mendeleev Ridge is characterized by a fairly uniform sedimentary layer that thickens to the south. As with most of the central Arctic far from coastal influences, sedimentation is dominated by particulate fluxes strictly linked to ice-rafted debris (IRD), plus some unknown but minor amount of advected sediment in the form of nepheloid transport or turbidity flows above the bottom (Fahl and Nöthig 2007; Hwang et al. 2008), and to a very minor extent to particles linked to productivity in the ice and water column and eolian particles (Darby et al. 1989). This property makes this site ideal for investigating the behavior of U-series isotopes (^{210}Pb, ^{226}Ra, ^{230}Th).

1.2.2. Sedimentological analyses

Multicores were sampled at half-centimetre intervals. The sediment was dried and ground in an agate mortar. Particle-size analyses were performed as follows: Na-hexametaphosphate was added to deflocculate the sediment by tumble mixing for 3 h in deionized water. Samples were treated in an ultrasound bath for 10 min followed by rotated

agitation for 3 min. Sediments were sieved (2 mm) then disaggregated in an ultrasonic bath for 90 s prior to their analysis. The disaggregated sediment samples were analyzed with a laser-diffraction particle-size analyzer (LS13320, Beckman-Coulter). Only particle sizes between 0.04 and 2000 μm were analyzed. Laser calibration was verified before and after analyses using three standards (Latron 300-0.3 μm, G15-15 μm, and GB500-500 μm). Analyses of 6–14 spectra are necessary to obtain enough stability on the spectrum to compare results. The mean of the last two spectra is weighted to 100% to minimize minor statistical deviations. The particle-size data and granulometric statistics are then processed with the Gradistat program (Blott and Pye 2001).

Organic and inorganic carbon contents (OC and IC, respectively) were measured with a Carlo Erba™ elemental analyzer. A first aliquot is dried and analyzed as evolved CO_2 for its total carbon content. A second aliquot is acidified twice with HCl (1 N) to dissolve carbonates and then analyzed in a similar fashion for its residual carbon content considered to represent OC. IC was then calculated by balancing the difference between the two measurements. IC and OC are both expressed in dry weight percent (dw%) of total sediment and represent the mean of two analyses. Uncertainties ($\pm 1\sigma$), as determined from replicate measurements of standard materials, average ±0.06% for IC (i.e., ±0.6% for its expression as $CaCO_3$ equivalent). Although fast, this method may result in biases for IC calculations when HCl (1 N) hydrolysable minerals (e.g., chlorite) or compounds (e.g., Fe and Mn oxyhydroxydes) are present in the sediment (e.g., Leventhal and Taylor 1990; Raiswell et al. 1994), thus resulting in higher apparent OC contents in the second acidified sample aliquot and in a subsequent underestimation of the IC content. In the present case, the sediment shows low OC values in comparison with the IC except in the upper 7 cm (Table 3). Some underestimation of the IC content thus seems likely, notably near core top. Semi-quantitative X-ray diffraction measurements of mineralogical assemblages (Not et al. 2007) indeed suggest a slightly higher carbonate content in the sediment, particularly in the upper few centimetres, and also indicate that it consists, in average, of ~75% dolomite and ~25% calcite.

1.2.3. Radioactive isotope measurements

1.2.3.1. Lead-210 analyses

Lead-210 (half life $t_{1/2}$ = 22.6 year) activities were measured on bulk sediment samples, dried, and ground in an agate mortar. Measurements were made by α counting of the activity of ^{210}Pb-daughter isotope, ^{210}Po ($t_{1/2}$ = 138.4 days, α = 5.30 MeV). Measurements were performed about 200 days following sampling. A few replicate measurements were carried out ~1 year later to verify the achievement of equilibrium between the two isotopes in the study samples. All replicate data were identical to the first set of measurements within counting errors. Chemical extraction and counting efficiencies were determined using a ^{209}Po spike. Chemical procedures for ^{210}Po extraction followed Baskaran and Naidu (1995) (i.e., with a classical HCl–HNO_3–HF treatment), and samples were deposited on a silver disk (Flynn 1968). The ^{209}Po and ^{210}Po activities were measured in a silicon surface barrier α spectrometer (EGG and ORTEC type 576A). Uncertainties were estimated as 1σ standard deviation for counting statistics (~2%–4% of the value obtained).

1.2.3.2. Cesium-137 analyses

Cesium-137 ($t_{1/2}$ = 30.17 years) was measured on ~1 cm^3, bulk, dried, and ground subsamples by γ-ray spectrometry at 661.6 keV (γ ray yield = 85.0%), using a low-background high-purity Ge well detector (Canberra). IAEA-300 sediment was used to calibrate the yield of the detector. Uncertainties were estimated for counting errors.

1.2.3.3. Radium-226 analyses

Aliquots of geochemical subsamples were weighed and spiked with a ^{228}Ra solution processed for dissolution, chemical separation, and purification of Ra through MnO_2 precipitation following Ghaleb et al. (2004). Data acquisition used a Daly-ion counter by peak jumping mode on a VG sector-54 mass spectrometer. Analytical uncertainty represents two standard errors and was ~1% for the majority of the samples.

1.2.3.4. Thorium isotope analyses

Thorium isotopes (^{230}Th and ^{232}Th) were extracted and measured following conventional techniques (Lally 1982) by α spectrometry after separation on an anion exchange resin (AG1-X8, 200–400 mesh), purification of thorium using the anion exchange resin. The thorium was then deposited on steel disks by electrodeposition (Lally 1982). Activities were measured using α spectrometry (EGG and ORTEC type 576A). ^{228}Th-spike solution was used to calculate chemical extraction and counting efficiencies (natural ^{228}Th was assumed to be in secular equilibrium to ^{232}Th). Analytical uncertainties were estimated from counting statistics to ~3% for all Th isotopes. All other isotopes activities reported in Tables 2–4 are expressed in disintegrations per minute and per gram of dry bulk sediment (dpm g^{-1}).

1.3. Results and discussion

1.3.1. Lead-210 in Arctic Ocean sediments

The nine cores from the trans-Arctic transect depict two patterns of ^{210}Pb distribution in subsurface sediments (Figs. 2, 3). In the first pattern (Fig. 2A), ^{210}Pb activities decrease sharply in the first 1–2 cm then show a reverse increasing trend deeper in the sediment. In the second pattern (Fig. 2B), ^{210}Pb activities decrease more steadily to deeper depths (~4–5 cm). In the very first 0.5 cm of sediment, ^{210}Pb activities of both patterns differ by almost one order of magnitude (i.e., between 9 and 72 dmp g^{-1}). These two broad patterns of ^{210}Pb distribution thus respond to distinct sedimentological settings and overall sedimentation rates. The first one seems exclusive to ridges in the central Arctic Ocean, i.e., at sites below permanent sea-ice cover. The ^{210}Pb distribution in core MC-14 (Fig. 2C) corresponds to the first pattern although the near-surface maximum is missing due to the loss of ~1 cm of core-top sediment when this core tube was extruded from the multicorer. The second pattern corresponds to cores from much shallower water depths, where particulate organic carbon fluxes and mixing depths are higher. This is quite consistent with previous studies on ^{210}Pb in the Arctic (Clough et al. 1997).

1.3.2. Sedimentological properties and sedimentation rates in the Mendeleev Ridge cores

MC-11 and MC-12 are 38.5 and 34.5 cm in length, respectively. The sediment is characterized by alternating brown – dark-brown and yellowish-brown layers. It shows an alternation of fine carbonate-rich layers with coarser grain units. Accelerator mass spectrometry (AMS) ^{14}C ages were obtained on low-abundance assemblages of *Neogloboquadrina pachyderma* (left-coiled) in core MC-11 at depths of 0.25, 4.25, 8.25, and 12.25 cm (Table 3). Although the ages at 4.25 and 12.25 cm are near ^{14}C dating limits with respect to deep-sea core carbonates, they may indicate the presence of shells reworked from marine isotope stage (MIS) 3 or older possibly carried to the site through ice rafting. Nonetheless, the ^{14}C age of ~27 ka at 8.25 cm provides a lower limit of the mean sedimentation rate for the upper 8 cm of sediment. It corresponds to a calibrated age of about 33 ka, using the calibration model of Fairbanks et al. (2005). Potential errors in estimating the calibrated age notably due to uncertainties about reservoir age correction for Arctic Ocean surface waters during the late MIS 3 should not be of major importance here. This date results in a sedimentation rate of ~3.1 mm ka^{-1}. Another approach consists of using the ^{14}C age of ~8.5 ka at 0.5 cm (i.e., ~9.5 calibrated ka; cf. Reimer et al. 2004) in the mixed layer (Table 3) to estimate the most recent sedimentation rate. Using a simple model based on a constant ^{14}C-carrier flux to the sea floor and a homogeneous-mixed layer (e.g., Berger and Johnson 1978), the age at the core top (T) can be expressed as follows:

$$[1] \quad T = 1/\lambda \ln(1+(\lambda X/S)$$

where λ is the decay constant of ^{14}C (1.21×10^{-4} a^{-1}), S is the sedimentation rate, and X is the mixed layer thickness.

As for most low sedimentation rate sites investigated in this study, the mixed layer thickness for ^{14}C-carrier material should be at least equal to the depth penetration of $^{210}Pb_{xs}$, here $X \approx$ 10 mm (see the following and Fig. 2), assuming that this excess is due to mechanical mixing more than diffusion. This approach yields a sedimentation rate of about ~1 mm ka^{-1} or significantly less than the linear radiocarbon calculation of ~3 mm ka^{-1} or more. This means that the flux of ^{14}C carriers cannot be considered constant or the mixed layer thickness for these ^{14}C carriers is much higher than that for ^{210}Pb (or both). Using the 3 mm ka^{-1} estimate

from previous for S, a value of ~50 mm could be calculated for the theoretical thickness of the ^{14}C-carrier mixed layer in this second hypothesis (e.g., see Boudreau and Imboden 1987 for deep burrowing impact on mixing models). Since foraminifer shells at a depth of 4.25 cm yielded and age of ~32 ka, one can discard the second hypothesis. The mixing of "old" material with recent shells seems indeed more likely. Note that using eq. [1] with an S value of 3 mm ka^{-1} and the 10 mm thickness for the mixed layer X, a constant ^{14}C-carrier flux would have resulted in a ^{14}C age of ~3 ka instead of the calibrated age of 9.5 ka. Nevertheless, ^{230}Th–^{231}Pa analyses in MC-11 (Not et al. 2007) indicate that MIS 5 sediments are present below 25 cm in this core, thus suggesting a mean sedimentation rate in the 2–3 mm ka^{-1} range. Similarly, Sellen et al. (2007) reported ^{10}Be evidence for sedimentation rates of ~2 mm ka^{-1} in MC-14, a nearby core showing sedimentological and geochemical features almost identical to those of MC-11 (Fig. 2). Thus, we will retain the estimate of ~3 mm ka^{-1} for the mean sedimentation rate of MC-11 and, as will be seen in the following, for MC-12 as well. Consequently, the excess ^{210}Pb seen in core tops of low sedimentation rate sites (Fig. 2A) illustrates either mechanical mixing by bioturbations and (or) chemical diffusion as documented by Courcelles (1998) in very low sedimentation rate lacustrine sequences.

A few ^{137}Cs measurements were performed as a means to document the distribution in the sediment of the post-1950 A.D. thermonuclear signal (Table 4). ^{137}Cs activity is observed down to 1 cm in cores MC-11, MC-12 and MC-18 (Fig. 2A) and down to 4 cm in core MC-22 (Fig. 2B). In the second case, mechanical mixing down to this 4 cm seems probable. In the first case, both diffusion and mixing could also explain the ^{137}C distribution in the upper centimetre of sediment. Other studies of sedimentation rates in the Arctic report values ranging from 10 to 0.2 mm ka^{-1} based on different proxies, such as ^{14}C (Ku and Broecker 1965; Darby et al. 1997, 2006; Polyak et al. 2007), ^{230}Th (Ku and Broecker 1965; Huh et al. 1997), paleomagnetism (Jones 1987), and micropaleontology (Aksu and Mudie 1985). However, recent reviews propose that the key issue to constrain Arctic sedimentation rates is not only the choice of the proxy but the significant variability of sedimentation rates across the Arctic Ocean with the lowest rates characteristic of the central areas of the Amerasian basin, such as the Alpha and northern Mendeleev ridges, as also illustrated here (Backman et

al. 2004; Sellen et al. 2008). Nonetheless, if the distribution of the $^{210}Pb_{xs}$ in such settings cannot be used to estimate recent sedimentation rates, it may be used as a proxy for the downcore distribution of ^{226}Ra–^{230}Th parent isotopes and thus as a stratigraphic tool, as discussed in the following section.

1.3.3. ^{210}Pb–^{226}Ra systematics in MC-11

The excess ^{210}Pb ($^{210}Pb_{xs}$), i.e., the fraction exceeding parent-isotope activity, has been determined in core HLY0503-11MC by subtracting ^{226}Ra activity (available down to 7.5 cm) from the total ^{210}Pb activity. This excess is only seen in the top centimetre of the sediment (Fig. 3). Below, the ^{210}Pb seems to be nearly all supported by ^{226}Ra, which shows a decreasing trend from ~7 cm to the core top in response to an upward diffusive gradient. Below ~7 cm, both isotopes seem to closely follow their parent ^{230}Th activity except for some diffusion of ^{226}Ra below ^{230}Th peaks (Fig. 3). Worth of mention is the fact that ^{230}Th is in excess relative to its parent uranium in the MC-11 sequence (Not et al. 2007), thus representing the ^{230}Th fraction scavenged by sinking particles when deposited but for the radioactive decay since their deposition. One sample at 21.25 cm below sediment surface (dbsf) shows a minimum ^{230}Th activity (~1 dpm g^{-1}), possibly representative of the detrital heritage of ^{230}Th and its daughter products.

Nonetheless, the ^{210}Pb activity that is strictly representative of ^{210}Pb fluxes from the overlying water column can differ slightly from the Pb_{xs} previously estimated by subtracting ^{226}Ra activity from that of total ^{210}Pb in the core-top samples. Two processes may account for such a slight difference: (1) the diffusive ^{226}Ra may not be totally in radioactive equilibrium with its daughter ^{210}Pb (i.e., produced in situ; cf. Cochran 1992); and (2) some diffusion of the intermediate gaseous ^{222}Rn isotope could also result in a slight imbalance between ^{226}Ra and its daughter ^{210}Pb. This diffusion of ^{226}Ra is generally thought to have little impact on estimates of the supported fraction of ^{210}Pb (Key et al. 1979; Imboden and Stiller 1982; Baskaran and Naidu 1995). However, the effect of ^{226}Ra diffusion is not necessarily negligible. Deschamps (1997) has illustrated large deficits (~40%) in ^{228}Ra, but excesses in daughter ^{228}Th (versus their parent ^{232}Th) in fine particles sedimenting in the modern St. Lawrence estuary linked to processes occurring during their water transport and earlier

terrestrial evolution in soils. Assuming a similar behavior for ^{226}Ra in the Mendeleev Ridge sediment, ^{226}Ra diffusion during particle transport would result in some excess of the "inherited" fraction of ^{210}Pb versus its parent "detrital" ^{226}Ra fraction. In an opposite way, ^{226}Ra fluxes resulting from the excess ^{230}Th in core-top sediments may result in some daughter ^{210}Pb deficit linked to the time interval it needs to reach equilibrium with its parent ^{226}Ra. Fortunately, here, the very low sedimentation rate but high residence time of particles in the upper sedimentary column (~3 ka, as previously estimated) should carry back these potential disequilibria to nearly secular equilibrium conditions at the ^{210}Pb time scale, as discussed in the following.

There is no correlation between water depth and ^{210}Pb distribution in surface sediment and downcore. MC-11 and MC-12 raised from depths of 2570 and 1586 m, respectively, present similar $^{210}Pb_{xs}$ distributions (Fig. 4), suggesting that the particle flux is identical at these two sites. In earlier studies of $^{210}Pb_{xs}$ distribution in Arctic sediment cores (Clough et al. 1997; Huh et al. 1997; Smith et al. 2003), the reverse trend at a few centimetres below the surface has been reported in several cases; Smith et al. (2003) explained it using a bioturbational mixing, whereas Clough et al. (1997) presented it most likely as a result of ^{226}Ra ingrowth. As illustrated in Fig. 4, this pattern is closely controlled by the subsurface diffusion gradient of ^{226}Ra produced by the excess in parent ^{230}Th that characterizes the most recent sediment from core tops.

1.3.4. ^{226}Ra diffusion at MC-11 site

The ^{226}Ra distribution in MC-11 typically corresponds to a diffusion profile in Arctic Ocean sediments previously noted (Baskaran and Naidu 1995). This diffusion pattern combines diffusion of ^{226}Ra ejected from particles by alpha recoil and diffusion of ^{226}Ra from adsorbed ^{230}Th on grains. Unfortunately, without pore-water ^{226}Ra data, direct diffusion rates cannot be calculated. Cochran (1980) proposed a method to estimate ^{226}Ra fluxes from deep sediments using ^{226}Ra activities of sediment. This method is based on a box model where the ^{226}Ra concentration is maintained in the mixed core-top layer by balancing its sources (production of ^{226}Ra by ^{230}Th + ^{226}Ra in freshly deposited sediment) and losses (radioactive decay of ^{226}Ra + burial).

Under steady state conditions,

$$[2]\ \lambda_{Ra} A^{X}_{Th} \rho X + S A^{0}_{Ra} \rho = \lambda_{Ra} A^{X}_{Ra} \rho X + S A^{X}_{Ra} \rho$$

where X is the mixed layer thickness (here about 10 mm), S is the sedimentation rate (here ~3 mm ka^{-1}), A^{X}_{Th} is the total ^{230}Th activity in the mixed layer, A^{X}_{Ra} is the total ^{226}Ra activity in the mixed layer, A^{0}_{Ra} is the activity of ^{226}Ra linked to detrital sources (about 1 dpm g^{-1} here as estimated above), ϱ is the sediment density (in g cm^{-3}), and λ_{Ra} is the decay constant of ^{226}Ra (in ka^{-1}).

Here, the term $SA^{0}_{Ra}\varrho$ is negligible versus $\lambda_{Ra}A^{X}_{Th}\varrho X$ when comparing the total ^{230}Th activity near the core top with the activity of its "detrital fraction" (~1 dpm g^{-1}), seen as a proxy for A^{0}_{Ra} (Fig. 3). Using this model, about 60% of ^{226}Ra losses from the mixed layer would occur at this site through radioactive decay and about 40% through burial. One useful information gained from this exercise is that any initial disequilibrium between ^{210}Pb, ^{226}Ra, and ^{230}Th disequilibrium in the detrital fraction of the sediment should be largely reduced at burial stage, i.e., below the mixed layer, as previously estimated from the age of the mixed layer above.

As a consequence, in such low sedimentation rate sites, with shallow mixing (if any), a direct estimate of the ^{226}Ra flux can be obtained by the depth-integrated (0.5 cm integration step) deficiency in ^{226}Ra inventory relative to the ^{230}Th inventory (see later in the text for details on inventory estimates) down to ~7.5 cm. The obtained ^{226}Ra flux is ~0.043 dpm cm^{-2} a^{-1}. This estimate of the ^{226}Ra flux over the Mendeleev Ridge is in the upper range of values reported previously from Pacific and Atlantic sediments (Cochran 1980; Cochran and Krishnaswami 1980; Moore and Dymond 1991; Moore 1999; Hancock et al. 2000). Cochran (1980) suggested an inverse and nonlinear correlation between ^{226}Ra fluxes from sediments and sedimentation rates. Our estimate (0.043 dpm cm^{-2} a^{-1}) thus corresponds to values expected in very low sedimentation rate areas.

1.3.5. ^{210}Pb behavior downcore

A striking feature is the similarity of ^{210}Pb vertical distribution in cores MC-11 and MC-12 despite their ~1 km bathymetric difference (Fig. 4). Below the high activity of the surface layer (25 dpm g^{-1} in the top 0.5 cm), there is (*i*) a decreasing trend of $^{210}Pb_{xs}$ from core top

down to ~1.5 cm, linked to its return to equilibrium with parent ^{226}Ra with likely some diffusion–mixing from the sediment–water interface; (*ii*) a reverse increasing trend down to ~7.5 cm following the upward diffusion gradient of ^{226}Ra; and (*iii*) a fluctuating ^{210}Pb distribution below, still closely following ^{226}Ra distribution. Downcore, ^{226}Ra follows the ^{230}Th distribution except for some diffusion below activity peaks of this isotope, thus suggesting an overall pattern primarily governed by the distribution of residual excesses in ^{230}Th linked to its variable scavenging rates through time and its decay since deposition (Figs. 3, 4). ^{210}Pb and ^{230}Th distributions show two major peaks downcore, between 15 and 20 cm and between 27 and 32 cm, with a slight decoupling between ^{210}Pb distribution and ^{230}Th profiles due to ^{226}Ra diffusion away from the ^{230}Th peaks.

The second step in ^{210}Pb distribution, i.e., its increase from ~1.5 to 7.5 cm here, is found in other Arctic sediments (Clough et al. 1997) and was explained as the result of growth of ^{226}Ra in sediments. Our study provides supporting ^{226}Ra data to validate this hypothesis of ^{226}Ra ingrowth from $^{230}Th_{xs}$ decay and further documents the diffusion pattern of ^{226}Ra. ^{230}Th distribution (and thus ^{210}Pb distribution) downcore closely follows the carbonate content and inversely correlates with grain size (Fig. 3), thus pointing to variable scavenging rates due to particle availability and size. Between peaks, we observe a larger particle size and a lower carbonate content, possibly linked to the minimum sedimentary supply during glacial periods, essentially represented by relatively coarse but scarce IRDs (Fig. 2; see also Moran et al. 2006).

1.3.6. Lead-210 excess inventories in MC-11 and MC-12

Inventories of $^{210}Pb_{xs}$ in deep-sea sediments are calculated from measurements of ^{210}Pb minus the supported fraction estimated ideally from parent-isotope activity (^{226}Ra) using the equation:

$$[3]\ I = \sum_i (\rho_i A^i_{xs} \Delta X_i)$$

where I is the inventory of $^{210}Pb_{xs}$ (in dpm g^{-1}), ϱ_i is the dry bulk density (in g dry sediment per cm^3 of wet sediment) of the ith depth interval, A^i_{xs} is the $^{210}Pb_{xs}$ activity (in dpm g^{-1}) of the ith depth interval, and ΔX_i is the thickness of ith depth interval (in cm). ^{210}Pb inventories of 12 and 14 dpm cm^{-2} are measured in cores MC-11 and MC-12, respectively, and are within

a range of values for the Arctic (Baskaran and Naidu 1995; Huh et al. 1997; Smith et al. 2003). The small difference in $^{210}Pb_{xs}$ inventories between MC-11 and MC-12 is not significant, considering the potential errors in sediment-depth measurements and in dry bulk-density estimates. This similarity in $^{210}Pb_{xs}$ inventories at the two sites representing distinct water depths (~2.6 versus ~1.6 km) suggests that $^{210}Pb_{xs}$ inventories in Mendeleev Ridge surface sediments do not simply reflect the production of ^{210}Pb from ^{226}Ra and ^{222}Rn decay in their overlying water column and losses by advection must occur.

$^{210}Pb_{xs}$ in sediments includes fractions from both its atmospheric fallout and production in the water column. In the following calculations, we use a flux of atmospheric ^{210}Pb of ~0.08 dpm cm^{-2} a^{-1} measured near Point Barrow in Alaska. We expect some variability in ^{210}Pb fluxes due to its relatively large range in Arctic haze aerosols (from 0.0134 to 0.0613 dpm m^{-3}; see Moore and Smith 1986; Weiss and Naidu 1986; Bacon et al. 1989; Baskaran and Shaw 2001; Smith et al. 2003). Production rate of ^{210}Pb in the water column is dictated by the distribution of ^{226}Ra, and the scavenging flux can be estimated from the disequilibrium between ^{226}Ra and ^{210}Pb in water column. Although water column ^{226}Ra and ^{210}Pb data are not available at MC-11 and MC-12 core sites, data from nearby in the Canada Basin are available (Moore and Smith 1986; Bacon et al. 1989; Smith and Ellis 1995). Thus, assuming that the ^{226}Ra–^{210}Pb disequilibrium relationship shows minimum variability across the basin, a theoretical scavenging rate of $0.16 \times Z$ dpm cm^{-2} a^{-1} can be estimated in the water column using a 0.16 value derived from the average ^{210}Pb deficiency (relative to ^{226}Ra), where Z is the water depth in kilometres (Huh et al. 1997). In this scenario, as illustrated in Table 5, the $^{210}Pb_{xs}$ inventory in MC-12 would represent 128% of the total flux (from the atmosphere and the water column), whereas in MC-11, it would represent only 75% of this flux. However, if these values do illustrate some ^{210}Pb missing at the deep site (MC-11) in comparison with the shallower one (MC-12), they must be used carefully. For example, Masque et al. (2007) showed that sea ice intercepts the atmospheric flux of ^{210}Pb and transports at least some of it out of the Arctic. Nonetheless, this imbalance with vertical production rates implies some boundary scavenging responsible for an export of dissolved ^{210}Pb (Huh et al. 1997; Smith et al. 2003).

Thus, despite the bathymetric differences, $^{210}Pb_{xs}$ profiles in MC-11 and MC-12 are nearly similar, which allows us to conclude that the vertical particle fluxes are identical at the two sites and these particles do not scavenge additional ^{210}Pb at least below 1600 m. One possible explanation linked to the scarcity of scavenging particles in such a setting (already evoked by Bacon et al. 1989) would relate to the saturation of these particles in adsorbed heavy metals, like ^{210}Pb and ^{230}Th. Studies on ^{222}Rn escape rates in the northern polar regions highlight the fact that the ^{210}Pb fallout at this high latitude is fairly low. The average estimate of ^{222}Rn escape rate is ~0.3 atom cm^{-2} s^{-1} (Baskaran and Naidu 1995). Using the sediment inventory of $^{210}Pb_{xs}$ and reported flux (flux = $^{210}Pb_{xs}$ inventory / mean life of ^{210}Pb, 31.9 a), a ^{222}Rn escape rate of ~0.22 atom cm^{-2} s^{-1} can be estimated, assuming that the sediment inventory contains all the ^{210}Pb produced in situ by ^{222}Rn. This ^{222}Rn escape rate over the Mendeleev Ridge is similar to that obtained on the continental shelf of the East Chukchi Sea (Baskaran and Naidu 1995).

1.4. Conclusion

Lead-210 distribution in the Arctic sedimentary sequences investigated here show distinct profiles partly independent of the water depth but closely linked to sedimentological settings. For example, cores in ridge environments show a shallow mixing–diffusion depth (~1 cm). Analyses of parent isotopes of ^{210}Pb show that the ^{210}Pb distribution below this layer is controlled by the ^{226}Ra distribution. This isotope shows a steep diffusive gradient towards the water column in the top few centimetres of the sedimentary column, then a distribution governed by that of excesses in the parent ^{230}Th below except for some diffusion from abundance peaks of $^{230}Th_{xs}$. The diffusive flux of ^{226}Ra towards the water column estimated at 0.043 dpm cm^{-2} a^{-1} on the Mendeleev Ridge is consistent with the very low sedimentation rate estimated over the ridge (~3 mm ka^{-1}). In such environments, the patterns of ^{210}Pb distribution indicate that ^{210}Pb can be a proxy for the downcore distribution of parent ^{226}Ra and ^{230}Th except for the slight decoupling of ^{226}Ra and ^{230}Th at the core top and from ^{230}Th peaks, downcore due to ^{226}Ra diffusion. Therefore, ^{210}Pb can have a potential stratigraphic use in correlating cores in such environments where the usual stratigraphic tools have limited resolution or are unavailable. The $^{210}Pb_{xs}$ inventory of the shallower core MC-12 indicates

that the ^{210}Pb present in the sediment probably represents the sum of the atmospheric and water column ^{210}Pb fluxes. However, in the deeper water MC-11 core, an almost similar $^{210}Pb_{xs}$ inventory indicates a deficit of ^{210}Pb in comparison with ^{210}Pb fluxes from the atmosphere and water column, thus there is probably export of part of the ^{210}Pb in the water column through boundary scavenging. However, the scarcity of particles to scavenge particle-reactive nuclides can account for their possible saturation in adsorbed heavy metals. Thus, suspended and particulate water-column measurements are needed to better document such processes.

1.5. Acknowledgements

We wish to acknowledge Captains Dan Oliver and Thomas Arnell, the crews of US Coast Guard Cutters *Healy* and *Oden*, Martin Jakobsson and Anders Karlgvist, respectively, chief scientist and project director onboard the *Oden*, for their support during the 2005 HOTRAX cruise. We are grateful to J.K. Cochran and one anonymous reviewer for helpful suggestions. Thanks are also due to Dr. Sandrine Solignac for onboard sampling, Dr. Guillaume St-Onge for particle size analyses, and Agnieska Adamowicz for carbon analyses. HOTRAX was funded by the US National Science Foundation's Office of Polar Programs (OPP-0352395), the US Coast Guard, the Swedish Polar Research Secretariat, and the Swedish Science Council. The present study is a contribution to the Polar Climate Stability Network program (Canadian Foundation for Climate and Atmospheric Sciences). Support from Natural Sciences and Engineering Research Council of Canada and the Killam Foundation to CHM and Fonds Québecois de la Recherche sur la Nature et les Technologies (GEOTOP grant and a team grant to de Vernal et al.) is also acknowledged.

1.6. References

Aksu, A.E., and Mudie, P.J. 1985. Magnetostratigraphy and palynology demonstrate at least 4 milion years of Arctic Ocean sedimentation. Nature **318**: 280-283.

Backman, J., Jakobsson, M., Lovlie, R., Polyak, L., and Febo, L.A. 2004. Is the central Arctic Ocean a sediment starved basin? Quaternary Science Reviews **23**(11-13): 1435-1454.

Bacon, M.P., Huh, C.A., and Moore, C.M. 1989. Vertical profiles of some natural radionucleides over the Alpha Ridge, Arctic Ocean. Earth and Planetary Science Letters **95**: 15-22.

Baskaran, M. 2005. Interaction of sea ice sediments and surface sea water in the Arctic Ocean: Evidence from excess ^{210}Pb. Geophysical Research Letters **32**(12): 1-4.

Baskaran, M., Asbill, S., Santschi, P., Brooks, J., Champ, M., Adkinson, D., Colmer, M.R., and Makeyev, V. 1996. Pu, 137Cs and excess 210Pb in Russian Arctic sediments. Earth and Planetary Science Letters **140**(1-4): 243-257.

Baskaran, M., Asbill, S., Schwantes, J., Santschi, P., Champ, M.A., Brooks, J.M., Adkinson, D., and Makeyev, V. 2000. Concentrations of 137Cs, 239,240Pu and 210Pb in sediment samples from the Pechora Sea and biological samples from the Ob, Yenisey Rivers and Kara Sea. Marine Pollution Bulletin **40**(10): 830-838.

Baskaran, M., and Naidu, A.S. 1995. 210Pb-derived chronology and the fluxes of 210Pb and 137Cs isotopes into continental shelf sediments, east Chukchi Sea, Alaskan Arctic. Geochimica et Cosmochimica Acta **59**(21): 4435-4448.

Baskaran, M., and Shaw, G.E. 2001. Residence time of arctic haze aerosols using the concentrations and activity ratios of Po-210, Pb-210 and Be-7. J Aerosol Sci **32**(4): 443-452.

Berner, R.A. 1980. Early diagenesis - A theoretical approach. Princeton, Princeton, N. J.
Blott, S.J., and Pye, K. 2001. Gradistat: A grain size distribution and statistics package fro the analysis of unconsolidated sediments. Earth Surface Processes and landforms **26**: 1237-1248.

Clough, L.M., Ambrose Jr, W.G., Cochran, J.K., Barnes, C., Renaud, P.E., and Aller, R.C. 1997. Infaunal density, biomass and bioturbation in the sediments of the Arctic Ocean. Deep-Sea Research Part II: Topical Studies in Oceanography **44**(8): 1683-1704.

Cochran, J.K. 1980. The flux of 226Ra from deep-sea sediments. Earth and Planetary Science Letters **49**(2): 381-392.

Cochran, J.K. 1992. The oceanic chemistry of the uranium and thorium series nuclides. *In* Uranium-series disequilibrium : applications to earth, marine, and environmental science.

Edited by M. Ivanovich and R.S. Harmon. Clarendon Press ; Oxford University Press, Oxford New York. pp. 335-395.

Cochran, J.K., and Krishnaswami, S. 1980. Radium, thorium, uranium, and Pb210 in deep-sea sediments and sediment pore waters from the North Equatorial Pacific. American Journal of Science **280**(9): 849-889.

Cochran, J.K., McKibbin-Vaughan, T., Dornblaser, M.M., Hirschberg, D., Livingston, H.D., and Buesseler, K.O. 1990. 210Pb scavenging in the North Atlantic and North Pacific Oceans. Earth & Planetary Science Letters **97**(3-4): 332-352.

Cook, H.E., Johnson, P.D., Matti, J.C., and Zemmels, I. 1975. Methods of sample preparation and X-ray diffraction data analysis, University of California, Riverside, Washington.

Darby, D.A., Bischof, J.F., and Jones, G.A. 1997. Radiocarbon chronology of depositional regimes in the western Arctic Ocean. Deep-Sea Res Pt Ii **44**(8): 1745-1757.

Darby, D., Polyak, L., Jakobsson, M., Berger, G., Lovlie, R., Perovich, D., Grenfell, T., Kikuchi, T., and Tateyama, K. 2005a. HLY0503 Cruise Report.

Darby, D.A., Jakobsson, M., and Polyak, L. 2005b. Ice breaker Expedition collects key Arctic Seafloor and Ice data. EOS **86**(52): 549-552.

Darby, D., Polyak, L., and Bauch, H.A. 2006. Past glacial and interglacial conditions in the Arctic Ocean and marginal seas-a review. Progress in Oceanography **71**: 129-144.

Dyke, A.S., McNeely, R.N., and Hooper, J. 1996. Marine reservoir corrections for bowhead whale radiocarbon age determinations. Canadian Journal of Earth Sciences **33**(12): 1628-1637.

Flynn, W.W. 1968. The determination of low levels of polonium-210 in environmental materials. Analytica Chimica Acta **43**(2): 221-226.

Ghaleb, B., Pons-Branchu, E., and Deschamps, P. 2004. Improved method for radium extraction from environmental samples and its analysis by thermal ionization mass spectrometry. J Anal Atom Spectrom **19**(7): 906-910.

Hancock, G.J., Webster, I.T., Ford, P.W., and Moore, W.S. 2000. Using Ra isotopes to examine transport processes controlling benthic fluxes into a shallow estuarine lagoon. Geochimica Et Cosmochimica Acta **64**(21): 3685-3699.

Hermanson, M.H. 1990. 210Pb and 137Cs chronology of sediments from small, shallow Arctic lakes. Geochimica et Cosmochimica Acta **54**(5): 1443-1451.

Huh, C.A., Pisias, N.G., Kelley, J.M., Maiti, T.C., and Grantz, A. 1997. Natural radionuclides and plutonium in sediments from the western Arctic Ocean: sedimentation rates and pathways of radionuclides. Deep-Sea Research Part I-Topical Studies in Oceanography **44**(8): 1725-1743.

Imboden, D.M., and Stiller, M. 1982. The influence of radon diffusion on the 210Pb distribution in sediments. Journal of Geophysical Research **87**(C1): 557-565.

Jakobsson, M., Lovlie, R., Al-Hanbali, H., Arnold, E., Backman, J., and Morth, M. 2000. Manganese and color cycles in Arctic Ocean sediments constrain Pleistocene chronology. Geology **28**(1): 23-26.

Jakobsson, M., Lovlie, R., Arnold, E.M., Backman, J., Polyak, L., Knutsen, J.O., and Musatov, E. 2001. Pleistocene stratigraphy and paleoenvironmental variation from Lomonosov Ridge sediments, central Arctic Ocean. Global and Planetary Change **31**(1-4): 1-22.

Jones, G.A. 1987. The central Arctic Ocean sediment record: Current progress in moving from a litho- to a chronostratigraphy. Polar Research **5**(3): 309-311.

Key, R.M., Guinasso, N.L., and Schink, D.R. 1979. Emanation of radon-222 from marine sediments. Marine Chemistry **7**(3): 221-250.

Ku, T.-L., and Broecker, W.S. 1965. Rates of sedimentation in the Arctic ocean. Progress In Oceanography **4**: 95-104.

Lally, A.E. 1982. Chemical procedures. *In* Uranium Series Disequilibrium: Application to Environmental Problems. *Edited by* M. Ivanovich and R.S. Harmon. Clarendon Press-Oxford, New York. p. 571.

Masque, P., Cochran, J.K., Hirschberg, D.J., Dethleff, D., Hebbeln, D., Winkler, A., and Pfirman, S. 2007. Radionuclides in Arctic sea ice: Tracers of sources, fates and ice transit time scales. Deep Sea Research Part I: Oceanographic Research Papers **54**(8): 1289-1310.

Moore, C.M., and Smith, J.N. 1986. Disequilibria between 226Ra, 210Pb and 210Po in the Arctic Ocean and the implications for chemical modification of the Pacific water inflow. Earth and Planetary Science Letters **77**: 285-292.

Moore, D.M., and Reynolds, R.C. 1989. X-ray Diffraction and the indentification and analysis of clay minerals, Oxford.

Moore, W.S. 1999. The subterranean estuary: a reaction zone of ground water and sea water. Marine Chemistry **65**(1-2): 111-125.

Moore, W.S., and Dymond, J. 1991. Fluxes of Ra-226 and Barium in the Pacific-Ocean - the Importance of Boundary Processes. Earth and Planetary Science Letters **107**(1): 55-68.

Moran, K., Backman, J., Brinkhuis, H., Clemens, S.C., Cronin, T., Dickens, G.R., Eynaud, F., Gattacceca, J., Jakobsson, M., Jordan, R.W., Kaminski, M., King, J., Koc, N., Krylov, A., Martinez, N., Matthiessen, J., McInroy, D., Moore, T.C., Onodera, J., O'Regan, M., Palike, H., Rea, B., Rio, D., Sakamoto, T., Smith, D.C., Stein, R., St John, K., Suto, I., Suzuki, N., Takahashi, K., Watanabe, M., Yamamoto, M., Farrell, J., Frank, M., Kubik, P., Jokat, W., and Kristoffersen, Y. 2006. The Cenozoic palaeoenvironment of the Arctic Ocean. Nature **441** (7093): 601-605.

Polyak, L., Curry, W.B., Darby, D.A., Bischof, J., and Cronin, T.M. 2004. Contrasting glacial/ interglacial regimes in the western Arctic Ocean as exemplified by a sedimentary record from the Mendeleev Ridge. Palaeogeogr Palaeocl **203**(1-2): 73-93.

Polyak, L., Darby, D., Bischof, J., and Jakobsson, M. 2007. Stratigraphic constraints on late Pleistocene glacial erosion and deglaciation of the Chukchi margin, Arctic Ocean. Quaternary Research **67**: 234-245.

Poore, R.Z., Ishman, S.E., Phillips, R.L., and McNeil, D.H. 1994. Quaternary stratigraphy and paleoceanography of the Canada Basin, western Arctic Ocean. US Geological Survey Bulletin **2080**.

Sellen, E., Jakobsson, M., and Backman, J. 2008. Sedimentary regimes in Arctic's Amerasian and Eurasian Basins: Clues to differences in sedimentation rates. Global and Planetary Change **61**(3-4): 275-284.

Smith, J.N., and Ellis, K.M. 1995. Radionuclide tracer profiles at the CESAR ice station and Canadian Ice Island in the western Arctic Ocean. Deep-Sea Research, Part II **42**(6): 1449-1470.

Smith, J.N., Ellis, K.M., Naes, K., Dahle, S., and Matishov, D. 1995. Sedimentation and mixing rates of radionuclides in Barents Sea sediments off Novaya Zemlya. Deep-Sea Research, Part II **42**(6): 1471-1493.

Smith, J.N., Moran, S.B., and Macdonald, R.W. 2003. Shelf-basin interactions in the Arctic Ocean based on Pb-210 and Ra isotope tracer distributions. Deep-Sea Res Pt I **50**(3): 397-416.

Stein, R. 2007. Upper Cretaceous/lower Tertiary black shales near the North Pole: Organic-carbon origin and source-rock potential. Marine and Petroleum Geology **24**(2): 67-73.

Turekian, K.K., Nozaki, Y., and Benninger, L.K. 1977. Geochemistry of atmospheric radon and radon products. Earth & Planetary Science Letters **5**: 227-255.

Weiss, H., V., and Naidu, A.S. 1986. ^{210}Pb flux in an Arctic Coastal Region. Arctic **39**(1): 59-64.

Station	Water depth (m)	Latitude N	Longitude	Location
HLY0501-04	462	72°41.56' N	157°27.13'	Upper mid-slope
HLY0503-08	2791	79°35.653' N	172°27.535' W	Ridge
HLY0503-11	2570	83°07.730' N	174°41.570' W	Ridge
HLY0503-12	1586	83°17.797' N	171°54.994' W	Ridge
HLY0503-14	1874	84°18.482' N	149°05.902' W	Ridge
HLY0503-18	2654	88°26.228' N	146°40.989' E	Ridge
HLY0503-NP	4224	89°59.333' N	158°01.305' E	Basin
HLY0503-21	2015	86°39.595' N	056°56.207' E	Ridge
HLY0503-22	783	80°28.704' N	007°43.880' E	Plateau

Table 1: Locations and water depth of multicores retrieved during the HOTRAX expedition analyzed in this study.

Depth in core (cm)	Ages (Libby's years)
0.25	8525 ± 35
4.25	32630 ± 510
8.25	27010 ± 250
12.25	33550 ± 540

Table 2: AMS ^{14}C ages in HLY0503-11MC. Ages were performed on *Neogloboquadrina pachyderma*. Ages are expressed in Libby's years.

Core	Water depth (m)	Inventory in sediments (dpm cm^{-2})	Flux* to sediments (dpm cm^{-2} y^{-1})	Scavenging rate in water column (dpm y^{-1})	Atmospheric flux (dpm cm^{-2} y^{-1})	Fraction** of total flux accountable in sediments
HLY0503-11MC	2570	12	0.36	0.41	0.08	0.73
HLY0503-12MC	1586	14	0.43	0.25	0.08	1.28

* Flux to sediments = inventory in sediment/mean-life of ^{210}Pb.
** Calculated by dividing flux to sediments by the sum of atmospheric flux and water column scavenging flux.

Table 3: ^{210}Pb budget, inventories and fluxes

Depth (cm)	^{137}Cs (dpm/g)	± 1σ	^{210}Pb (dpm/g)	± 1σ	^{226}Ra (dpm/g)	± 2σ	^{230}Th (dpm/g)	± 1σ	^{232}Th (dpm/g)	± 1σ
0.25	0.15	0.04	22.42	0.58	4.91	0.02	25.37	0.23	2.00	0.07
0.75	0.00		9.96	0.28						
1.25	0.00		8.68	0.28	7.39	0.10	20.94	0.07	1.75	0.02
1.75			8.24	0.27						
2.25			9.66	0.31	8.58	0.11	29.42	0.09	2.39	0.03
2.75			9.46	0.30						
3.25			9.71	0.18	9.24	0.47	37.54	0.33	3.29	0.10
3.75			10.36	0.19						
4.25			11.94	0.24	9.66	0.11	13.05	0.05	1.18	0.01
4.75			11.40	0.20						
5.25			11.17	0.18	10.35	0.11	19.30	0.08	2.03	0.03
5.75			12.52	0.24						
6.25			13.95	0.42	16.97	0.14	17.15	0.19	2.62	0.07
6.75			14.61	0.48						
7.25			14.03	0.45	13.82	0.12	9.29	0.05	1.63	0.02
7.75			12.04	0.44						
8.25			10.53	0.35			4.95	0.04	1.59	0.02
8.75			7.72	0.24						
9.25			5.99	0.20			2.90	0.08	2.27	0.07
9.75			5.25	0.18						
10.25			4.49	0.20			2.70	0.03	1.95	0.03
10.75			4.09	0.16						
11.25			3.93	0.16			3.14	0.03	1.69	0.02
11.75			3.78	0.17						
12.25			4.06	0.12			3.37	0.06	2.22	0.05
12.75			4.12	0.15			1.99	0.05	1.84	0.05
13.25			4.00	0.16			2.34	0.05	2.05	0.04
14.25			3.11	0.12			2.28	0.05	2.21	0.05
15.25			3.17	0.12			6.95	0.12	2.47	0.07
16.25			4.73	0.19			8.28	0.08	2.47	0.04
17.25			5.62	0.15			5.11	0.10	2.64	0.07
18.25			3.42	0.11			1.67	0.04	1.90	0.05
19.25			2.73	0.09			1.89	0.05	2.25	0.05
20.25			2.28	0.07			1.45	0.03	1.94	0.03
21.25			2.13	0.69			1.03	0.04	1.66	0.05
22.25			1.90	0.08			1.35	0.04	2.21	0.05
23.25			1.68	0.07			1.18	0.04	1.79	0.05
24.25			1.89	0.07			1.28	0.04	1.99	0.05
25.25			1.93	0.07			5.10	0.09	2.55	0.07
26.25			3.44	0.11			5.41	0.07	2.21	0.04

27.25	5.07	0.15	5.22	0.09	2.33	0.06
28.25	5.29	0.18	5.94	0.10	3.22	0.07
29.25	5.52	0.15	4.47	0.07	2.24	0.05
30.25	5.87	0.16	3.96	0.04	2.17	0.03
31.25	5.82	0.17	2.84	0.03	2.21	0.03
32.25	4.86	0.13	2.55	0.04	2.09	0.03
33.25	4.97	0.12	2.64	0.07	2.29	0.07
34.25						
35.25	3.90	0.11				
36.25	3.06	0.10				
37.25	2.68	0.11				
38.25	1.79	0.07				

Table 4: Activities of ^{210}Pb, ^{137}Cs, ^{226}Ra, ^{230}Th and ^{232}Th in sediments of the core HLY0503-11MC.

Depth (cm)	HLY05 01-04	± 1σ	HLY05 03-08	± 1σ	HLY05 03-12	± 1σ	HLY05 03-14	± 1σ	HLY05 03-18	± 1σ	HLY05 03-NP	± 1σ	HLY050 3-21	± 1σ	HLY05 03-22	± 1σ
0.25	18.37	0.58	65.77	1.37	26.69	0.72	9.02	0.27	72.63	1.43	43.62	0.82	14.47	0.30	42.89	0.89
0.75	18.33	0.43	24.69	0.52	9.46	0.27	9.74	0.30	25.86	0.52	50.57	0.82	6.66	0.16	35.81	0.66
1.25	18.92	0.68	11.30	0.30	8.02	0.25	7.66	0.28	9.04	0.25	12.92	0.32	2.38	0.08	28.90	0.63
1.75	18.55	0.52	11.78	0.28	9.08	0.30	8.48	0.25	7.35	0.19	6.26	0.14	3.07	0.08	26.91	0.46
2.25	18.59	0.67	12.66	0.30	9.57	0.31	9.28	0.29	6.85	0.19	6.97	0.18	2.13	0.07	23.02	0.37
2.75	19.50	0.58	13.99	0.33	9.96	0.33	9.36	0.24	7.45	0.22	7.98	0.20	2.32	0.09	20.76	0.45
3.25			13.09	0.32	9.42	0.29	9.93	0.30	6.46	0.28	8.42	0.19	2.30	0.07	14.63	0.29
3.75	18.23	0.42	13.99	0.32	10.32	0.31	10.22	0.28	7.70	0.31	8.79	0.19	2.52	0.08	7.70	0.17
4.25	18.53	0.48	12.89	0.33	12.87	0.59	13.37	0.39	7.69	0.19	9.45	0.19	2.39	0.08	10.46	0.24
4.75	17.06	0.43	12.52	0.30	11.18	0.30	12.45	0.38	8.03	0.29	8.90	0.19	2.39	0.07	6.61	0.15
5.25	15.20	0.44	10.05	0.22	12.33	0.31	12.33	0.37	8.17	0.31	9.44	0.20	2.40	0.07	6.89	0.16
5.75	14.94	0.34	9.51	0.25	12.95	0.38	11.18	0.38	8.38	0.34	9.96	0.21	2.51	0.08	5.19	0.12
6.25	13.40	0.31	13.95	0.42	13.68	0.46	10.09	0.19	9.83	0.34	10.02	0.24			4.85	0.12
6.75	11.75	0.28	6.87	0.23	12.89	0.40	9.31	0.16	10.82	0.42	10.03	0.27			5.00	0.14
7.25	11.65	0.29	8.84	0.34	12.86	0.39	11.06	0.28	10.34	0.43	10.41	0.32			4.99	0.16
7.75	10.06	0.27	7.37	0.26	12.20	0.38	7.74	0.19	10.51	0.40	11.71	0.40			5.90	0.18
8.25	9.11	0.24	4.73	0.18	9.84	0.31	5.31	0.13	10.33	0.39	11.64	0.41			6.76	0.17
8.75			6.86	0.33	7.68	0.27	4.05	0.11	11.11	0.35	11.92	0.39			7.46	0.22
9.25	8.09	0.16	7.18	0.29	5.56	0.17	2.88	0.10	11.57	0.35	11.92	0.39			9.66	0.28
9.75	8.08	0.17	6.40	0.23	4.11	0.15	2.60	0.07	12.33	0.40	12.47	0.38			11.23	0.27
10.25	7.81	0.17	7.24	0.27	3.12	0.12	2.36	0.06	11.61	0.41	12.36	0.37			11.68	0.27
10.75	5.58	0.16	7.27	0.26	2.89	0.11	2.05	0.06	12.43	0.45	12.15	0.40			10.56	0.27
11.25	7.26	0.19	6.73	0.24	2.49	0.10	2.02	0.06	12.73	0.42	11.91	0.43			8.34	0.22
11.75	9.64	0.21	8.08	0.32	2.41	0.09			6.50	0.21	11.68	0.41			7.03	0.26

Table 5: Activities of ^{210}Pb in sediments of the Arctic Ocean.

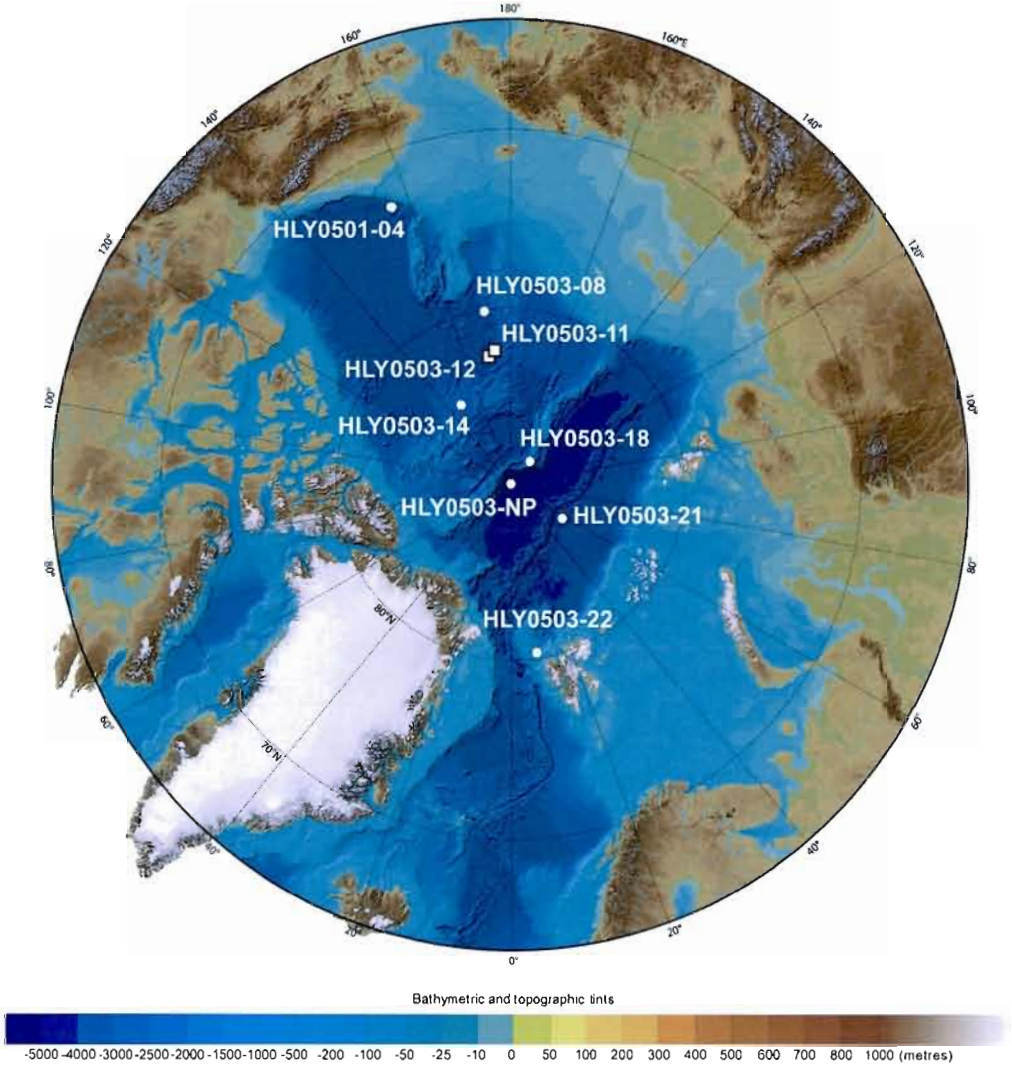

Figure 1. Locations of multicores from the HOTRAX 2005 expedition. Bathymetry from International Bathymetric Chart of the Arctic Ocean (IBCAO; Jakobsson et al 2008). Circles indicate lead analyses and squares indicate lead, radium and thorium analyses.

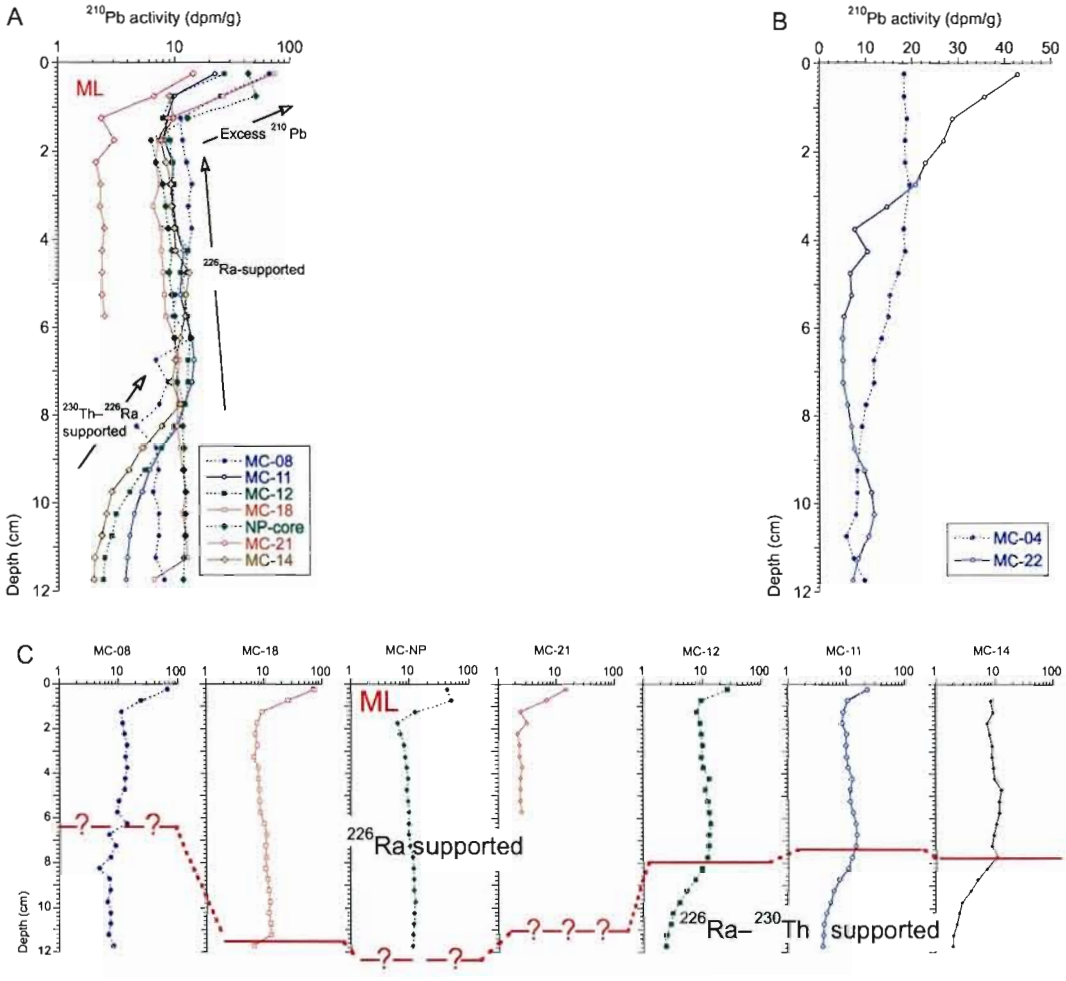

Figure 2. ^{210}Pb activities in multicores: (A) and (B) represent the two distribution patterns observed; (C) illustrates the profiles from all cores following the (A) pattern.

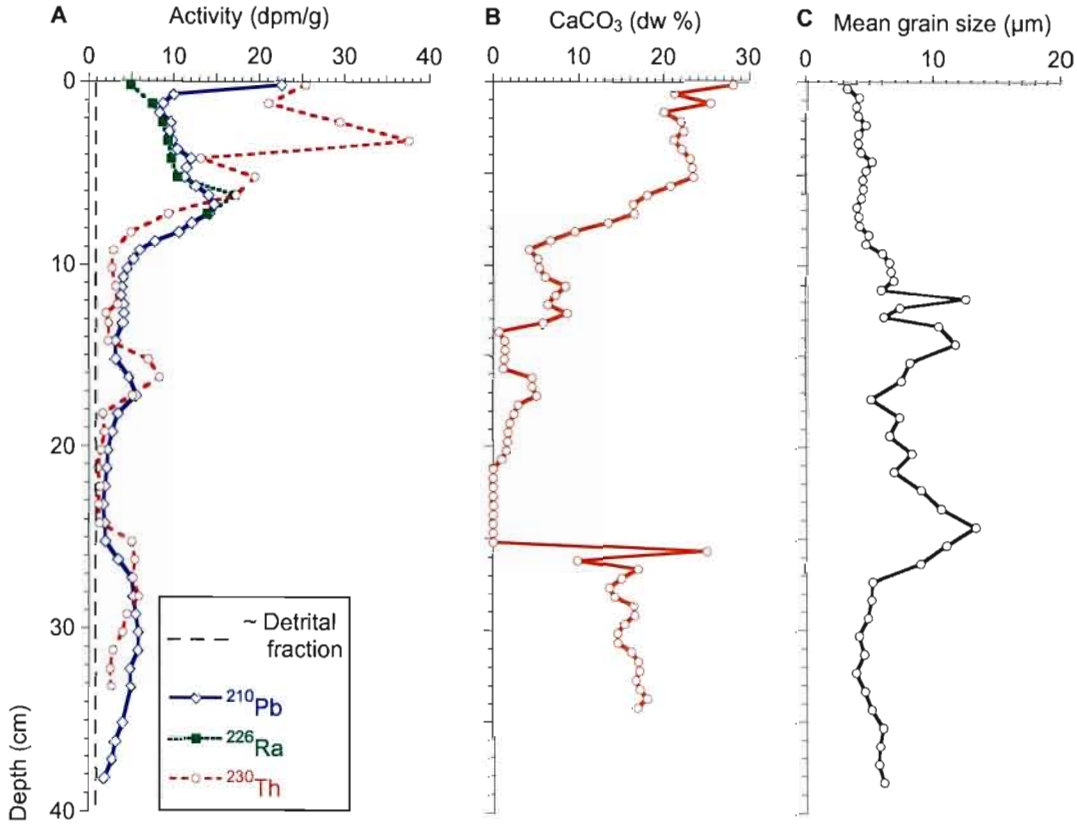

Figure 3. (A) ^{210}Pb, ^{226}Ra, and ^{230}Th measurements in MC-11; (B-C) inorganic carbon content and mean particle size of bulk sediment sample, respectively.

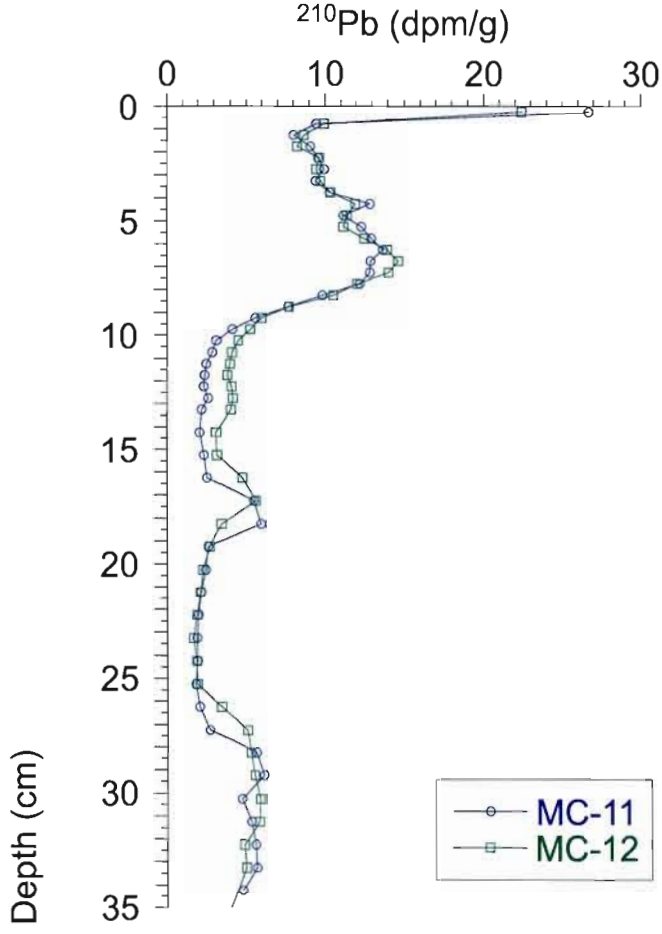

Figure 4. ^{210}Pb profiles in MC-11 and MC-12 raised from distinct water depths (~ 2.6 and ~1.6 km, respectively).

CHAPITRE 2

TIMES CONSTRAINTS FROM ^{230}Th AND ^{231}Pa DATA IN LATE QUATERNARY, LOW SEDIMENTATION RATE SEQUENCES FROM THE ARCTIC OCEAN: AN EXAMPLE FROM THE NORTHERN MENDELEEV RIDGE

Christelle Not[1], Claude Hillaire-Marcel[1]

[1]GEOTOP, Université du Québec à Montréal, C. P. 8888, Montréal, QC, H3C 3P8, Canada

Article publié en 2010 dans Quaternary Science Reviews, 29: 3665-3675, doi:10.1016/ j.quascirev.2010.06.042

Résumé

En l'absence de stratigraphie basée sur les isotopes de l'oxygène, l'élaboration d'une chronostratigraphie couvrant la période du Quaternaire pour des environnements à faible taux de sédimentation de l'océan Arctique est souvent délicate. Dans cette étude, nous utilisons des enregistrements sédimentaires provenant de la ride Mendeleev, à une profondeur d'environ 1600 m (multicore HLY0503-12) et 2500 m (multicore and trigger HLY0503-11), pour analyse des actinides à des fins chronostratigraphiques. Des analyses granulométrique, minéralogique, géochimique (C_{org}, C_{inorg}) et isotopique (^{210}Pb, ^{238}U, ^{234}U, ^{232}Th, ^{230}Th, ^{231}Pa) ont été faites sur du sédiment total et broyé, alors que les analyses isotopique suivante, ^{14}C, $\delta^{13}C$ et $\delta^{18}O$ ont été faites sur les foraminifères planctoniques lorsqu'ils étaient présents. Les deux multicores ont des profils très similaires malgré leur différence de bathymétrie. Ils sont caractérisés par trois unités principales. L'unité supérieure (0-8 cm) et l'unité inférieure (26-38 cm) sont caractérisées par un contenu elevé en argile et en carbonate, alors que l'unité intermédiaire (8-26 cm) est caractérisée par une haute concentration en sable et une faible concentration en argile et carbone inorganique. Un événement ponctuel, caractérisé par un pic d'argile et de carbone inorganique est enregistré à ~17 cm. Des excès de ^{230}Th et ^{231}Pa sont observés jusqu'à 35 et 27 cm, respectivement, impliquant des âges de ~340 ka et ~140 ka à ces profondeurs. Le modèle d'âge obtenu, à partir des actinides, permet d'attribuer l'intervalle du stade isotopique 1-3 à l'unité supérieure, et la transition des stades 8 à 7 à l'unité inférieure. L'unité intermédiaire correspondrait donc aux deux derniers cycles glaciaires, interrompu par un événement rapide correspondant possiblement à la transition du stade 6 à 5. Les données de la carotte par gravité permettent d'étendre la stratigraphie jusqu'au stade 13. Cette étude suggère un taux de sédimentation moyen de 1,5 $mm.ka^{-1}$ dans le secteur de la ride Mendeleev, ce qui est compatible avec les taux de sédimentation estimés à partir des données de ^{10}Be dans des sites proche de cette étude.

Abstract

Due to the lack of 'conventional' oxygen isotope stratigraphies, the setting of unquestionable time frames in Late Quaternary records from low sedimentation rate settings of the Arctic Ocean often encounters difficulties. Here we use HOTRAX cores raised from the Mendeleev Ridge (multicore HLY0503-12, ~1600 m water depth; multicore and trigger weight core HLY0503-11, ~2500 m warer depth) to demonstrate that U-series data may supply reliable time constraints and sedimentation rate estimates. Grain size, mineralogical, geochemical (C_{org}, C_{inorg}) and isotopic (^{210}Pb, ^{238}U, ^{234}U, ^{232}Th, ^{230}Th, ^{231}Pa) measurements were made on ground bulk sediment, whereas isotopic (^{13}C, ^{14}C, ^{18}O) measurements were performed on planktonic foraminifers when present. The two multicores present remarkably similar profiles despite their >1 km-bathymetric difference. Both show three majors units. The top (0-8 cm) and bottom (26-38 cm) units have high clay and carbonate contents, whereas the intermediate unit (8-26 cm) shows high sand and low clay and inorganic carbon contents. An apparently short event with higher clay and inorganic content is recorded at ~17 cm. ^{230}Th-excess and ^{231}Pa-excess are observed down to 35 and 27 cm, respectively, thus locking minimum ages of ~ 340 ka and ~140 ka at these depths. Age-model estimates allowed us to assign the top unit to the Marine Isotopic Stages (MIS) 1-3 interval, and the bottom unit to the Termination III-MIS 7 interval. The intermediate unit would represent the last two glacial cycles, interrupted by a short Termination II-MIS 5e "excursion". Data from the TWC allow this stratigraphy to be extended to MIS 13. Glacial units correspond to very low sedimentation rates essentially linked to ice rafting deposition, as indicated by their high sand content. This study suggests a mean sedimentation rate of about 1.5 $mm.ka^{-1}$ for this sector of the Mendeleev Ridge, which supports the very low sedimentation rate suggested by ^{10}Be data in a nearby site from other studies.

2.1. Introduction

Setting stratigraphies in Arctic Ocean deep-sea sediment sequences is often difficult (Backman et al., 2004; Sellén et al., 2009). Low productivity, low species diversity and poor preservation of microfossils seriously limit the establishment of conventional eco/climatic- or bio-stratigraphies, as well as the setting of stable isotope stratigraphies from foraminifer assemblages. When present, such microfossils can only be ^{14}C-dated up to 30-40 ka. For these reasons, attempts at using other geochemical approaches have been made. For example, in cores from the northern Mendeleev Ridge recovered during the HOTRAX cruise (Fig. 1), Kaufman et al., (2008) and Polyak et al., (2009) estimated average sedimentation rates varying from 5 $mm.ka^{-1}$ to 15 $mm.ka^{-1}$ based on amino-acid racemization rates, whereas Sellén et al., (2009) proposed a lower ~2.7 $mm.ka^{-1}$ rate, from ^{10}Be analyses.

Here, we use ^{230}Th and ^{231}Pa to put some temporal constraints on the late Quaternary sections of such low sedimentation rate sites. Both ^{230}Th (half-life ($t_{1/2}$) = 75,690 years) and ^{231}Pa (half-life ($t_{1/2}$) = 32,760 years) are particle-reactive radionuclides produced uniformly in the ocean by alpha decay of soluble ^{234}U and ^{235}U, respectively. The rapid removal of ^{230}Th and ^{231}Pa isotopes from seawater is reflected by their very low seawater activities compared with parent uranium isotopes (Moore and Sackett, 1964). These particle-reactive radionuclides are primarily removed locally through scavenging by suspended particulate matter, rather than transported through advection. The excess of ^{230}Th ($^{230}Th_{xs}$) in sediments corresponds to the fraction of ^{230}Th unsupported by uranium decay in crystal lattices or authigenic grain coating of sediments. This fraction is assumed to mostly derive from its production in the water column. Hence, concentrations of $^{230}Th_{xs}$ and $^{231}Pa_{xs}$ in the sediment depend on particle scavenging, which, in turn, depends on the depth of the water column, the sedimentation rate and the age of the sediment. Excess in ^{230}Th can provide rough estimates of deep-sea core chronology. For example, when some $^{230}Th_{xs}$ is measurable in a sample, the sample age must be less than five or six half-lives of ^{230}Th, which are roughly 375-450 ka, within statistical constraints of the measurement precision. Therefore, the downcore distribution of $^{230}Th_{xs}$ and $^{231}Pa_{xs}$ could provide some temporal benchmarks. Most previous studies have concluded to a significant deficit in the Arctic sedimentary accumulation of ^{230}Th relative to its production in the water column (Edmonds et al., 2004; Huh et al., 1997; Moran et al., 2005; Scholten et al.,

1995). However, in a recent study of a Western Arctic area, a balanced budget has been observed in last-deglacial to Holocene sediments (Hoffmann and McManus, 2007). Under such conditions, $^{230}Th_{xs}$ should reveal a powerful tool to document sedimentation rates and sedimentary events, such as turbidites or hiatuses, both of which can influence the stratigraphy of Arctic cores (Grantz et al., 1996 and Poore et al., 1999).

In this study, we present high resolution measurements of ^{230}Th and ^{231}Pa in two cores from the Mendeleev Ridge. The cores were acquired during the Healy-Oden Trans Arctic Expedition (HOTRAX) in summer 2005 (Darby et al., 2005). The aim of this study is to investigate the behavior of ^{230}Th and ^{231}Pa in relation with sedimentological changes downcore, and to assess their suitability to set time constraints in such records.

2.2. Materials and methods

During the HOTRAX 2005 expedition, sediment cores were collected from the northern part of the Mendeleev Ridge in different bathymetric settings (Fig. 1). In this study, we present results for two multicores (HLY0503-11MC8; henceforth 11-MC, 83°07.730'N, 174°41.570'W, 2570 m water depth, and HLY0503-12MC8; henceforth 12-MC, 83°17.797'N, 171°54.994'W, 1586 m water depth) and the upper part (down to 60 cm) of a trigger weight core from HLY0503-11MC8 (henceforth 11-TWC, 83°08.615'N, 174°32.231'W, 2644 m water depth). The multicores are characterized by alternating brown/ dark-brown and yellowish-brown sediment layers. These sediment cycles have been interpreted to reflect interglacial and glacial variability and have been observed throughout the Arctic Ocean (Jakobsson et al., 2000; O'Regan et al., 2008; Phillips and Grantz, 1997; Polyak et al., 2004; Stein, 2008a). The upper part of trigger weight core 11-TWC is composed of an alternation of brown to yellowish layers with pinkish clasts at 27 cm.

Measurements of thorium, uranium, protactinium and lead (^{210}Pb) isotopes, of some geochemical properties (i.e. total carbon, organic carbon, inorganic carbon and total nitrogen), as well as grain size and mineralogical composition were made every 1 cm. All geochemical analyses were performed on dried, ground and well-mixed sediment.

Analytical procedures for uranium (U) and thorium (Th) separation were as follows. The sediment was treated by HCl-HNO_3-HF acid attack, and spiked using a ^{233}U-^{236}U-^{229}Th

solution before the U and Th separation followed using anion exchange column (Dowex AG 1x8 resin) with a modified two stage extraction with 6N HCl for U and 7N HNO_3 for Th (Edwards et al., 1987). Purification of the Th fraction was done with an anion exchange column (Dowex AG 1x8 resin) and U purification using UTEVA® resin. Measurements were made using a Micromass IsoProbe ™ MC-ICP-MS at the GEOTOP Research Center. Uranium measurements were made using the procedure for data acquisition, tailing correction and mass discrimination correction described in Deschamps et al. (2003). The overall uranium analytical reproducibility, as estimated from replicate analyses of one selected sample, is 4% for ^{234}U and 6% for ^{238}U ($\pm 2\sigma$). Thorium measurements were made in two sequences on a Daly detector, one for mass 229 and another one for mass 230. In this sequence the mass 229 is measured in axial, the mass 232 in collector H1 and masses 235 and 238 in collectors H2 and H3 respectively. U-500 standard was used for mass fractionation correction assuming U and Th have the same ionization efficiency. Validation of the Th measurements by ICP-MS was obtained from the comparison of alpha and ICP-MS data (see supplementary material). The thorium analytical reproducibility, as estimated from replicate analyses of one selected sample, is 4% for ^{230}Th and 6% for ^{232}Th ($\pm 2\sigma$).

The ^{231}Pa concentration in sediment was measured by isotopic dilution (^{233}Pa spike) at the Pacific Centre for Isotopic and Geochemical Research (University of British Columbia). Following acid digestion, ^{231}Pa was extracted from the sediment samples by anion exchange chromatography following Choi et al. (2001), and samples were measured by single collector sector-field inductively coupled plasma mass spectrometer (SF-ICP-MS, Finnigan Element 2) (Choi et al., 2001; Pichat et al., 2004). The instrumental mass fractionation was evaluated by measurement of U-500 standard. The signal was corrected for the contribution of the instrumental background, dark noise, blanks linked to the chemical procedure and blanks linked to spike addition. The mean analytical error associated with ^{231}Pa measurements is <5% ($\pm 2\sigma$); however, it varied from 1 to 15 % depending on the concentration of ^{231}Pa, the chemical yield and the counting efficiency. Calculations of excesses in ^{230}Th and ^{231}Pa, i.e., of fractions scavenged in the water column during particle sedimentation, were made by subtracting respectively ^{234}U and ^{235}U (calculated using a $^{238}U/^{235}U$ activity ratio of 0.046) activities in order to estimate those of ^{230}Th and ^{231}Pa fractions supported by parent isotopes

(i.e., respectively ^{234}U and ^{235}U) linked to detrital particle lattice, thus of "detrital" origin (see supplementary material).

Lead-210 ($t_{1/2}$ = 22.6 a) activities were measured by alpha counting of the activity of ^{210}Pb-daughter isotope, ^{210}Po ($t_{1/2}$ = 138.4 days: α = 5.30 MeV). Measurements were performed approximately 200 days following sampling. A few replicate measurements were carried out approximately a year later in order to verify if the equilibrium between the two isotopes prevailed in the study samples. All replicate data were identical to the first set of measurements within counting errors. Chemical extraction and counting efficiencies were determined using a ^{209}Po spike. Chemical procedures for ^{210}Po extraction followed Baskaran and Naidu (1995) (i.e., with a classical HCl/HNO_3/HF treatment), and samples were deposited on a silver disk (Flynn, 1968). The ^{209}Po and ^{210}Po activities were measured in a silicon surface barrier α-spectrometer (EGG and ORTEC type 576A). Uncertainties were estimated as ±1 standard deviation for counting statistics (approx. 2 to 4% of the value obtained).

Total carbon content was measured using a Carlo Erba™ elemental analyzer. The error, based on standard deviation of results of replicate analyses for one sample, is estimated at ± 0.05%. The percent inorganic carbon (C_{inorg}) was calculated by substracting the organic C from the total C, following usual weight normalization. The carbon isotopic composition of organic matter ($\delta^{13}C$) was measured by continuous-flow mass spectrometry using a Carlo Erba elemental analyzer connected to an Isoprime™ mass spectrometer. Results are presented in the standard δ notation versus VPDB. A precision of ± 0.1‰ (±1σ) is estimated based on replicate analyses of standard samples.

The foraminifer samples used for isotopic investigation consist of sieved then hand-picked ~ 80 µg sub-assemblages of *Neogloboquadrina pachyderma* (left coiled), i.e., about 10 to 12 shells. Samples were analyzed with a Micromass Isoprime™ isotope ratio mass spectrometer in dual inlet mode coupled to a MultiCarb™ preparation system. CO_2 was extracted at 90°C by acidification with 100% concentration H_3PO_4. Measurements were made with internal reference carbonate material calibrated against the VPDB scale. The analytical reproducibility determined by replicate measurements of the internal standard carbonate

material (UQ6a; $\delta^{13}C$= 2.25 ‰; $\delta^{18}O$= -1.4 ‰) was routinely better than 0.05 % for both $\delta^{13}C$ and $\delta^{18}O$.

Particle-size analyses were performed as follows: Na-hexametaphosphate was added to deflocculate the sediment by tumble mixing for 3 h in deionized water. Samples were treated in an ultrasound bath for 10 min followed by rotated agitation for 3 min. For core 11-MC, sediments were sieved (2 mm) then disaggregated in an ultrasonic bath for 90 s prior to their analysis. The disaggregated sediment samples were analyzed with a laser-diffraction particle-size analyzer (LS13320, Beckman-Coulter). Only particle sizes between 0.04 and 2000 mm were analyzed. Laser calibration was verified before and after analyses using three standards (Latron 300-0.3 mm, G15-15 mm, and GB500-500 mm). Analyses of 6-14 spectra are necessary to obtain enough stability on the spectrum to compare results. The mean of the last two spectra was weighted to 100% to minimize minor statistical deviations. The particle-size data and granulometric statistics were then processed with the Gradistat program (Blott and Pye, 2001). A similar procedure was used for core 12-MC. However, it seems that grain size measurements were made on a fraction below 100 μm in this core due to some laboratory mistake. Coulter counter statistics yielded barely any sand fraction in 12-MC, whereas weighted fractions >106 μm recovered for micropaleontological studies are almost identical to those observed in 11-MC (see supplementary material). Mineralogical assemblages were determined by X-ray diffraction (XRD) using a Siemens D5000 with CoKα1,2 radiation and a Si detector. Aliquots of dry bulk sediment were dispersed in distilled water, and then sieved on a 63 μm mesh. Following this sieving, samples from core 11-MC were then sieved on a 10 μm mesh, whereas samples from core 12-MC were sieved on a 20 μm mesh. Each sample was placed on an X-ray diffractometer three times, one with no additional treatment to what is described above, one with heat treatment and one with ethylene-glycol treatment. Semi-quantitative estimations N ($\pm 1\sigma \sim 5\%$) of the main mineral species were based on the area of the diffraction peak for each mineral corrected for quartz. The carbonate fraction is defined as the sum of calcite and dolomite contents.

2.3. Results

2.3.1. Major sedimentological features

In core 11-MC, the mean grain size varies between 4 and 16 μm. Percent sand varies from 0 to 26%, and percent clay varies from 15 to 35% (Fig. 2). The observed mean grain size variations are mostly explained by the percentage of sand. Furthermore, percent clay and the mean grain size delimit three distinct layers, with finer grain sizes at depth intervals of 0-8 cm, 16-18 cm and 26-38 cm. Percent inorganic carbon shows parallel variations in these layers, ranging from 1 to 4%. Percent organic carbon is stable along the core at approximately 0.22±0.13% (±1σ), with a maximum of 0.50%. Similarly, in core 12-MC, the mean grain size varies from 4 to 6 μm. However the sand fraction is practically absent and the silt fraction corresponds to 70 to 80% of the total, whereas the clay fraction varies between 20 and 30%. Percent inorganic carbon varies between 0 to 6% and percent organic carbon (0.23±0.12%) is as stable downcore as in 11-MC. The clay fraction distribution also shows the same peaks as described for core 11-MC, again at practically identical depths. However, as explained above, one cannot compare directly the coarse fraction contents of the two cores based on the Coulter counter statistics, due to a laboratory error procedure when processing core 12-MC. Nonetheless, based on the fine fraction distributions and coarse (> 106 μm) material contents (supplementary material), one may conclude that both cores are practically similar from a sediment grain size perspective.

The carbonate fraction varies from 2% to more than 46% in core 11-MC. Three peaks are observed, one near the surface (0-8 cm), the second between 16 and 18 cm, and the bottom one from 26 cm to core bottom (Fig. 3). If some planktonic and benthic foraminifers are present in these layers, they represent a very small percentage of this carbonate fraction, which is mostly composed of an even proportion of fine-grained calcite and dolomite from detrital origin. The isotopic composition ($\delta^{13}C$ and $\delta^{18}O$) of *Neogloboquadrina pachyderma* (left coiled) -henceforth Npl- assemblages is shown in Figure 3. $\delta^{18}O$ values vary between +1 and +2.5‰, which corresponds to an offset of the calcite in equilibrium with VSMOW standard within Arctic temperature ranges (Hillaire-Marcel et al., 2004). $\delta^{13}C$ values vary from +0.5 to 1‰, which is consistent with values abundantly reported in literature for interglacial assemblages of Npl in the sub-Arctic North Atlantic (Poore et al 1999, Stein,

2008b for review; Hillaire-Marcel et al., submitted). In order to investigate a longer sediment record at the HLY0503-11 site, we analyzed the upper part of the trigger weight core corresponding to the 11-MC multicore. Figure 4 presents percent inorganic carbon, ^{210}Pb and ^{230}Th analyzed in the multicore and the trigger weight core. As shown by Not et al (2008), ^{210}Pb data are a direct consequence of variations of its parent isotopes ^{226}Ra and ^{230}Th. The combination of percent inorganic carbon and ^{210}Pb allows us to correlate the two cores as indicated in Figure 4. Based on this correlation, we conclude that the top 18 cm of sediment are missing in the TWC. Furthermore, the TWC sequence shows a compaction of about 35%, compared with 11-MC. The first peak of inorganic carbon in the trigger weight core matches the third one in 11-MC and three other peaks are observed below, from 25 to 36 cm, 44 to 46 cm and at ~ 58 cm.

2.3.2. U and Th Series Data

As shown in Figure 5, the ^{234}U/^{238}U activity ratio varies between 0.97 and 0.84 in core 11-MC, and between 0.95 and 0.86 in core 12-MC. All values lower than 1 indicate that the sediment has undergone U losses with preferential departure of ^{234}U during particle transport, scavenging and/or post depositional diagenetic processes. Furthermore, values lower than 1 in the top part of cores indicate the lack of any diagenetic U-uptake that one could link to the low C_{org} abundance (Gariepy et al., 1994). The ^{238}U/^{232}Th activity ratio varies between 1.03 and 0.58 in core 11-MC, and between 0.79 and 0.42 in core 12-MC.

Downcore ^{230}Th distribution is similar at the two sites and shows three peaks in both MC's, from 0 to 8 cm, 16 to 18 cm, and from 26 cm to core-bottom. These peaks correspond to the layers with lower mean grain size, high clay content, and high inorganic carbon content. Within these peaks ^{230}Th activity varies between 30 and 2 dpm/g in both cores, whereas in the other layers it ranges from 1 to 2 dpm/g (Fig. 6). Downcore 11-MC ^{231}Pa distribution shows ^{231}Pa activity varying between 1.15 and 0.5 dpm/g. Unfortunately, due to analytical problems, there is a gap in the data set between 5 and 13 cm.

2.4. Discussion

2.4.1. Two sedimentary regimes

Based on sedimentological features, two distinct sedimentary regimes can be identified at sites 11-MC and 12-MC. The first regime (0-8 cm, 16-18 cm and 26-38 cm in MCs) is characterized by carbonate "pulses" and high clay content. The carbonate supplies represent 15 to 45 % of the sediment and are mostly a mixture of equal amounts of calcite and dolomite. These high carbonate content layers may be seen as resulting from high supplies of fine detrital carbonates, mostly from the Canadian Archipelago, where dolomite is abundant (Stein, 2008b). Erosion of Paleozoic carbonates by the Laurentide Ice Sheet and their subsequent release in the Western Arctic have been long recognized as a prominent feature in sedimentary sequences from the area (Bischof et al., 1996; Darby et al., 2002; Polyak et al., 2004). However, these layers also contain foraminifer shells, mostly Npl. Their $\delta^{18}O$ values show an offset with theoretical calcite produced at mid-pycnocline depth. Hillaire-Marcel and de Vernal (2008) explained this ^{18}O-offset as the result of sea ice production processes leading to the distillation of isotopically light brines sinking in the water column and providing suitable salinity conditions for the species to develop. Based on the scarcity of foraminifer and their ^{18}O offset, it appears that in the Arctic environment ^{18}O-data should be carefully interpreted and cannot be directly linked to reference curves. However, the foraminifer $\delta^{13}C$ signature still follows a North Atlantic pattern (Hillaire-Marcel et al., 2004). In the studied sequences, it is characteristic of interglacial periods even though it is slightly heavier compared to North Atlantic records, due to the very low Arctic temperatures. Foraminifers from the first centimeter yielded a ^{14}C age of 8500 years (Libby's years), suggesting relatively high biogenic fluxes during the early Holocene thermal optimum, since bioturbation is limited here to the top 0.5 cm layer as shown by ^{137}Cs data (Not el al., 2008). Below this layer, scattered foraminifer shells down to about 12 cm, yielded Libby's ages ranging from 27 to 33 ka with reversals, suggesting that this section might incorporate some reworked material. The ^{14}C-age distribution also indicates an extremely low sedimentation, if any, during MIS2.

The second regime (8-16 cm and 18-28 cm in MCs) corresponds mostly to ice-rafted deposition (IRD) with possibly some post- and/or syn-depositional losses of fine fractions

(e.g., Haley et al 2008, and below). The corresponding layers have a higher sand content (2 mm to 63 μm fraction in 11-MC), a low carbon content and no foraminifer shells (11-MC and 12-MC). The mineralogical composition is ~15% mica, ~20% quartz, ~30% feldspar and ~30% plagioclase.

Assuming an age of ~ 30 ka at 9 cm and a nearly constant IRD sedimentation rate back in time, an age model can be tentatively developed, in a first estimate, from the sand-fraction cumulative inventory downcore 11-MC, where reliable measurements of coarse fractions have been made (Fig. 7). In this scenario, involving a steady IRD supply through time, the mean sedimentation rate obtained is estimated at 1.2 $mm.ka^{-1}$, whereas the sedimentation rate for the glacial period sensu stricto is estimated at 0.7-0.75 $mm.ka^{-1}$. This model provides a first order chronostratigraphy for the two sites. As seen below, nearly constant ^{238}U and ^{232}Th activities of ~ 1.5 and ~ 2 dpm/g, respectively, are observed in the glacial intervals, when IRD supplied most of the sediment, but for the later post- and/or syn-depositional loss of fine fractions. Deglacial-interglacial intervals, with higher clay and carbonate fractions, show slightly higher ^{232}Th activities (~ 2.5 dpm/g), linked to ^{232}Th-enriched clay minerals, but surprisingly almost identical ^{238}U activities.

In summary, we associate the first sedimentary regime, characterized by high contents in foraminifer shells, clays, and inorganic carbon, to deglacial and/or interglacial periods and the second regime, characterized by high coarse fraction content (mostly IRD deposition), to glacial periods, which is consistent with the interpretation of Arctic sedimentary features proposed in the literature (e.g., Spielhagen et al., 2004, O'Regan et al., 2008, Polyak et al., 2009).

2.4.2. Time constraint from U series isotopes

In the sediment, ^{230}Th-contents depend mostly upon i) the production rate of ^{230}Th in the water column, ii) the efficiency of ^{230}Th scavenging on particles, iii) the sedimentation rate, iv) the age of the sediment leading to the decay of the unsupported fraction and v) the fraction carried with detrital supplies.

In the ocean as a whole, and for many specific basins, an approximate balance between uranium dissolved in the ocean, which controls the production rate of ^{230}Th, and the ^{230}Th

added to sediments has been demonstrated (Ku and Broecker, 1967). Even if some debate remains about the balance of the production of ^{230}Th in the water column and its accumulation in the underlying surface sediment, our first assumption is that all the ^{230}Th produced in the water column is found in the sediment, at least under the present interglacial conditions (see inventories and flux section below). In other words, lateral transport and boundary scavenging are not considered a significant source of ^{230}Th in recent sediment *a priori*. The fraction of ^{230}Th that comes from the water column is referred to as ^{230}Th-excess ($^{230}Th_{xs}$), as opposed to the ^{230}Th produced in the sediment by the radioactive decay of parent (^{234}U), to which we will refer to as "supported" or "detrital" ^{230}Th, since there is little evidence for any significant addition of diagenetic U in the sediment. If totally scavenged from the water column, $^{230}Th_{xs}$ activity in the sediment depends on the production rate (i.e. thickness of the water column), the sedimentation rate and the age of the sediment (Hoffmann and McManus, 2007). Nonetheless, $^{230}Th_{xs}$ can provide a rough chronological benchmark in Arctic cores. Assuming broadly similar statistical errors on the supported and excess fraction estimates, the error on the difference between the minimum measurable excess above supported ^{230}Th-activity can be estimated as ~ [^{230}Th-supported + (2σ * $\sqrt{2}$)]. When the $^{230}Th_{xs}$ falls within the error bars of the supported fraction, one may conclude with a 95% probability that there is no "measurable" excess left. At such depths, one may thus presume that the limit of the ^{230}Th-dating method is attained. In sediment almost totally deprived of diagenetic uranium, as in the studied cores (see supplementary material for details), the $^{230}Th_{xs}$ can be estimated by subtracting the ^{234}U activity from the measured ^{230}Th activity. In the same way, $^{231}Pa_{xs}$ can be estimated by subtracting the ^{235}U activity. A time limit can then be calculated as follows:

$$T_{lim} \sim (1/\lambda)*\mathrm{Ln}\ (A_{xs}/Er_{(2\sigma * \sqrt{2})})$$

Where: T_{lim} is the time limit (ka), λ is the decay constant of the concerned isotope (ka^{-1}), A_{xs} is the top core (maximum) reference activity of the excess of this isotope activity and Er the mean error (in $dmp.g^{-1}$) on the difference between the residual excess in the isotope and its supported fraction, i.e. about (2σ * $\sqrt{2}$) with σ standing for the mean absolute error on the measurement of the activity of the supported fraction. As illustrated in Figure 6, minimum

measurable residual activities yield ages of ≥ 340 ka ($^{230}Th_{xs}$) here, at depths of 36 or >34 cm, respectively in 11-MC and 12-MC, and of ≥ 140 ka ($^{231}Pa_{xs}$), at a depth of 29 cm, in 11-MC. Whereas in the literature, oscillations of $^{230}Th_{xs}$ in the western Arctic Ocean, the Norwegian Sea, Fram Strait and the eastern Arctic Basin have been related to oxygen isotope stages (Eisenhauer et al., 1994; Huh et al., 1997; Scholten et al., 1990), here they follow the two distinct sedimentary regimes highlighted by the sedimentological data (Fig. 6). The glacial regime seems to be associated with a very low $^{230}Th_{xs}$, whereas deglacial/interglacial periods are characterized by a higher $^{230}Th_{xs}$ activity. Assuming a constant scavenging rate during all the deglacial/interglacial intervals, we can propose that the decrease of $^{230}Th_{xs}$ in similar downcore units is only due to $^{230}Th_{xs}$ radioactive decay. Based on this hypothesis, a time period can be determined between each of these layers (Fig. 6). For example ~140 ka is estimated between 2 and 17 cm in core 11-MC, and ~ 60 ka between 17 and 27 cm. Similarly, ^{231}Pa profiles can be used to set some time constraints, and a time period of ~120 ka is obtained between 1 and 16 cm (Fig. 6). Based on these estimates, the three peaks in ^{230}Th are assigned to Terminations (T) and Marine Isotopic Stages (MIS) MIS 1-3, T 2/MIS 5 and T 3/ MIS 7, respectively, thus suggesting a very low mean sedimentation rate (~ 1.5 $mm.ka^{-1}$) for this part of the Arctic Ocean. Note that this estimate does not drastically differ from the ~ 1.2 $mm.ka^{-1}$ value obtained assuming a constant IRD supply, as explained above. Furthermore, the $\delta^{13}C$-values in Npl thought to represent "interglacial" conditions, match each of the Termination-Interglacial intervals identified from the rough $^{230}Th_{xs}$ and $^{231}Pa_{xs}$ chronologies. It is worth mentioning that in 11-MC and 12-MC, MIS 2 is not recognized by distinct sedimentological changes, due to both or either its relatively short duration and smoothing in the records, or an absence of sedimentation. The deglacial-interglacial transitions illustrated in Figure 9 present features not unlike those described in other Arctic areas (Haley et al., 2008; Norgaard Pedersen et al., 1998 and Spielhagen et al., 2004). However, the time resolution of the study cores does not allow resolving unquestionably MIS 2 and the MIS3/ MIS1 transition. A complete stop in deposition during MIS 2 is not required, but due to the time resolution achieved here and the mean glacial sedimentation rate estimated above, a maximum of 0.5 cm would have been deposited during MIS2: A layer smoothed out in the record.

The ^{230}Th budget in the Arctic Ocean is still fragmentarily established. First studies on surface sediments led to the conclusion that some sedimentary $^{230}Th_{xs}$ deficit could exist. For example, Ku and Broecker (1967) first suggested that $^{230}Th_{xs}$ concentrations, which they measured in sandy layers from an Alpha Ridge core, were lower than expected from a purely radioactive-decay-driven profile, possibly due to a lack in suitable particles to effectively scavenge ^{230}Th in the water column or to their loss through sedimentary processes . This conclusion was put forth in more recent studies on surface sediment across the Artic Ocean (Edmonds et al., 2004; Edmonds et al., 1998; Huh et al., 1997; Moran et al., 2005). However a recent study, which focuses on the last 40 ka, suggests a balance of ^{230}Th from water column production with ^{230}Th inventories in sediments from the Western Arctic area during the Holocene and the deglacial period (Hoffmann and McManus, 2007). Such contradictory inferences in the ^{230}Th budget of Arctic sediments are due to either weak time constrains on the sequences investigated (see Hoffmann and McManus, 2007 for details) or sedimentary losses in carrier fractions, or to both.

Here, we will estimate ^{230}Th budget changes throughout the last two climatic cycles identified from sedimentological and geochemical inferences discussed above. Assuming that all ^{230}Th produced in the water column was scavenged to the seafloor at each site, the corresponding cumulative inventories were calculated using the equation of Suman and Bacon (1989):

Production (dpm cm^{-2} ky^{-1}) = 0.00263*water column depth (m).

Inventories of $^{230}Th_{xs}$ in the cored sediment were calculated from measurements of ^{230}Th, using the equation:

$$I = \sum_i (\varrho_i A^i_{xs} \Delta X_i)$$

Where: I = Inventory of $^{230}Th_{xs}$ (dpm.g^{-1}); ϱ_I = dry bulk density (g dry sediment.cm^{-3} wet sediment) of the i^{th} depth interval; A^i_{xs} = $^{230}Th_{xs}$ activity (dpm.g^{-1}) of the i^{th} depth interval; and ΔX_i = thickness of i^{th} depth interval (cm).

^{230}Th inventories in cores 11-MC and 12-MC and ^{230}Th water column production were obtained: i) using the equation described above for the two distinct regimes, ii) assuming a constant initial sedimentary $^{230}Th_{xs}$-flux during each of these regimes and iii) using the age models developed above (Fig. 5). Figure 8 presents the water column production over each coring site and the inventories for the glacial vs deglaciation/interglacial regimes in the

corresponding cores. The ^{230}Th budget seems to be in balance during deglaciation/interglacial periods, but in deficit during glacial periods. This conclusion is consistent with Hoffmann and McManus (2007) with respect to the late glacial-Holocene section. Nonetheless during glacial intervals, a significant amount of the ^{230}Th produced in the water column seems to be missing in the sedimentary record from the northern Mendeleev Ridge. In opposition, the Lomonosov Ridge area does not show any obvious ^{230}Th-deficit in glacial sediments (Not and Hillaire-Marcel, submitted), possibly due to the significantly higher sedimentation rates and higher fine particle contents observed in the Lomonosov Ridge area and/or to differences in depositional processes.

The mechanism of $^{230}Th_{xs}$ scavenging is still unclear. Recently, Roy-Barman et al. (2009) proposed that lithogenic particles and Mn oxides should be the main ^{230}Th scavengers. Thus, ^{230}Th would not be scavenged significantly by carbonate particles and organic matter, but indirectly through its adsorption by Mn-oxyde crystals forming over carbonates (biogenic, possibly detrital). Considering the Mn enrichment of Arctic interglacial sediment (O'Regan et al., 2009) and the correlation between interglacial and $^{230}Th_{xs}$, Mn coatings can be considered as potential Th-scavengers. Nonetheless, in the Arctic Ocean where biological productivity is very low, ice-rafted clay-size lithogenic particles are considered as the major scavengers of ^{230}Th (Edmonds et al., 1998, Trimble et al., 2004). Thus, we may have here, over Mendeleev Ridge, a situation where some continuous scavenging would occur in relation to lithogenic particle fluxes, but with additional scavenging in Mn-oxide crystals when carbonate sedimentation occurs. This could have led to a reduction in ^{230}Th-fluxes to the sea-floor during intervals when fluxes of carbonates collapsed, especially glacial intervals (Edmonds et al., 1998, Roy-Barman et al., 2009).

Another process could also account for the deficit in $^{230}Th_{xs}$ of the glacial sedimentary units: some winnowing of fine $^{230}Th_{xs}$-carrier particles over the ridge, independently of the bathymetry since both sites depict similar deficits despite their ~ 1 km depth-difference. Haley et al, (2008) provided evidence for brine rejection linked to sea ice formation, on and near the Siberian shelves, during glacial times. The sinking of such brines could have possibly washed out fines from surface sediments or even carried away fine fractions from IRD during their deposition, by increasing the intermediate and deep water velocity. Such a

process would account for both the larger grain-size of glacial sediments and the loss of most of the scavenged $^{230}Th_{xs}$. However, the striking similarity of lithostratigraphies and ^{230}Th inventories at both sites separated by a ~1 km-bathymetric difference would require an absolutely identical winnowing, to occur at both sites. Thus, unless stronger evidence is found in favor of this scenario, that of a glacial deficit in $^{230}Th_{xs}$ due to a lesser efficiency of scavenging particles (almost no carbonates, and no Mn-oxide coatings) and/or to a lack of fine scavenging material in general, must also be considered. This would involve some export of dissolved ^{230}Th towards the deep basins, Arctic margins and/or even through Fram Strait, which is the largest outlet for Arctic waters towards the sub-arctic seas. Until evidence for ^{230}Th-focussing either in deep basins and or along the Arctic margins is found, either both some specific export of fine particles or their saturation in scavenged-^{230}Th, below 1600 m, remain possible explanations.

2.4.3. The proposed stratigraphy

Based on the time estimates and the association of specific sedimentary layers to termination-interglacial intervals, the stratigraphy developed in Figure 9, with reference to Marine Isotopic Stages (MIS), can be put forth. Peaks of ^{210}Pb and inorganic carbon content highlight the last few deglacial/interglacial periods. Peaks associated with T 2/MIS 5 and T 5/MIS 11 seem less pronounced than those of MIS 1, 7 and 9. A substantially reduced Greenland ice volume is suggested during MIS 5 and 11 (de Vernal and Hillaire-Marcel, 2008). A stronger zonal circulation in the North Atlantic could then paradoxically result in a significant sea-ice cover in the Arctic. Nevertheless, glacial stages seem to be restricted to discrete coarse-grained IRD layers, and depict overall lower sedimentation rates ($\leq$ 1 mm.ka^{-1}); in some cases such intervals could be unrecorded and/or undetected at the resolution achievable in such low sedimentation rate settings. In both multicores 11-MC and 12-MC, the lack of sedimentological changes in near core tops that could be associated with the Last Glacial Maximum (MIS 2) further indicates very low sedimentation rates (thus reduced IRD) during this interval, as already suggested by Poore et al. (1999). However, our overall sedimentation rate estimate (~ 1.5 mm.ka^{-1}) also leads to conclude that any average 1 cm-sample encompasses a ~ 6.5 ka interval. This reduced the probability of detecting MIS 2.

The mean sedimentation rate of 1.5 mm ka^{-1} obtained here is close to that estimated for the top of the sequence, based on ^{14}C measurements (1.6 mm/ka in core HLY0503-11MC2; Polyak et al. 2009). It however invalidates estimates of 4.6 mm ka^{-1} from amino-acid racemisation rates (Polyak et al., 2009 and Kaufman et al., 2008). Since Be isotope data on Mendeleev and Alpha ridges (Sellèn et al., 2009) yielded values in the range suggested by U-series, we consider that ^{230}Th and ^{231}Pa may reveal instrumental in developing a robust multi-proxy time scale in such very low sedimentation rate settings.

2.5. Conclusion

Sedimentation rates in the western Arctic Ocean seem about one order of magnitude lower than those of the eastern Arctic Ocean, or of other high northern latitude areas. At rates of 1-3 $mm.ky^{-1}$, the ^{14}C method is applicable only in the top few centimeters of sediments. The lack of planktonic foraminifers in Arctic sediments, especially during glacial periods, and their isotopic properties precludes dating by $\delta^{18}O$ stratigraphy. Thus, $^{230}Th_{xs}$ and Be-isotopes (Sellèn et al., 2009) appear viable geochemical tool for dating sediments in this part of the Arctic Ocean. In this study, sedimentological observations define two different depositional regimes; one with nearly exclusive IRD deposition (i.e. glacial periods) and a second one, during deglaciations, when marginal-ice and drainage events supply additional material. Over Mendeleev Ridge, these sedimentary pulses originated essentially from the Canadian margin, as indicated by the abundance of dolomitic carbonates from this source area. In such a setting, ^{230}Th and ^{231}Pa provide tools for defining a chronostratigraphy spanning the last few climatic cycles, but also for the characterization of glacial and deglacial-interglacial times.

Finally, if the ^{230}Th budget seems to be in balance during deglacial/interglacial periods, even under such low sedimentation rate conditions, some ^{230}Th is missing from the glacial sedimentary column. Either some ^{230}Th-export occurred in the water column, or losses occurred through fine carrier-particle removal at the water/sediment interface. An unambiguous determination of glacial ^{230}Th dynamics remains to be achieved by working on glacial records from deep basins, margins and possibly the Fram Strait area.

2.6. Acknowledgements

We owe thanks to Dennis Darby, Leonid Polyak and Martin Jakobsson for providing access to material recovered during the 2005 HOTRAX cruise. We thank Dr. Roger François for providing facilities for Pa analyses at the University of British Columbia. Support from GEOTOP members has been essential for the achievement of the exhaustive analytical program behind this study, in particular from Bassam Ghaleb, Guillaume St-Onge, Michel Preda, Jennifer McKay (now at Oregon State University) and Agnieska Adamowicz. Substantial comments from Martin Frank, Robert Spielhagen and Mathew O'Regan, who reviewed this paper, led to significant changes and improvements in the manuscript. HOTRAX was funded by the U.S. National Science Foundation's Office of Polar Programs (OPP-0352395), the U.S. Coast Guard, the Swedish Polar Research Secretariat, and the Swedish Science Council. The present study is a contribution to the Polar Climate Stability Network program (*Canadian Foundation for Climate and Atmospheric Sciences*). Funding from the *Natural Sciences and Engineering Research Council* of Canada (Claude Hillaire-Marcel) and the *Fonds Québecois de la Recherche sur la Nature et les Technologies* (GEOTOP grant and team grant to de Vernal et al.) is also acknowledged.

2.7. References

Aagaard, K., Coachman, L. K., and Carmack, E. (1981). On the halocline of the Arctic Ocean. *Deep Sea Research Part A. Oceanographic Research Papers* **28,** 529-545.

Backman, J., Jakobsson, M., Lovlie, R., Polyak, L., and Febo, L. A. (2004). Is the central Arctic Ocean a sediment starved basin? *Quaternary Science Reviews* **23,** 1435-1454.

Baskaran, M., and Naidu, A. S. (1995). 210Pb-derived chronology and the fluxes of 210Pb and 137Cs isotopes into continental shelf sediments, east Chukchi Sea, Alaskan Arctic. *Geochimica et Cosmochimica Acta* **59,** 4435-4448.

Bischof, J., Clark, D. L., and Vincent, J. S. (1996). Origin of ice-rafted debris: Pleistocene paleoceanography in the western Arctic Ocean. *Paleoceanography* **11,** 743-756.

Blott, S. J., and Pye, K. (2001). Gradistat: A grain size distribution and statistics package fro the analysis of unconsolidated sediments. *Earth Surface Processes and landforms* **26,** 1237-1248.

Choi, M. S., Francois, R., Sims, K., Bacon, M. P., Brown-Leger, S., Fleer, A. P., Ball, L., Schneider, D., and Pichat, S. (2001). Rapid determination of Th-230 and Pa-231 in seawater by desolvated micro-nebulization Inductively Coupled Plasma magnetic sector mass spectrometry. *Marine Chemistry* **76,** 99-112.

Darby, D. A., Bischof, J. F., Spielhagen, R. F., Marshall, S. A., and Herman, S. W. (2002). Arctic ice export events and their potential impact on global climate during the late Pleistocene. *Paleoceanography* **17,** 15-15.

Darby, D. A., Jakobsson, M., and Polyak, L. (2005). Ice breaker Expedition collects key Arctic Seafloor and Ice data. *EOS* **86,** 549-552.

de Vernal, A., and Hillaire-Marcel, C. (2008). Natural Variability of Greenland Climate, Vegetation, and Ice Volume During the Past Million Years. *Science* **320,** 1622.

Deschamps, P., Doucelance, R., Ghaleb, B., and Michelot, J. L. (2003). Further investigations on optimized tail correction and high-precision measurement of uranium isotopic ratios using multi-collector ICP-MS. *Chemical Geology* **201,** 141-160.

Edmonds, H. N., Moran, S. B., Cheng, H., and Edwards, R. L. (2004). Th-230 and Pa-231 in the Arctic Ocean: implications for particle fluxes and basin-scale Th/Pa fractionation. *Earth and Planetary Science Letters* **227,** 155-167.

Edmonds, H. N., Moran, S. B., Hoff, J. A., Smith, J. N., and Edwards, R. L. (1998). Protactinium-231 and thorium-230 abundances and high scavenging rates in the western Arctic Ocean. *Science* **280,** 405-407.

Edwards, R. L., Chen, J. H., and Wasserburg, G. J. (1987). 238U 234U 230Th 232Th systematics and the precise measurement of time over the past 500,000 years. *Earth and Planetary Science Letters* **81,** 175-192.

Eisenhauer, A., Spielhagen, R. F., Frank, M., Hentzschel, G., Mangini, A., Kubik, P. W., Dittrich-Hannen, B., and Billen, T. (1994). 10Be records of sediment cores from high northern latitudes: Implications for environmental and climatic changes. *Earth and Planetary Science Letters* **124,** 171-184.

Flynn, W. W. (1968). The determination of low levels of polonium-210 in environmental materials. *Analytica Chimica Acta* **43,** 221-226.

Gariepy, C., Ghaleb, B., Hillaire-Marcel, C., Mucci, A., and Vallieres, S. (1994). Early Diagenetic Processes in Labrador Sea Sediments : Uranium-Isotope Geochemistry. *Canadian Journal of Earth Sciences* **31,** 28-37.

Haley, B. A., Frank, M., Spielhagen, R. F., and Eisenhauer, A. (2008). Influence of brine formation on Arctic Ocean circulation over the past 15 million years. *Nature Geosciences* **1**, 68-72.

Hillaire-Marcel, C., and de Vernal, A. (2008). Stable isotope clue to episodic sea ice formation in the glacial North Atlantic. *Earth and Planetary Science Letters* **268,** 143-150.

Hillaire-Marcel, C., de Vernal, A., Polyak, L., and Darby, D. (2004). Size-dependent isotopic composition of planktic foraminifers from Chukchi Sea vs. NW Atlantic sediments - implications for the Holocene paleoceanography of the western Arctic. *Quaternary Science Reviews* **23,** 245-260.

Hoffmann, S., and McManus, J. (2007). Is there a 230Th deficit in Arctic sediments? *Earth and Planetary Science Letters* **258,** 516-527.

Huh, C. A., Pisias, N. G., Kelley, J. M., Maiti, T. C., and Grantz, A. (1997). Natural radionuclides and plutonium in sediments from the western Arctic Ocean: sedimentation rates and pathways of radionuclides. *Deep-Sea Research Part I-Topical Studies in Oceanography* **44,** 1725-1743.

Jakobsson, M., Lovlie, R., Al-Hanbali, H., Arnold, E., Backman, J., and Morth, M. (2000). Manganese and color cycles in Arctic Ocean sediments constrain Pleistocene chronology. *Geology* **28,** 23-26.

Jakobsson, M., Macnab, R., Mayer, L., Anderson, R., Edwards, M., Hatzky, J., Schenke, H. W., and Johnson, P. D. (2008). An improved bathymetric portrayal of the Arctic Ocean: Implications for ocean modeling and geological, geophysical and oceanographic analyses. *Geophys. Res. Lett.* **35,** L07602.

Kaufman, D. S., Polyak, L., Adler, R., Channell, J. E. T., and Xuan, C. (2008). Dating late Quaternary planktonic foraminifer Neogloboquadrina pachyderma from the Arctic Ocean using amino acid racemization. *Paleoceanography* **23**.

Ku, T.-L., and Broecker, W. S. (1967). Rates of sedimentation in the Arctic ocean. *Progress In Oceanography* **4,** 95-104.

Moore, W. S., and Sackett, W. M. (1964). Uranium and Thorium Series Inequilibrium in Sea Water. *J. Geophys. Res.* **69**.

Moran, S. B., Shen, C. C., Edwards, R. L., Edmonds, H. N., Scholten, J. C., Smith, J. N., and Ku, T. L. (2005). Pa-231 and Th-230 in surface sediments of the Arctic Ocean: Implications for Pa-231/Th-230 fractionation, boundary scavenging, and advective export. *Earth and Planetary Science Letters* **234,** 235-248.

Norgaard-Pedersen, N., Spielhagen, R. F., Thiede, J., and Kassens, H. (1998). Central Arctic surface ocean environment during the past 80,000 years. *Paleoceanography* **13**, 193-204.

Not, C., Hillaire-Marcel, C., Ghaleb, B., Polyak, L., and Darby, D. (2008). 210Pb-226Ra-230Th systematics in very low sedimentation rate sediments from the Mendeleev Ridge (Arctic Ocean). *Canadian Journal of Earth Sciences* **45,** 1207-1219.

O'Regan, M., King, J., Backman, J., Jakobsson, M., Pa?like, H., Moran, K., Heil, C., Sakamoto, T., Cronin, T. M., and Jordan, R. W. (2008). Constraints on the Pleistocene chronology of sediments from the Lomonosov Ridge. *Paleoceanography* **23**.

Phillips, R. L., and Grantz, A. (1997). Quaternary history of sea ice and paleoclimate in the Amerasia Basin, Arctic Ocean, as recorded in the cyclical strata of Northwind Ridge. *Bulletin of the Geological Society of America* **109,** 1101-1115.

Pichat, S., Sims, K. W. W., Francois, R., McManus, J. F., Brown Leger, S., and Albarade, F. (2004). Lower export production during glacial periods in the equatorial Pacific derived from (231Pa/230Th)xs,0 measurements in deep-sea sediments. *Paleoceanography* **19**.

Polyak, L., Curry, W. B., Darby, D. A., Bischof, J., and Cronin, T. M. (2004). Contrasting glacial/interglacial regimes in the western Arctic Ocean as exemplified by a sedimentary record from the Mendeleev Ridge. *Palaeogeography Palaeoclimatology Palaeoecology* **203,** 73-93.

Scholten, J. C., Botz, R., Mangini, A., Paetsch, H., Stoffers, P., and Vogelsang, E. (1990). High resolution 230Thex stratigraphy of sediments from high-latitude areas (Norwegian Sea, Fram Strait). *Earth and Planetary Science Letters* **101,** 54-62.

Scholten, J. C., VanderLoeff, M. M. R., and Michel, A. (1995). Distribution of Th-230 and Pa-231 in the water column in relation to the ventilation of the deep Arctic basins. *Deep-Sea Research Part Ii-Topical Studies in Oceanography* **42,** 1519-1531.

Sellèn, E., Jakobsson, M., Frank, M., and Kubik, P. W. (2009). Pleistocene variations of beryllium isotopes in central Arctic Ocean sediment cores. *Global and Planetary Change* **68,** 38-47.

Spielhagen, R. F., Baumann, K. H., Erlenkeuser, H., Nowaczyk, N. R., Norgaard-Pedersen, N., Vogt, C., and Weiel, D. (2004). Arctic Ocean deep-sea record of northern Eurasian ice sheet history. *Quaternary Science Reviews* **23**, 1455-1483.

Stein, R. (2008a). Glacio-Marine Sedimentary Processes. *In* "Developments in Marine Geology." pp. 87-132. Elsevier.

Stein, R. (2008b). Quaternary Variability of Palaeoenvironment and Its Sedimentary Record. *In* "Developments in Marine Geology." pp. 287-437. Elsevier.

Suman, D. O., and Bacon, M. P. (1989). Variations in Holocene sedimentation in the North American Basin determined from 230Th measurements. *Deep Sea Research Part A. Oceanographic Research Papers* **36,** 869-878.

2.8. Suplementary Material

In this section we provide complementary information relating to methodology and calculation.

Comparison of ^{230}Th analyses from ICP-MS and Alpha measurements.

Figure 1 show the correlation between two different methods (Alpha Spectrometry and MC-ICP-MS measurements) for ^{230}Th analysis. In general, the correlation is good for both cores, however higher activities are not as well correlated, which could be due to mineralogical heterogeneities in the crushed sediment despite efforts to homogenize it.

Estimation of ^{230}Th and ^{231}Pa excesses

Thorium-230 excess ($^{230}Th_{xs}$) is considered to represent the fraction of ^{230}Th scavenged from the water column by organo-mineral matter. In practice it is assimilated to the unsupported ^{230}Th in the sediment at the moment it settles. An approach to calculate $^{230}Th_{xs}$ is to assume a constant U/Th ratio in the detrital fraction and secular equilibrium conditions within ^{238}U-^{234}U-^{230}Th series. Assuming constant $^{238}U/^{232}Th$ ratio and secular equilibrium between ^{234}U and ^{238}U in the detrital fraction, the excess daughter products are as follows (Lao et al., 1993):

$$^{230}Th_{xs} = {}^{230}Th_m - R*{}^{232}Th_m - 1.14*({}^{238}U - R*{}^{232}Th)$$

$$^{231}Pa_{xs} = {}^{231}Pa_m - (0.0046*R*{}^{232}Th_m) - 0.0046*({}^{238}U_m - R*{}^{232}Th_m)$$

"xs" stands for "excess"; "m" stands for measured; 0.0046 is the activity ratio of $^{235}U/^{238}U$ in natural material; "R" is the $^{238}U/^{232}Th$ activity ratio in the detrital fraction; 1.14 stands for the $^{234}U/^{238}U$ activity ratio in seawater (Lao et al., 1993). This method also implies that there is no diagenic U uptake or losses in the sediment (see discussion in Veiga-Pires and Hillaire-Marcel., 1999). For core HLY0503-11MC, the $^{238}U/^{232}Th$ ratio peaks at 1.25 cm and 26.25 cm (Fig. 5). However, $^{234}U/^{238}U$ ratios do not show these two peaks that are simply due to lower ^{232}Th activity at theses depths. We may thus postulate minimum U uptake in the study cores where oxidizing conditions linked to very low C_{org} fluxes prevail (Fig. 5). Thus, on the contrary, some U losses from the sediment forward seafloor with preferential leaching of ^{234}U could occur, as suggested by $^{234}U/^{238}U$ activity ratios < 1 in the sub-surface sediment (Fig. 5). As suggested in Veiga-Pires and Hillaire-Marcel (1999), a better estimate of the $^{230}Th_{xs}$ could be made with references to parent activity (^{234}U) in such cases. In a first estimate, the ^{234}U

losses occurred within the last 30 ka, below, the $^{234}U/^{238}U$ ratio seems to return more or less to secular equilibrium (Fig. 5). We have thus neglected here the impact of these losses on $^{230}Th_{xs}$ estimates. We have thus calculated the $^{230}Th_{xs}$ as follows:

$$^{230}Th_{xs} = {}^{230}Th_m - {}^{234}U_m$$

The notation "m" corresponds to measured values.

This $^{230}Th_{xs}$ remains a first order estimate since we ignore the precise timing of U-losses in sub-surface sediment. It will likely overestimate the ^{230}Th setup time from scavenging processes in the upper 10 cm and underestimate it slightly below.

References

Lao, Y., Anderson, R. F., Broecker, W. S., Hofmann, H. J., and Wolfli, W. (1993). Particulate fluxes of 230Th, 231Pa, and 10Be in the northeastern Pacific Ocean. Geochimica et Cosmochimica Acta 57, 205-217.

Veiga-Pires, C. C., and Hillaire-Marcel, C. (1999). U and Th isotope constraints on the duration of Heinrich events H0-H4 in the southeastern Labrador Sea. Paleoceanography 14, 187-199.

Depth (cm)	HLY0503-11MC		HLY0503-12MC
	$^{230}Th_{xs}$ (dpm.g^{-1})	$^{231}Pa_{xs}$ (dpm.g^{-1})	$^{230}Th_{xs}$ (dpm.g^{-1})
0.25	21.75±0.92	1.23±0.17	15.65±0.68
1.25	23.28±1.00	1.09±0.12	18.39±0.80
2.25	27.96±1.18	1.08±0.18	28.23±1.18
3.25	28.01±1.18	0.83±0.15	22.43±0.96
4.25	25.96±1.10	0.59±0.10	16.92±0.74
5.25	17.75±0.78	0.48±0.10	12.27±0.54
6.25	12.23±0.54	-	8.97±0.40
7.25	9.59±0.44	-	7.85±0.38
8.25	4.31±0.24	-	4.67±0.24
9.25	0.94±1.10	-	1.43±0.12
10.25	1.05±0.05	-	0.46±0.10
11.25	2.01±0.14	-	0.16±0.08
12.25	1.20±0.10	-	0.17±0.08
13.25	0.84±0.10	-	0.20±0.08
14.25	0.93±0.10	-	0.38±0.10
15.25	0.74±0.10	-	0.47±0.06
16.25	5.14±0.26	-	0.36±0.08
17.25	7.79±0.36	-	3.54±0.20
18.25	2.84±0.16	-	5.95±0.30
19.25	0.46±0.08	-	0.63±0.08
20.25	0.24±0.08	-	0.11±0.08
21.25	0.19±0.08	-	0.00±0.00
22.25	0.02±0.06	0.00±0.00	0.07±0.06
23.25	0.00±0.00	0.00±0.00	0.11±0.08
24.25	0.00±0.00	0.00±0.00	0.03±0.06
25.25	0.01±0.06	0.00±0.00	0.02±0.06
26.25	2.66±0.14	0.02±0.00	0.02±0.04
27.25	4.48±0.24	0.02±0.00	2.58±0.16
28.25	3.76±0.22	0.01±0.00	3.70±0.20
29.25	3.66±0.20	0.00±0.00	3.36±0.18
30.25	3.26±0.20	0.00±0.00	2.74±0.18
31.25	2.71±0.18	0.00±0.00	2.61±0.16
32.25	1.74±0.14	0.00±0.00	3.07±0.16
33.25	1.43±0.12	0.00±0.00	3.03±0.18
34.25	1.17±0.12	0.00±0.00	2.10±0.12
35.25	0.83±0.10	0.00±0.00	
36.25	0.44±0.08	0.00±0.00	
37.25	0.22±0.08	0.00±0.00	

Table S1: $^{230}Th_{xs}$ and $^{231}Pa_{xs}$ data in core HLY0503-11MC and $^{230}Th_{xs}$ data in core HLY0503-12MC.

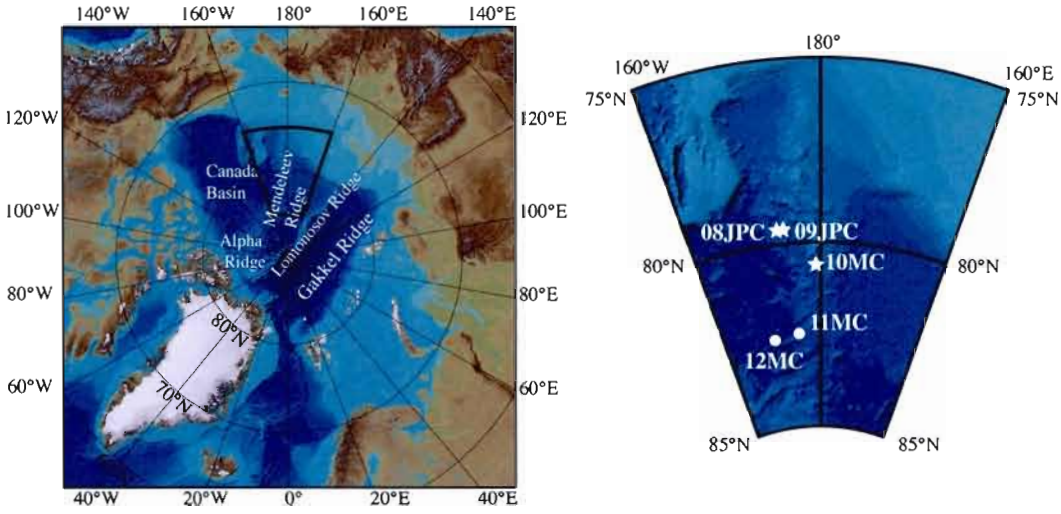

Figure 1: Location of multicores from the HOTRAX 2005 expedition used in this study (circles) and from references (stars) used for comparison. The Bathymetry from the International Bathymetric Chart of the Arctic Ocean (Jakobsson et al., 2008).

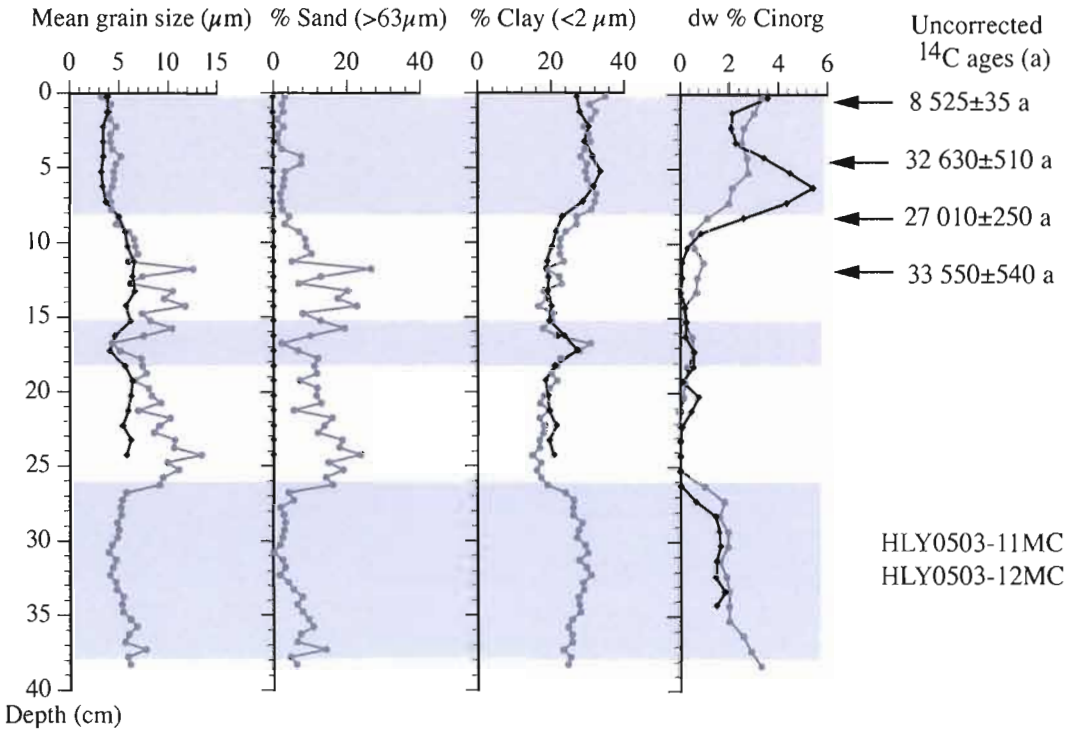

Figure 2: Sedimentological properties of cores HLY0503-11MC8 (grey) and HLY0503-12MC8 (black) and ^{14}C measurements on *Neogloboquadrina pachyderma* assemblages. The mean grain size, sand %, clay %, the inorganic carbon content, show two distinct regimes, one assigned to glacial periods (blank layers) and the other one to deglacial/ interglacial intervals (grey layers). The ^{14}C ages presented here are uncorrected conventional ages at depths of 0.25 cm, 4.25 cm, 8.25 cm and 12.25 cm, respectively. The grain size distribution in core 11MC8 relates to a fraction sieved at 2 mm, whereas that of core 12MC8 was likely sieved at ~ 100 μm (see text).

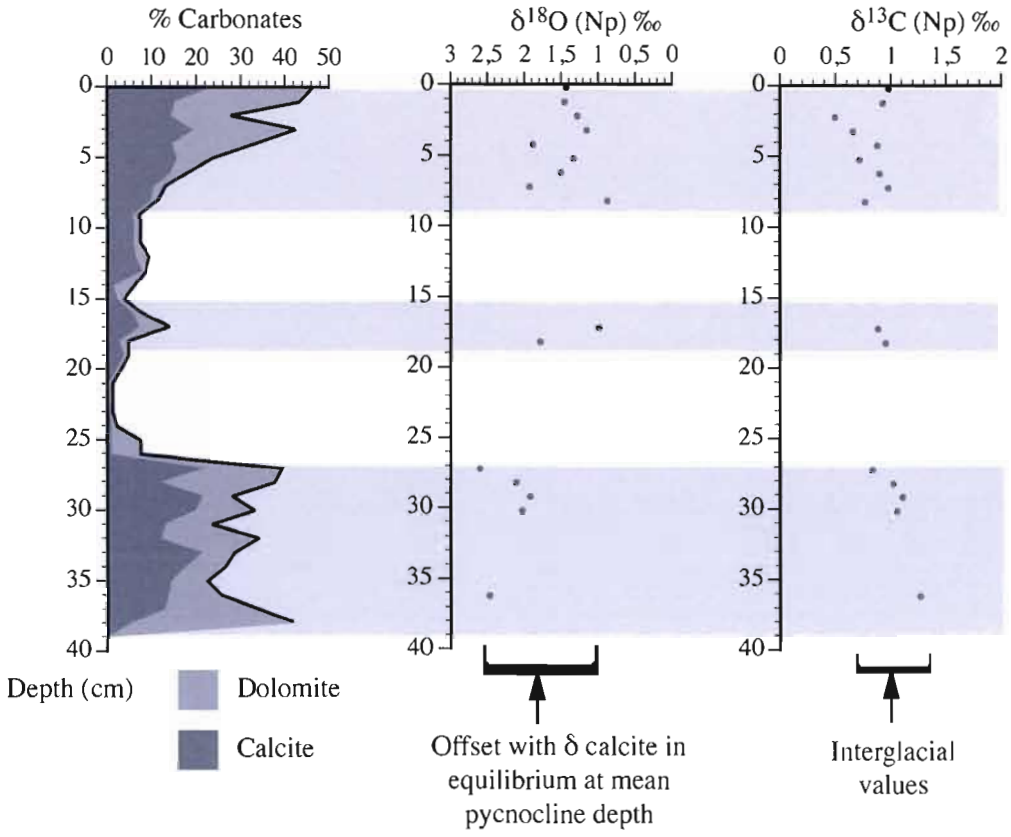

Figure 3. Carbonate characterization for core HLY0503-11MC8. Carbonate content vary between 2 and 46%, with higher contents during deglacial/interglacial periods (grey layers). The carbonates are consistently composed of 50% of calcite and 50% of dolomite downcore. $\delta^{18}O$ and $\delta^{13}C$ values were measured on *Neogloboquadrina pachyderma* shells, at depths where shells were present (deglacial/interglacial intervals with high detrital carbonate contents). The $\delta^{13}C$ values are consistent with "interglacial" marine carbon values from literature. However, the $\delta^{18}O$ presents an offset linked to the production of isotopically "light" brines during sea-ice growth (see Hillaire-Marcel and deVernal, 2008).

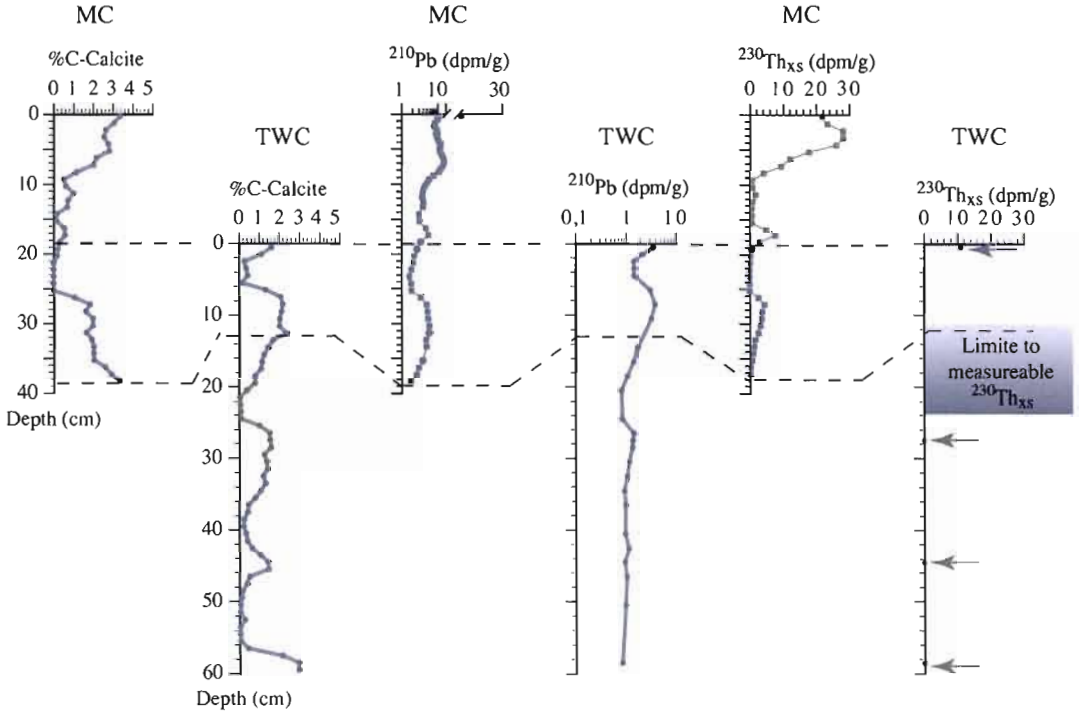

Figure 4. Percent C_{inorg}, ^{210}Pb and $^{230}Th_{xs}$ activities in HLY0503-11MC8 and HLY0503-11TWC. The correlation between the two records indicates a loss of the top-18 cm and a compaction of about 35% in the trigger weight core. Arrows show $^{230}Th_{xs}$ measurements in the TWC.

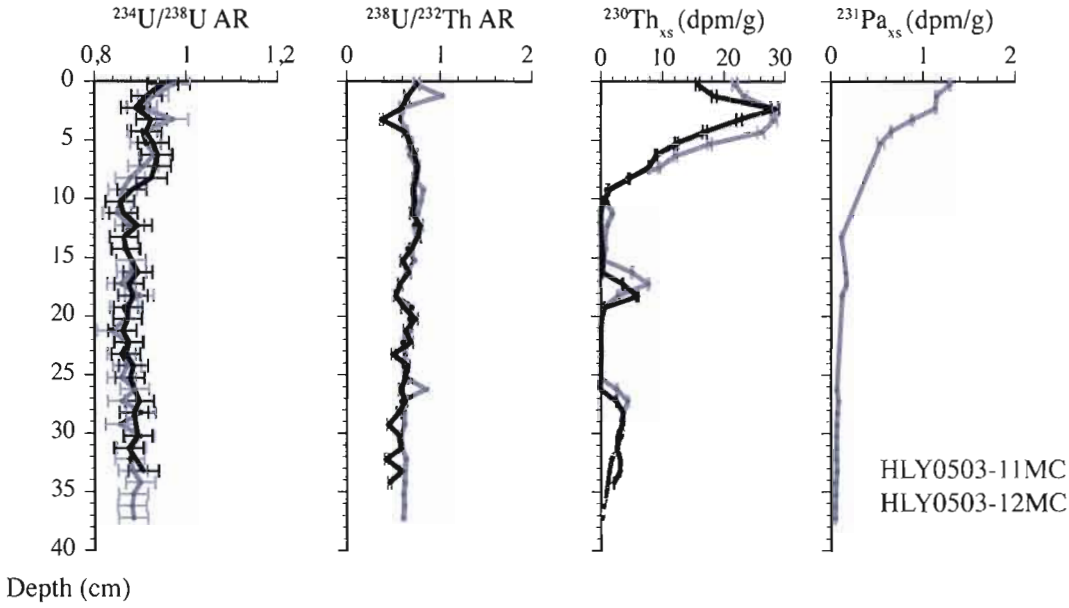

Figure 5. $^{234}U/^{238}U$ activity ratio (AR), $^{238}U/^{232}Th$ activity ratio, $^{230}Th_{xs}$ and $^{231}Pa_{xs}$ in core HLY0503-11MC8 (grey) and $^{234}U/^{238}U$ activity ratio (AR), $^{238}U/^{232}Th$ activity ratio, $^{230}Th_{xs}$ in core HLY0503-12MC8 (black). See supplementary material for excess calculations.

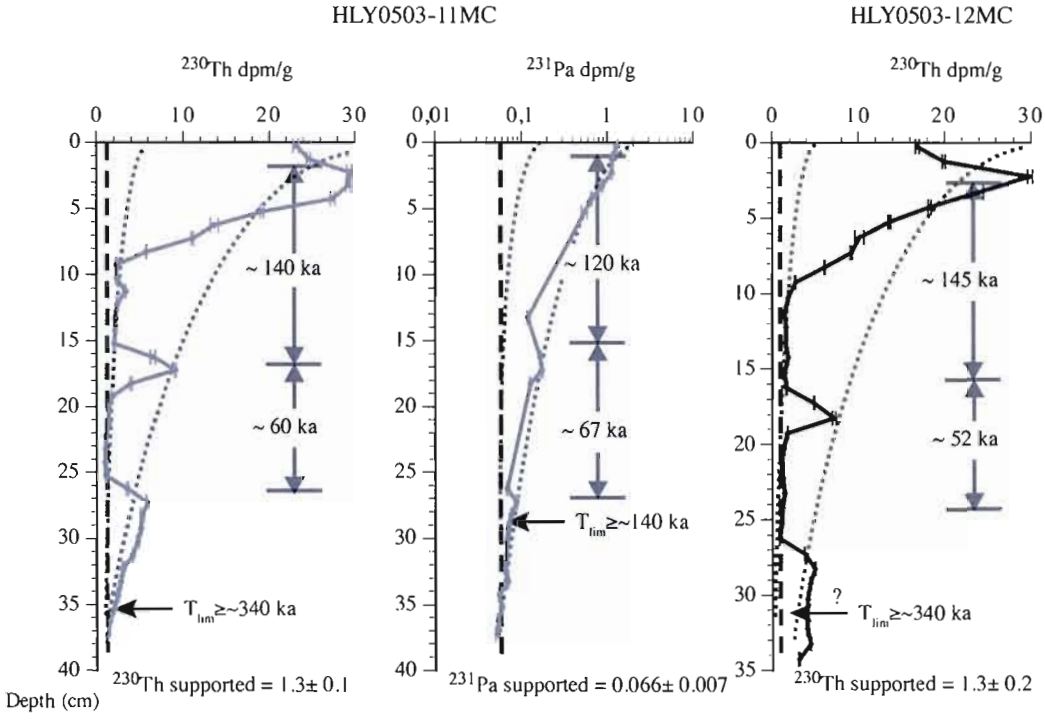

Figure 6. Time constraints based on U-series isotopes in cores HLY0503-11MC8 (grey) and HLY0503-12MC8 (black). Dotted lines illustrate two distinct sedimentary flux regimes for ^{230}Th and ^{231}Pa. Dashed lines illustrate the ^{230}Th or ^{231}Pa "supported" fraction; details about precise calculation of these fractions are given in the supplementary material. Time period estimates are obtained using the radioactive decay of these isotopes for a given constant initial flux for each regime.

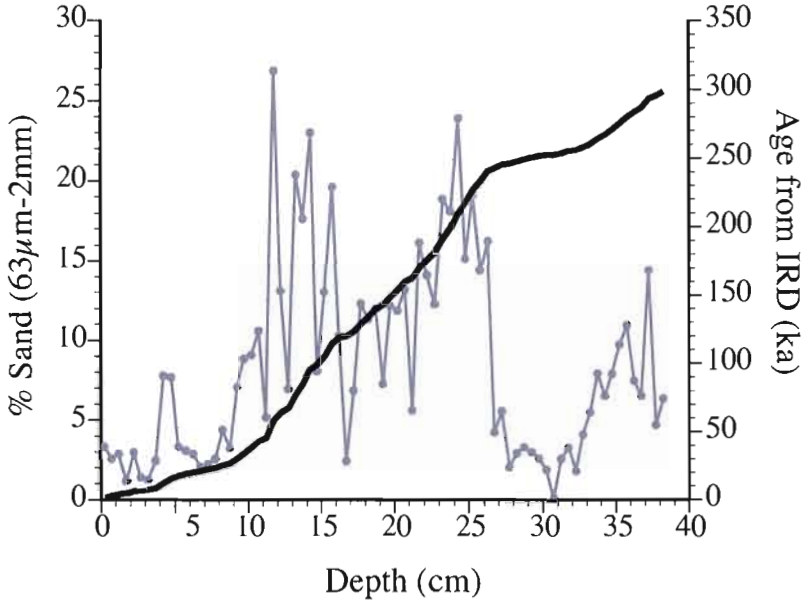

Figure 7. Age model based on a constant IRD flux downcore, and using the ^{14}C-age of ~ 30 ka at 9 cm for core HLY0503-11MC8. The IRD fraction is estimated here from the percentage of sand with a mean grain size between 63 μm and 2 mm. This age model yields a mean sedimentation rate of 1.2 mm.ka^{-1} for the core.

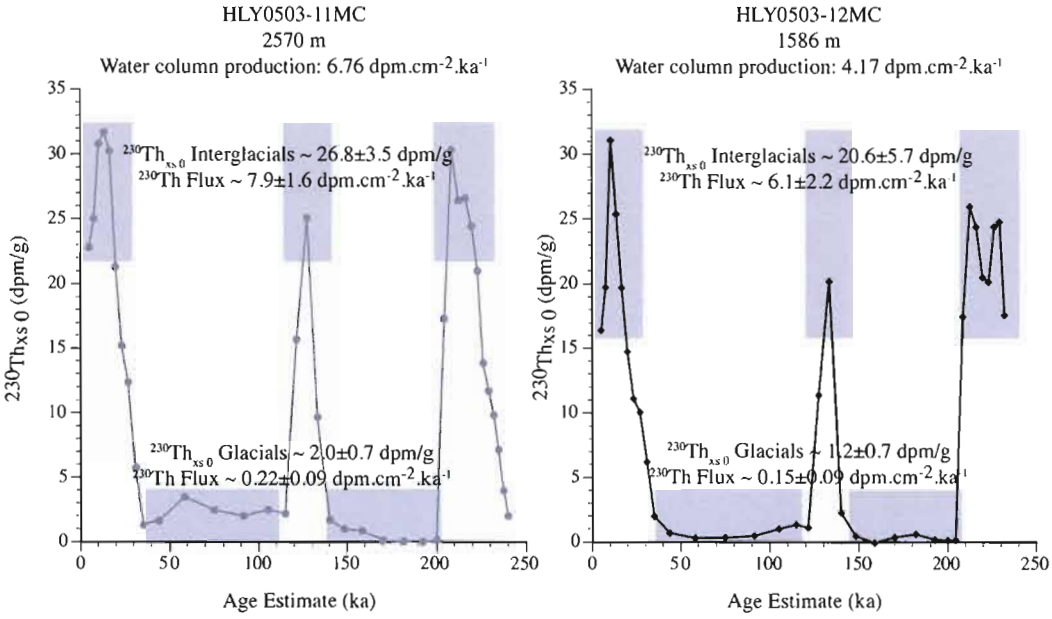

Figure 8. ^{230}Th fluxes in cores HLY0503-11MC8 and HLY0503-12MC8. The proposed water column production of ^{230}Th is based on Suman and Bacon (1989). Inventories and sediment fluxes are calculated distinctly for each sedimentary regime, and are assumed to be constant within error for each. During Arctic deglacial/interglacial periods, the ^{230}Th seems in balance between its production and sedimentary accumulation. However during glacial periods most of this ^{230}Th had to be exported, in the water column and/or through surface-sediment winnowing, to account for inventories such as those calculated here.

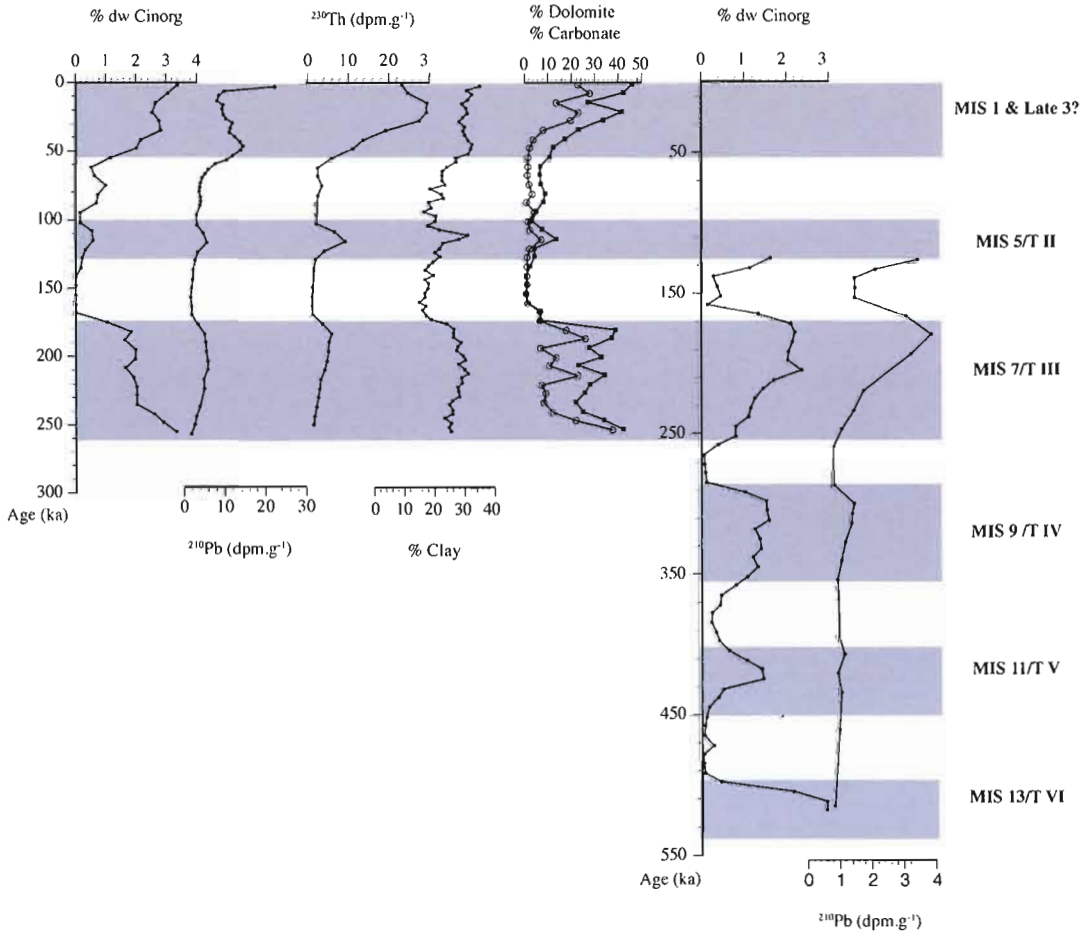

Figure 9. Age model in cores HLY0503-11MC8 (left) and HLY0503-11TWC (right). Ages are calculated using a mean sedimentation rate of 1.5 mm.ka^{-1}. Variations in the inorganic carbon content, ^{210}Pb, ^{230}Th, clay and carbonate contents (dolomite in open circle and total carbonate in black square) illustrate major sedimentological features. The Terminations (T) and Marine Isotopic Stages (MIS) are identified.

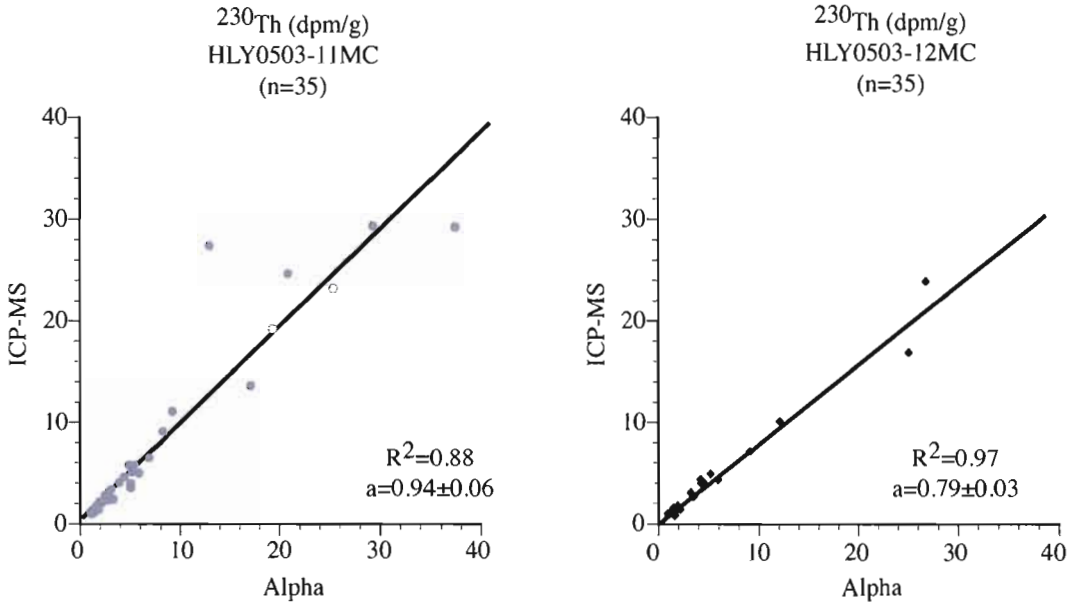

Figure S1. Comparison of ^{230}Th data from ICP-MS and Alpha measurement.

CHAPITRE 3

SEDIMENTOLOGICAL EVIDENCE FROM LOMONOSOV RIDGE FOR A WESTERN ARCTIC TRIGGER OF THE YOUNGER DRYAS

Christelle Not[1], Claude Hillaire-Marcel[1]

[1]GEOTOP, Université du Québec à Montréal, C. P. 8888, Montréal, QC, H3C 3P8, Canada

Article soumis à Geology

Résumé

Le refroidissement climatique du Younger Dryas et le ralentissement de la circulation Méridionale Atlantique conséquente, semble être due à l'apport important d'eau douce lors du drainage de lac Agassiz dans l'Atlantique Nord. Cependant le trajet de ce drainage fait encore largement l'objet de débat. Dans la littérature, différentes routes ont été proposées, en particulier, un passage vers l'est en direction du St-Laurent et une route vers l'Arctique canadien. Ce dernier scénario a fait l'objet d'une récente étude montrant un déversoir dans la région du Mackenzie. Cependant, il n'y a pas encore de preuves paléocéaniques de ce drainage. Dans cette étude, nous présentons des évidences d'un tel drainage dans un enregistrement sédimentaire provenant de la ride Lomonosov au centre de l'océan Arctique. L'unité sédimentaire correspondant au Younger Dryas est caractérisée par de fortes activités en actinides, liés à un fort flux de particules. L'unité est également caractérisée par un pic en matériel détritique carbonaté fin (calcite et dolomite), indiquant une provenance de la marge canadienne. Notre étude confirme un événement de déglaciation dans le secteur nord-ouest de la calotte Laurentidien lors de la phase initiale du Younger Dryas, daté à 12800-11700 ans.

Abstract

The Younger Dryas climate cooling event and related slowing of the Atlantic Meridional Overturning Circulation has been linked to a large array of processes. The most widely supported scenario involves an influx of freshwater into the North Atlantic Ocean linked to the partial drainage of glacial Lake Agassiz. Initially, an eastward route was suggested for this sudden outburst (via the Great Lakes and St. Lawrence River). More recently, some evidence for a northward drainage route, through the Mackenzie River outlet into the Arctic Ocean, has been found from land-based studies in the suspected drainage channel area. Here, we present complementary "marine" evidence for this northern route, based on sedimentological and geochemical data in marine sediment-cores obtained from the Lomonosov Ridge, in the central Arctic Ocean. A major drainage event, dated at ~13 to ~ 11.7 cal ka, was recorded in the sediments. They were marked by a pulse of detrital carbonates (with even amounts of calcite and dolomite), indicating a Mackenzie River sediment source area, and highlighted by a bottom peak in U-daughter isotopes, which we link to an enhanced flux of scavenging particles during the initial outburst. These findings support both the hypothesis of a glacial Lake Agassiz drainage trigger for the YD event, and of an Arctic routing for the freshwater pulse.

Keywords: Younger Drays, Arctic trigger, Lomonosov ridge, U-series.

3.1. Introduction

The Last Glacial Maximum (LGM) was followed by a deglaciation sequence punctuated by millennial-scale events, notably two major cold pulses: the Heinrich Event 1 and the Younger Dryas (YD). It is now generally accepted that both involved a significant reduction in the Atlantic Meridional Overturning Circulation (AMOC) attributed to enhanced meltwater inputs in the North Atlantic (e.g., Clark et al., 2001; McManus et al., 2004). The YD, spanning ~12 800 to ~11 700 cal years BP (Muscheler et al., 2008; Walker et al., 2009) corresponds to a period of cold conditions within the general climate warming that occurred during the transition from the LGM to the Holocene (Broecker, 2006; Peltier, 2007). If a large array of potential trigger mechanisms of the YD event have been put forth (see a review in Carlson, 2010; see also Broecker et al., 2010; Bradley and England, 2008), the most widely supported scenarios involve a major drainage pulse of glacial Lake Agassiz (Carlson, 2010), which surrounded the SW sector of the Laurentide Ice Sheet (LIS). A debate persisted with respect to the drainage route, either eastward, through the Great-Lakes - St. Lawrence system or, northward, through the Mackenzie River mouth area (e.g., Broecker et al., 1989; de Vernal et al., 1996; Carlson and Clark, 2008; Peltier et al., 2008). Recently, Murton et al. (2010) provided evidence for some drainage of Lake Agassiz, through the Mackenzie River mouth area, during the critical time interval. Optically Stimulated Luminescence measurements in eolian sands interbedded with coarse fluvial material, assigned to drainage pulses, yielded ages compatible with an YD assignment. These findings strongly support the northward route scenario put forth by Teller et al. (2005) and Teller and Boyd (2006). Polyak et al. (2007) also evoked this Arctic trigger scenario, based on a sedimentary record from the Chukchi margin. Unfortunately, one single ^{18}O depleted-value supports the extension of their record into the YD interval, not to mention uncertainties about the age model, based on three ^{14}C ages along the core, due to an open debate about the reservoir age correction for Arctic ocean paleowaters. Thus no clear "marine" evidence of a northwest route of Lake Agassiz outflow has yet been found. We present here this missing piece of information, based on detailed sedimentological and geochemical investigations on cores taken from the Lomonosov Ridge area, that record a strong meltwater pulse from the Mackenzie River mouth area during the YD time interval.

3.2. Samples and methods

Sedimentological and geochemical analyses were carried out on multi-core and trigger weight core sediments retrieved from the Lomonosov ridge during the HOTRAX 2005 expedition (Darby et al., 2005). Site HLY0503-18 is located at ~ 2500 m water depth in the Lomonosov Intra Basin (Fig. 1). The multi-core sequence (henceforth referred to as MC-18) is a 46 cm-long sequence of undisturbed fine-grained sediments (Hanslik et al., 2010). Sixteen radiocarbon analyses were performed on the trigger-core (henceforth TC-18) and used to construct an age model (Fig. 2). ^{14}C ages were calibrated with the Marine04 data set in OxCal 4.0 with 2-sigma standard deviation for four different marine reservoir ages (see Hanslik et al., In press). Lead-210 isotopes were measured by alpha counting, whereas uranium and thorium isotopes were measured by multi-collector-inductively coupled plasma-mass spectrometry on bulk sediment (see methodological details in Not and Hillaire-Marcel, 2010). Initial ^{230}Th-excess values ($^{230}Th_{XS})_0$ in the deglacial to Holocene sections were simply calculated by subtracting ^{234}U-activities, and correcting for decay based on interpolated ages from calibrated ages (see Veiga-Pires and Hillaire-Marcel, 1999, for the discussion of ways to calculate $^{230}Th_{XS}$ in sediments with abundant but variable detrital carbonate fractions).

Particle-size fractions were determined with a laser-diffraction particle-size analyser (LS13320 Beckman-Coulter) on bulk sediment, and granulometric statistics were processed with the Gradistat program (Blott and Pye, 2001). The silt fraction corresponds to the size fraction between 2 and 63 μm. Mineralogical assemblages were determined by X-ray diffraction (XRD) using a Siemens D5000 with CoKα1,2 radiation and a Si detector. Semi-quantitative estimations ($\pm 1\sigma \sim 5\%$) of the main mineral species were based on the area of the diffraction peak for each mineral corrected for quartz. The calcite and dolomite contents were measured in several fractions, in particular the >63 μm fraction, characteristic of ice-rafting sediment. The organic carbon (C_{org}) content was determined by the acidification of total sediment with HCl 1N and elemental-C analysis of the residual fraction with a Carlo Erba™ elemental analyzer. All detailed methodological settings are described in Not and Hillaire-Marcel (2010).

3.3. Results and discussion

In order to constrain the age of the event as recorded on Lomonosov Ridge, we used the ^{14}C chronology developed on TC-18 by Hanslik et al. (2010) transferring it to MC-18 using ^{210}Pb activity profiles for the correlation between the two cores (~2 km apart) as illustrated Fig. 2. Correlation of ^{210}Pb data indicates some compaction of TC-18 in comparison with MC-18, with possibly some smoothing. The first two centimetres in MC-18 correspond to the modern mixed layer (missing in TC-18; Fig. 2). From 2 to ~20 cm, four calibrated ages yield a sedimentation rate varying between 1.3 and 3.3 cm ka^{-1}. From ~ 20 to ~32 cm all ages fall into the range ~11.7-13.0 cal ka BP, indicating a substantial increase in the rate of sedimentation during that period with, possibly, a ^{14}C-plateau (cf. Broecker, 1992). Deeper along the core, two ages of almost 30 cal ka BP would indicate a late Marine Isotope Stage (MIS) 3 assignment for the lower part of the section. This would involve either a near complete stopping of sediment supply during MIS 2, or their removal through erosion. Erosion seems improbable, because the coring site is located in a small intra-ridge basin. Thus, we interpret the abrupt jump from ~13 to ~27 cal ka BP ages in the core, between 28 and 30 cm in the TC-18, as a near complete stop in sedimentation during MIS 2. This occurrence has also been suggested over the Mendeleev ridge area (Not and Hillaire-Marcel, 2010; Poore et al., 1999).

In MC-18, the 20 to 32 cm layer is characterized by higher values of ^{230}Th-excess vs its parent U-isotopes ($^{230}Thxs$) at the very bottom of the layer (Fig. 3). Enhanced $^{230}Thxs$ values are linked here to a high flux of scavenging particles, also indicated by the very high sedimentation rate of the interval (Fig. 2). Similar increases in $^{230}Th_{xs}$ features are observed in Mendeleev Ridge sequences deposited during Glacial/Interglacial transitions, where enhanced fluxes in ^{230}Th and ^{231}Pa match detrital carbonate pulses from the Canadian ice margin (Not and Hillaire-Marcel, 2010). In MC-18, $^{234}U/^{238}U$ activity ratios show a major change at a depth of 22 cm (Fig. 3). Above, ^{234}U is in deficit vs its parent ^{238}U, as is often observed in oxidized sub-surface sedimentary layers (e.g., Barnes and Cochran, 1990), whereas below, near equilibrium conditions exist between the two isotopes. This suggests a change in sediment source and/or accumulation rate (Klinkhammer and Palmer, 1991).

Because the ^{234}U-excess persists deeper in the core through layers assigned to MIS 2 and 3, without being affected by their drastic difference in sedimentation rates, a change in sediment source seems more likely. The possibility of a diagenetic uptake of uranium from seawater related to lower redox conditions (e.g., Gariépy et al., 1994), when sediments below 22 cm were deposited, is discarded, as the organic carbon content is practically unchanged on both sides of this transition (Fig. 3).

A closer look at sedimentological and geochemical features provides some evidence as to the precise source and mechanism leading to the dispersal of detrital carbonates as far as the Lomonosov Ridge area. In the critical layer the bulk mean grain size is very low, in comparison with the embedding sediments. This suggests enhanced supplies of suspended particulate matter greater than provided by an increase in Ice-Rafting Deposition (IRD), which should normally result in the deposition of coarser material (e.g., Hesse and Khodabakhsh, 1998). In this layer, the dolomite content increases mostly in the silt fraction, and, to a lesser extent, in the sand fraction (Fig 3). Here again, this feature suggests the deposition of silt-size detrital carbonates, initially produced by glacial erosion, and water-transported to the sedimentation area through a high-turbidity event (e.g., Andrews et al., 1988). Carbonates are predominantly composed of dolomite; such pulses of detrital, dolomite-rich carbonates are linked to the erosion of Lower Paleozoic strata in the Canadian Arctic by the LIS (Stein, 2008, Bischof et al 1996, Phillips and Grantz, 2001, Polyak et al, 2009). Paleozoic carbonate outcrops are located on Victoria Island, in the southern part of the Canadian Arctic Archipelago and in the Mackenzie Valley (based on the Canada Bedrock map, shown in Fig.1). Two mechanisms can introduce detrital carbonates into the deep Arctic Ocean: i) the drainage and dispersal of glacially-eroded carbonates from the Mackenzie area, i.e., from the only sector where the large Lake Agassiz, then spread along the western margin of the LIS, could have been drained (see discussion in Murton et al., 2010); ii) ice-rafting from paleo-ice streams (e.g. from M'Clure Strait, carrying Silurian carbonate material from Victoria Island; see Stokes and Tarasov, 2010). However, the mean grain size observed seems inappropriate for an IRD supply. Moreover, the critical layer depicts a huge bottom peak in ^{230}Th-excess ($^{230}Th_{xs}$; Fig. 4), which we interpret as marking a strong pulse of fine particulate

material, which was spread over large distances in the Arctic Ocean and thus could scavenge more $^{230}Th_{xs}$ than that produced in the overlying water column. Immediately above, $^{230}Th_{xs}$ returned to values in agreement with the vertical production of ^{230}Th, indicating a nearly complete interruption of lateral sedimentary supplies. Later on, during the Holocene, some $^{230}Th_{xs}$ is again observed, but with fluxes well below those accompanying the initial sedimentary pulse at the bottom of the critical layer (Fig. 4). Finally, worthy of mention is the fact that the corresponding layer, in TWC-18, is marked by a cluster of ^{14}C ages (Fig. 2; see also Hanslik et al., 2010). This can be partly due to enhanced sedimentation rates, but also very likely to the occurrence of the > 2 ka ^{14}C-plateau observed during the millennial scale Younger Dryas interval (Amman and Lotter, 1989; Broecker, 1992).

All sedimentological features examined above argue against a significant increase in IRD, but instead point to the occurrence of a sedimentological pulse linked to some major melt/ drainage event in the Mackenzie area. Murton et al. (2010) documented an overflow from Lake Agassiz through the Mackenzie River route, at the beginning of the YD (Murton et al 2010). Earlier, Tarasov and Peltier (2005, 2006), Peltier (2007) and Peltier et al. (2006), demonstrated that a northern route for the freshwater pulse, linked to Lake Agassiz drainage, would have been as efficient in shutting down the AMOC as an eastern or southern route from the SE margin of the LIS. All of the pieces of information thus concur to link the meltwater pulse at the origin of the YD to a drainage event from the Mackenzie basin into the Arctic Ocean.

3.4. Conclusion

The rapidly deposited unit identified in cores from the Lomonosov Ridge records a major deglacial event, with a detrital-dolomite signature labelling sediments originating from the Canadian Arctic and carried into the Arctic Ocean through the Mackenzie River mouth area. Radiocarbon data match the ^{14}C-plateau pattern of the Younger Dryas interval (cf. Broecker 1992), but unfortunately preventing precise estimates of sedimentation rate changes during the interval. Nonetheless, the abrupt increase in $^{230}Thxs$ at the base of the critical layer indicates a strong sedimentary pulse at its inception, thus supporting the scenario of a short

initial trigger linked to a huge drainage event in the Mackenzie River mouth area. The Lomonosov ridge cores thus provide "marine" evidence for an Arctic trigger for the YD-climate excursion, compatible with the recent findings of Murton et al. (2010), and the model experiments of Peltier and Tarasov (Peltier, 2007; Peltier et al., 2006; Tarasov and Peltier, 2005; Tarasov and Peltier, 2006).

3.5. Acknowledgments

This study, initiated within the *Polar Climate Stability Network* program (Canadian Foundation for Climate and Atmospheric Sciences), has been completed through support from the *Ministère du Développement économique, de l'innovation et de l'exportation* of Québec to the *Past4Future* research initiative. Funding from the Natural Sciences and Engineering Research Council and the *Fonds Québecois de la Recherche sur la Nature et les Technologies* (GEOTOP grant and team grant to de Vernal et al.) is also acknowledged. Support from GEOTOP members has been essential for the achievement of the exhaustive analytical program behind this study, with particular thanks to Bassam Ghaleb and Michel Preda.

3.6. References

Amman, B., and Lotter, A.F. (1989.) Late-glacial radiocarbon- and palynostratigraphy on the Swiss Plateau. *Boreas* **18**, 109–126.

Andrews, J.T., Geirsdóttir, A., and Jennings, A.E. (1988). Late Quaternary spatial and temporal changes in clay- and silt-size mineral assemblages of fiord and shelf cores, western Baffin Bay, northwest North Atlantic. *Continental Shelf Research* **9**, 445-463.

Barnes, C. E., and Cochran, J. K. (1990). Uranium removal in oceanic sediments and the oceanic U balance. *Earth and Planetary Science Letters* **97,** 94-101.

Bischof, J., Clark, D. L., and Vincent, J. S. (1996). Origin of ice-rafted debris: Pleistocene paleoceanography in the western Arctic Ocean. *Paleoceanography* **11,** 743-756.

Blott, S. J., and Pye, K. (2001). Gradistat: A grain size distribution and statistics package fro the analysis of unconsolidated sediments. *Earth Surface Processes and Landforms* **26,** 1237-1248.

Bradley, R. S., and England, J. H. (2008). The Younger Dryas and the Sea of Ancient Ice. *Quaternary Research* **70,** 1-10.

Broecker, W.S. (1992). Defining the boundaries of the late-glacial isotope episodes. *Quaternary Research* **38**, 135-138.

Broecker, W. S. (2006). Was the Younger Dryas triggered by a flood? *Science* **312,** 1146-1148.

Broecker, W. S., Kennet, J. P., Flower, B. P., Teller, J. T., Trumbore, S., Bonani, G., and Wolfli, W. (1989). Routing of meltwater from the Laurentide Ice Sheet during the Younger-Dryas cold episode. *Nature* **341,** 318-321.

Broecker, W.S., Denton, G.H., Edwards, R. L., Cheng, H. Alley, R. B., Putnam, A.E. (2010). Putting the Younger Dryas cold évent into context. Quaternary Science Review **29**, 1078-1081.

de Vernal, A., Hillaire-Marcel, C., and Bilodeau, G. (1996). Reduced meltwater outflow from the Laurentine ice margin during the Younger Dryas. *Nature* **381,** 774-777.

Carlson, A. E. (2010). What caused the Younger Dryas cold event? Geology, **38**, 383-384.

Carlson, A. E., and Clark, P. U. (2008). Rapid climate change and Arctic Ocean freshening: Comment. *Geology* **36,** e177.

Clark, P. U., Marshall, S. J., Clarke, G. K. C., Hostetler, S. W., Licciardi, J. M., and Teller, J. T. (2001). Freshwater forcing of abrupt climate change during the last glaciation. *Science* **293,** 283-287.

Darby, D. A., Jakobsson, M., and Polyak, L. (2005). Ice breaker Expedition collects key Arctic Seafloor and Ice data. *EOS* **86,** 549-552.

Gariepy, C., Ghaleb, B., Hillairemarcel, C., Mucci, A., and Vallieres, S. (1994). Early Diagenetic Processes in Labrador Sea Sediments - Uranium-Isotope Geochemistry. *Canadian Journal of Earth Sciences* **31,** 28-37.

Hanslik, D., Jakobsson, M., Backman, J., Bjorck, S., Sellen, E., O'Regan, M., Fornaciari, E., and Skog, G. (2010). Quaternary Arctic Ocean sea ice varaitions and deep water isolation times. *Quaternary Science Reviews* **29**,3430-3441.

Hesse, R. and Khodabakhsh, S. (1998). Depositional facies of late Pleistocene Heinrich events in the Labrador Sea. *Geology* **26**, 103-106.

Jakobsson, M., Macnab, R., Mayer, L., Anderson, R., Edwards, M., Hatzky, J., Schenke, H. W., and Johnson, P. D. (2008). An improved bathymetric portrayal of the Arctic Ocean: Implications for ocean modeling and geological, geophysical and oceanographic analyses. *Geophysical Research Letters* **35,** L07602.

Klinkhammer, G. P., and Palmer, M. R. (1991). Uranium in the oceans: where it goes and why. *Geochimica et Cosmochimica Acta* **55,** 1799-1806.

Lowell, T. V., Fisher, T. G., Comer, G. C., Hajdas, I., Waterson, N., Glover, K., Loope, H. M., Schaefer, J. M., Rinterknecht, V., Broecker, W., Denton, G., and Teller, J. T. (2005). Testing the Lake Agassiz meltwater trigger for the Younger Dryas. *EOS* **86,** 40.

Murton, J. B., Bateman, M. D., Dallimore, S. R., Teller, J. T., and Yang, Z. 2010. Identification of Younger Dryas outburst flood path from Lake Agassiz to the Arctic Ocean. *Nature* **464**, 740-743.

McManus, J. F., Francois, R., Gherardl, J. M., Kelgwin, L., and Drown-Leger, S. (2004). Collapse and rapid resumption of Atlantic meridional circulation linked to deglacial climate changes. *Nature* **428,** 834-837.

Muscheler, R., Kromer, B., Bjorck, S., Svensson, A., Friedrich, M., Kaiser, K. F., and Southon, J. (2008). Tree rings and ice cores reveal ^{14}C calibration uncertainties during the Younger Dryas. *Nature Geoscience* **1**, 263-267.

Not, C., and Hillaire-Marcel, C. (2010). U-series evidence for low Late Quaternary sedimentation rates (~1.5 mm/ka) over the northern Mendeleev Ridge, Arctic Ocean. *Quaternary Science Reviews* **29**, 3665-3675.

Peltier, W. R. (2007). Rapid climate change and Arctic Ocean freshning. *Geology* **35,** 1147-1148.

Peltier, W. R., Vettoretti, G., and Stastna, M. (2006). Atlantic meridional overturning and climate response to Arctic Ocean freshening. *Geophysical Research Letters* **33**. L06713.

Peltier, W. R., de Vernal, A., and Hillaire-Marcel, C. (2008). Rapid climate change and Arctic Ocean freshening: Reply. *Geology* **36,** e178.

Phillips, R. L., and Grantz, A. (2001). Regional variations in provenance and abundance of ice-rafted clasts in Arctic Ocean sediments: implications for the configuration of late Quaternary oceanic and atmospheric circulation in the Arctic. *Marine Geology* **172,** 91-115.

Polyak, L., Darby, D., Bischof, J., and Jakobsson, M. (2007). Stratigraphic constraints on late Pleistocene glacial erosion and deglaciation of the Chukchi margin, Arctic Ocean. *Quaternary Research* **67,** 234-245.

Polyak, L., Bischof, J., Ortiz, J. D., Darby, D. A., Channell, J. E. T., Xuan, C., Kaufman, D. S., Lovlie, R., Schneider, D. A., Eberl, D. D., Adler, R. E., and Council, E. A. (2009). Late Quaternary stratigraphy and sedimentation patterns in the western Arctic Ocean. *Global and Planetary Change* **68,** 5-17.

Poore, R.Z., Osterman, L., Curry, W.B., and Phillips, R.L. (1999). Late Pleistocene and Holocene meltwater events in the western Arctic Ocean. *Geology* **27**, 759-762.

Stein, R. (2008). Modern Environment and Its Record in Surface Sediments. *In* "Developments in Marine Geology", pp. 247-286. Elsevier.

Suman, D. O., and Bacon, M. P. (1989). Variations in Holocene sedimentation in the North American Basin determined from ^{230}Th measurements. *Deep Sea Research Part A. Oceanographic Research Papers* **36**, 869-878.

Tarasov, L., and Peltier, W. R. (2005). Arctic freshwater forcing of the Younger Dryas cold reversal. *Nature* **435,** 662-665.

Tarasov, L., and Peltier, W. R. (2006). A calibrated deglacial drainage chronology for the North American continent: evidence of an Arctic trigger for the Younger Dryas. *Quaternary Science Reviews* **25,** 659-688.

Teller, J. T., Leverington, D. W., and Mann, J. D. (2002). Freshwater outbursts to the oceans from glacial Lake Agassiz and their role in climate change during the last deglaciation. *Quaternary Science Reviews* **21,** 879-887.

Teller, J. T., Boyd, M., Yang, Z., Kor, P. S. G and Fard, A. M. (2005). Alternative routing of Lake Agassiz overflow during the Younger Dryas: new dates, paleotopography, and a re-evaluation. *Quaternary Science Reviews* **24**, 1890-1905.

Teller, J. T., and Boyd, M. (2006). Two possible routings for overflow from Lake Agassiz during the Younger Dryas: A Reply to Comment by T. Fisher, T. Lowell, H. Loope on "Alternative routing of Lake Agassiz overflow during the Younger Dryas: new dates, paleotopography, a re-evaluation". *Quaternary Science Reviews* **25,** 1142-1145.

Veiga-Pires, C., and Hillaire-Marcel, C. (1999). U and Th-isotope constraints on the duration of Heinrich events H0-H4 in the southern Labrador Sea. *Paleoceanography* **14**, 187-199.

Walker, M., Johnsen, S., Rasmussen, S. O., Popp, T., Steffensen, J. P., Gibbard, P., Hoek, W., Lowe, J., Andrews, J., Bjorck, S., Cwynar, L. C., Hughen, K., Kershaw, P., Kromer, B., Litt, T., Lowe, D. J., Nakagawa, T., Newnham, R., and Schwander, J. (2009). Formal definition and dating of the GSSP (Global Stratotype Section and Point) for the base of the Holocene using the Greenland NGRIP ice core, and selected auxiliary records. *Journal of Quaternary Science* **24,** 3-17.

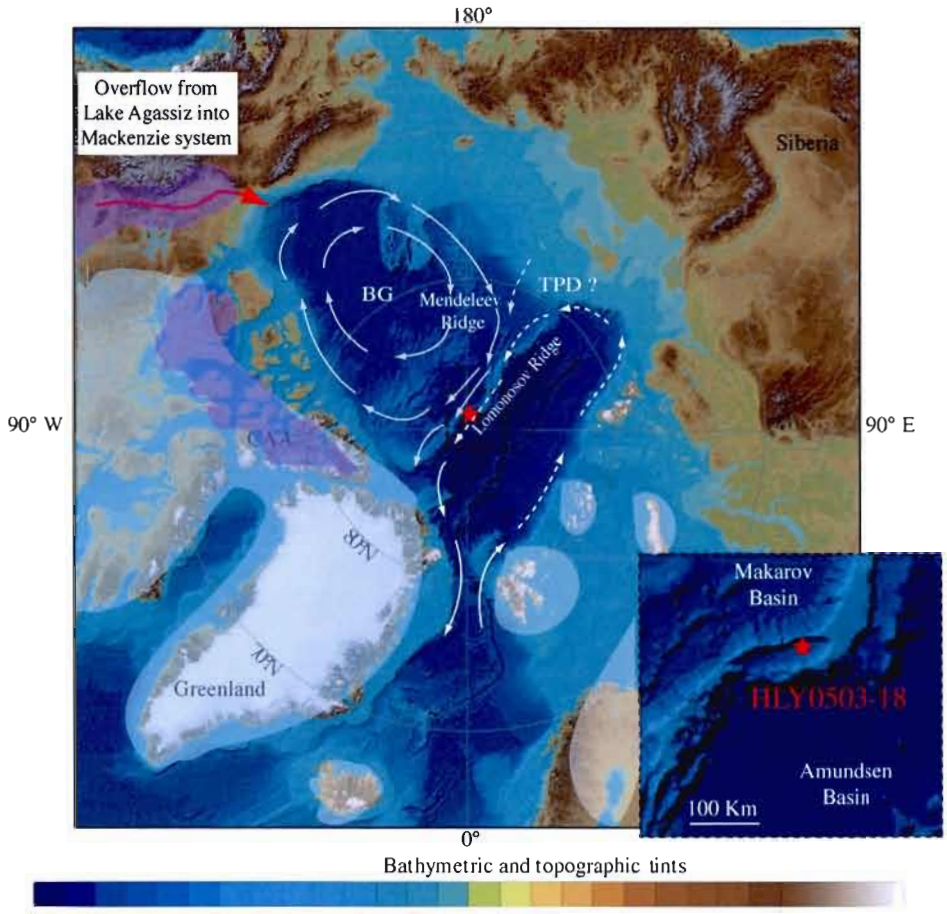

Figure 1: Location of sites HLY0503-18 on Lomonosov ridge in the Arctic ocean, with a close-up on the Lomonosov Intra Basin. Bathymetry is from the International Bathymetric Chart of the Arctic Ocean (Jakobsson et al., 2008). Mineralogical sources of calcite and dolomite (purple areas) are indicated based on Phillips and Grantz (2001) and the geological map of Canada. The white areas represent approximate positions of the Keewatin dome around 13 cal ka BP. The Agassiz drainage route described by Murton et al (2010) is indicated by the red arrow. Surface currents and sea-ice routes are represented by white arrows. We hypothezise an enhanced Beaufort Gyre (BG) during the drainage event.

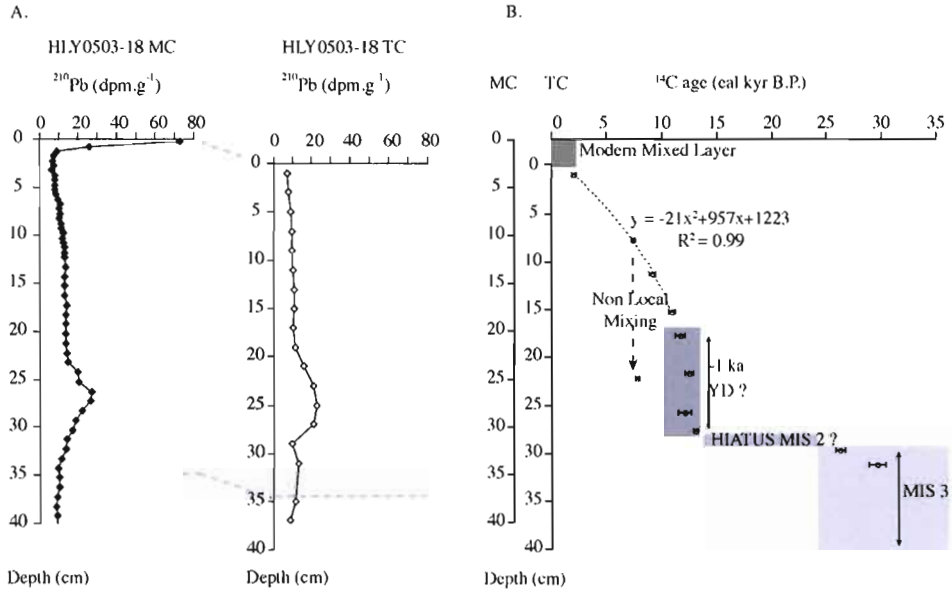

Figure 2: A. Correlation between HLY0503-18 TC and HLY0503-18 MC based on ^{210}Pb data. B. Chronology of multi-core HLY0503-18 based on the age model of Hanslik et al (2010) and ^{210}Pb correlation. The first two centimetres of the multi-core correspond to the modern mixed layer. Down to 18 cm, the ^{14}C chronology suggests a sedimentation rate of 1.3 to 3.3 cm ka^{-1}. The^{14}C cluster from 18 to 28 cm is assigned to a short millennial scale event of YD age. Below 28 cm, the sequence indicates very reduced sedimentation rates or even a hiatus during the LGM, and ages suggests a late MIS 3 assignment.

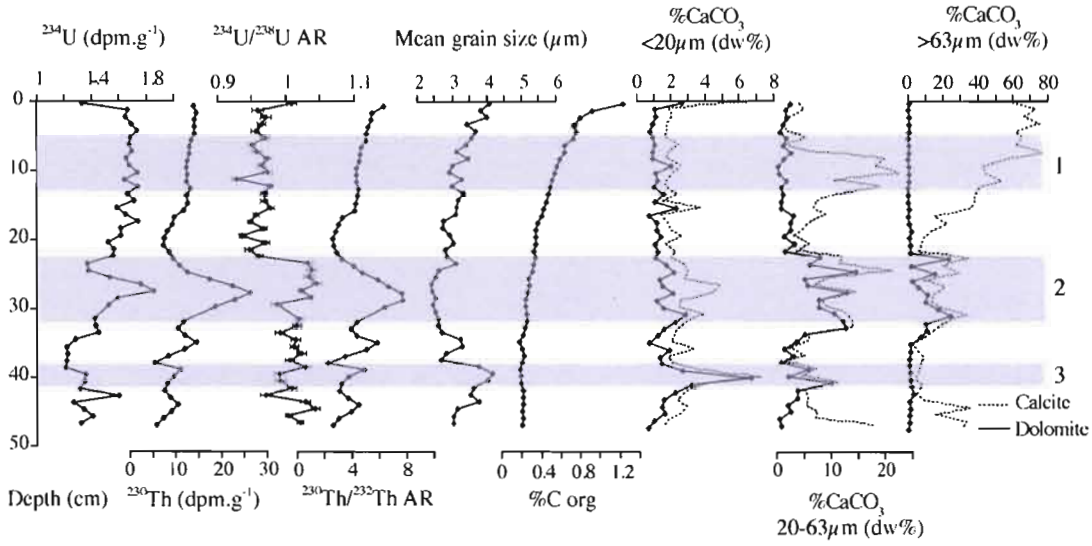

Figure 3: U-series isotope geochemistry (^{230}Th, ^{234}U activity and $^{230}Th/^{232}Th$, $^{234}U/^{238}U$ activity ratio; AR) and sedimentological properties of core HLY0503-18MC (dolomite with solid line and calcite with dashed line). Three distinct layers are observed: 1) The Holocene is marked by high carbonate calcite content in the coarse fraction and a calcite-peak in the silt range; a systematic deficit in ^{234}U (vs. ^{238}U) is attributed to a strong reduction in sedimentation rate throughout most of this interval and/or a significant change in sediment sources and properties; 2) The YD interval is highlighted by high U-series isotopes activities linked to distinct sediment sources (see ^{234}U-concentration) and increased sedimentation rates ($^{234}U/^{238}U$ AR near equilibrium); this unit is also characterized by its relatively high dolomite content in clay, silt and sand fractions, indicating a Canadian source for the detrital supplies, probably through flooding for clay and silt fractions, and ice-rafting for the sand fraction; 3) The late MIS 3 interval is characterized by a dolomite pulse in the clay to fine silt size range, but negligible changes in the coarse fraction. Most of the MIS 2 is missing here.

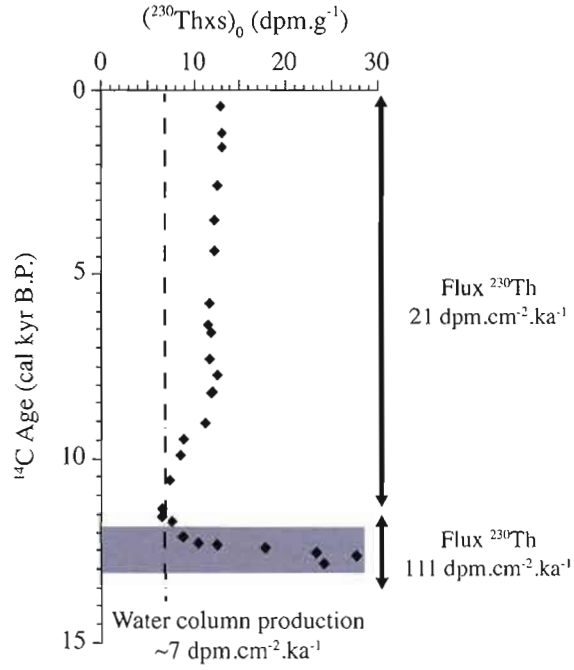

Figure 4: ^{230}Th-excesses (left) and fluxes (right) in core HLY0503-18MC8. The age-model used to calculate fluxes is illustrated in Fig.2. During the Holocene, and in particular during the first part of the YD, ^{230}Th depicts a strong excess well above its production in the overlying water column, indicating focusing at the coring site. The water column production of ^{230}Th is calculated based on Suman and Bacon (1989)

CONCLUSION

Dans cette thèse sont présentés les résultats de trois études portant sur l'utilisation des actinides dans les sédiments quaternaires de l'océan Arctique. La nécessité de comprendre les variations naturelles du climat arctique a motivé plusieurs missions océanographiques, dont la mission HOTRAX, qui a permis de récupérer du matériel sédimentaire dans les différents environnements arctiques. C'est grâce a l'acquisition de ce matériel que l'étude sur les actinides a débuté dans l'optique de mieux comprendre certain processus particuliers à l'océan Arctique, eu égard notamment aux vitesses d'accumulation de sédiment, parfois extrêmement faibles, et à leur variation spatio-temporelle. L'étude des actinides a permis l'établissement d'une chronostratigraphie pour certaines carottes sédimentaires, mais a également fourni des informations paléocéanographiques à partir de carottes de forage des deux rides principales de l'océan Arctique: la ride Mendeleev et la ride Lomonosov. Si cette thèse apporte des éléments d'information originaux et nouveaux, elle aussi met en évidence des zones d'ombres qui requerront des études particulières pour mieux cerner la variabilité naturelle du climat arctique.

Ainsi, c'est d'abord dans une optique chronostratigraphique que les actinides ont été utilisés aux fins de l'étude des sédiments de l'Arctique. Les données sur le ^{210}Pb ont été employées comme indicateurs des processus de mélange et, indirectement, via le comportement du ^{210}Pb soutenu, comme indicateurs chronostratigraphiques indirects. L'usage des actinides est motivé par les limitations intrinsèques voire l'impossibilité d'utiliser des méthodes plus conventionnelles de chronostratigraphie, telle la stratigraphie isotopique océanique (δ^{18}O des foraminifères) ou le ^{14}C. L'activité du ^{210}Pb a été déterminée dans neuf carottages courts représentant des environnements sédimentaires variés dans l'océan Arctique. L'activité du ^{210}Pb dans le sédiment est indépendante de la profondeur de la colonne d'eau mais dépendante de l'environnement sédimentaire. Dans le cas des sédiments provenant des plateaux continentaux, le profil de ^{210}Pb montre des profondeurs de mélange importantes. Dans le cas, des enregistrements provenant des rides ou des bassins profonds, l'excès de ^{210}Pb est limité au premier centimètre. L'étude des ascendants du ^{210}Pb dans deux carottages courts de la ride Mendeleïev a permis d'observer que le profil de ^{210}Pb était contrôlé par son ascendant direct, le ^{226}Ra, jusqu'à 8 cm, lequel était lui-même contrôlé principalement, plus

bas dans le profil, par l'activité du ^{230}Th ascendant. Ce profil particulier lié aux très faibles vitesses de sédimentation (< 3 mm a^{-1}), a permis de mettre en évidence une diffusion du ^{226}Ra importante à l'interface eau-sédiment, et moindre, mais perceptible, plus bas dans les profils sédimentaires, une diffusion du ^{226}Ra de part et d'autre des pics de ^{230}Th ascendant. Le flux diffusif de ^{226}Ra en surface est élevé (0,0043 dpm cm^{-2} a^{-1}) en relation avec les faibles vitesses de sédimentation. Finalement, le budget du ^{210}Pb a été établi sur deux carottages courts de la ride Mendeleïev. Ces deux enregistrements, distincts par 1000 m de différence de profondeur d'eau, ont permis de mettre en évidence que le ^{210}Pb en excès contenus dans le sédiment correspond à la somme des sources atmosphériques et de la colonne d'eau, à partir de ~ 1600 m de profondeur. Cependant, l'inventaire du ^{210}Pb en excès du carottage plus profond (~ 2500 m) est presque identique. On en a conclu à un transport latéral du ^{210}Pb et/ou à une capacité limitée d'adsorption particulaire.

Dans la mesure où le comportement du ^{210}Pb des enregistrements sédimentaires des rides océaniques arctiques indiquait un comportement fortement influencé par celui des isotopes ascendants, nous avons décidé de mesurer l'activité ^{226}Ra et ^{230}Th ascendants pour élucider les anomalies de distribution du ^{210}Pb, dans les profils, voire apporter des informations chronostratigraphiques, principalement sur la ride Mendeleïev où les vitesses de sédimentation paraissaient extrêmement faibles, d'après les études antérieures, mais ne faisaient pas l'objet d'un consensus. La colonne sédimentaire de la ride de Mendeleïev est caractérisée par deux régimes distincts, qui correspondent à la sédimentation des épisodes glaciaires et à la sédimentation des intervalles interglaciaires-tardiglaciaires. Les périodes glaciaires sont caractérisées par de très faibles flux particulaires, surtout représentés par du matériel de vêlage d'icebergs ou de glace (IRD). Les périodes de déglaciation (et/ou interglaciaires) sont à l'opposé caractérisées par des flux sédimentaires plus élevés (activités élevées en ^{230}Th, pics de carbonates détritiques et présence de foraminifères). En postulant un flux initial constant en ^{230}Th et en ^{231}Pa pendant les périodes de déglaciation et interglaciaires et en considérant que le seul processus influençant leur activité dans le sédiment est lié à la décroissance radioactive, des périodes de temps ont été estimées. Une vitesse de sédimentation moyenne de l'ordre de ~1 mm ka^{-1} a ainsi pu être estimée. Les caractéristiques sédimentologiques et géochimiques des deux régimes observés laissent croire à un transport latéral de ^{230}Th et de ^{231}Pa pendant les épisodes glaciaires. Deux possibilités pour la

focalisation de ces isotopes ont été retenues: vers les marges ou les bassins profonds de l'océan.

La ride de Lomonossov qui sépare l'océan Arctique entre les deux principaux bassins, eurasien et canadien, connaît des taux de sédimentation plus élevés que la ride de Mendeleev. Ici, notre étude porte sur un carottage court couvrant une partie des derniers ~ 35 000 ans. Les données sédimentologiques et géochimiques de cet enregistrement mettent en évidence une couche sédimentaire exceptionnelle, caractérisée par un très haut taux de sédimentation provenant d'un apport soudain de sédiments de l'Arctique Canadien. Cet événement daté à ~ 13 000-12000 ans (chronologie ^{14}C calibrée), a été attribué au Dryas récent. Il représente le premier enregistrement marin permettant de valider l'hypothèse du drainage du lac Agassiz, vers le nord, à l'origine de cet événement. Cependant, il serait intéressant, de ce point de vue, de comparer les enregistrements des derniers cycles climatiques de la ride de Mendeleïev à ceux de la ride de Lomonosov. Autrement dit, il serait intéressant d'analyser une séquence sédimentaire de celle-ci, plus longue et couvrant les derniers cycles climatiques. Grâce à la vitesse de sédimentation plus élevée sur cette ride, il serait alors possible d'augmenter la résolution temporelle et ainsi de mieux caractériser le comportement des ^{230}Th et ^{231}Pa pendant les périodes glaciaires et interglaciaires.

Relevons aussi que les inventaires de ^{230}Th dans les sédiments de surface des deux principales rides semblent très similaires, malgré des différences importantes et des vitesses de sédimentation variables. Il parait donc nécessaire d'élucider les mécanismes rendant compte de cette similarité. Des analyses du ^{230}Th et du ^{231}Pa des colonnes d'eau sus-jacentes ont été effectuées et devraient permettre, dans une étape ultérieure, de donner des éléments de réponse.

Finalement, dans le but de mieux caractériser les sédiments arctiques à travers le temps, il serait intéressant d'étudier la provenance des sédiments, grâce au traçage isotopique en Pb, Nd, Sr, des enregistrements étudiés et d'établir si possible le rôle des apports fluviatiles au niveau de la ride de Mendeleïev et la dualité entre la dérive transpolaire et la gyre de Beaufort sur les apports sédimentaires au-dessus de la ride de Lomonosov.

En conclusion, s'il est certain que les actinides apportent des informations pertinentes, aussi bien pour l'établissement d'une chronostratigraphie approximative (mais quasi exclusive ici)

que pour élucider les variations sédimentologiques ou paléocéanographiques, il reste que de nombreux points sont à éclaircir. Ils touchent aussi bien à la dynamique sédimentaire entre les plateaux et marges continentaux et les bassins, qu'au comportement des isotopes analysés dans la présente étude.

APPENDICE A

TABLEAUX DES DONNÉES DU CHAPITRE 2

Tableau A.1: Données géochimiques et sédimentologiques des échantillons de la carotte HLY0503-11MC.

Profondeur (cm)	Granulometrie (μm)	% Argile	% Sable	% C inorg	±	Calcite	Dolomite
0,25	3,27	35,17	3,35	3,37	0,06	23,73	22,78
0,75	4,26	30,79	2,61				
1,25	4,01	32,48	2,92	3,06	0,06	15,20	27,89
1,75	4,15	31,14	1,23				
2,25	4,78	29,21	3,00	2,64	0,06	14,34	13,50
2,75	4,18	30,48	1,46				
3,25	4,17	30,97	1,31	2,54	0,06	19,38	22,88
3,75	4,38	29,44	2,50				
4,25	5,26	28,31	7,81	2,77	0,06	14,58	19,60
4,75	4,76	30,09	7,72				
5,25	4,52	29,61	3,37	2,82	0,06	15,73	7,93
5,75	4,56	30,08	3,14				
6,25	4,41	31,19	2,90	2,16	0,06	14,25	3,68
6,75	4,05	32,63	2,09				
7,25	4,23	32,23	2,28	2,02	0,06	10,65	2,21
7,75	4,28	31,27	2,62				
8,25	5,02	27,25	4,44	1,16	0,06	9,87	1,49
8,75	4,77	27,25	3,28				
9,25	6,07	24,23	7,11	0,52	0,06	5,89	1,40
9,75	6,62	22,73	8,85				
10,25	6,75	22,66	9,09	0,63	0,06	5,88	1,24
10,75	6,99	22,66	10,61				
11,25	5,98	23,66	5,19	1,00	0,06	5,76	1,84

Profondeur (cm)	Granulometrie (μm)	% Argile	% Sable	% C inorg	±	Calcite	Dolomite
11,75	12,64	18,90	26,87				
12,25	7,46	22,44	13,13	0,74	0,06	6,35	3,17
12,75	6,18	23,13	6,98				
13,25	10,51	18,25	20,41	0,69	0,06	7,70	0,82
13,75	9,64	19,17	17,70				
14,25	11,83	16,74	23,05	0,15	0,06	1,46	4,13
14,75	7,41	20,68	8,10				
15,25	8,26	20,45	13,06	0,15	0,06	2,25	1,51
15,75	10,45	18,05	19,66				
16,25	7,58	21,84	10,28	0,54	0,06	5,86	2,12
16,75	4,33	31,08	2,43				
17,25	5,18	28,10	6,87	0,58	0,06	7,16	6,96
17,75	7,31	22,84	12,32				
18,25	7,44	21,82	11,35	0,31	0,06	2,75	2,04
18,75	7,87	20,36	12,00				
19,25	6,65	21,90	7,30	0,21	0,06	3,77	1,00
19,75	8,08	19,74	12,15				
20,25	8,41	18,26	11,87	0,18	0,06	2,07	1,08
20,75	9,29	17,21	13,21				
21,25	7,01	19,85	5,63	0,00	0,06	0,34	0,94
21,75	10,25	17,09	16,24				
22,25	9,14	18,30	14,12	0,01	0,06	0,47	1,06
22,75	8,64	18,08	12,29				
23,25	10,74	17,04	18,93	0,00	0,06	0,71	0,57

Profondeur (cm)	Granulometrie (μm)	% Argile	% Sable	% C inorg	±	Calcite	Dolomite
23,75	10,65	17,14	18,16				
24,25	13,46	15,10	23,95	0,00	0,06	0,99	1,24
24,75	9,93	17,43	15,24				
25,25	11,15	16,30	19,20	0,00	0,06	0,98	6,46
25,75	9,47	17,50	14,44				
26,25	9,14	19,19	16,34	1,05	0,06	0,98	6,46
26,75	5,75	24,13	4,26				
27,25	5,37	26,46	5,59	1,83	0,06	21,85	17,63
27,75	5,19	26,29	2,05				
28,25	5,27	26,25	2,91	1,63	0,06	11,93	25,87
28,75	4,84	28,77	3,32				
29,25	5,01	27,77	3,00	1,99	0,06	21,45	6,65
29,75	4,87	27,29	2,58				
30,25	4,32	29,52	1,89	1,97	0,06	19,78	13,43
30,75	3,97	30,30	0,10				
31,25	4,72	27,96	2,56	1,65	0,06	12,92	10,50
31,75	4,41	29,98	3,28				
32,25	4,09	31,19	1,82	1,92	0,06	11,89	22,82
32,75	4,68	28,93	4,11				
33,25	4,78	29,11	5,50	2,02	0,06	21,27	7,28
33,75	5,45	27,70	7,95				
34,25	5,30	27,95	6,54	2,03		17,53	8,89
34,75	5,40	28,21	7,93				
35,25	6,20	25,94	9,74	2,03	0,06	14,40	8,10

Profondeur (cm)	Granulometrie (μm)	% Argile	% Sable	% C inorg	±	Calcite	Dolomite
35,75	6,83	24,97	10,96				
36,25	6,00	25,94	7,49	2,60	0,06		
36,75	5,63	25,96	6,54				
37,25	7,79	23,51	14,42	2,91	0,06	12,68	21,74
37,75	5,90	25,56	4,71				
38,25	6,17	24,84	6,37	3,33	0,06	5,22	37,55

Tableau A.2 : Données géochimiques des isotopes des séries de l'uranium de la carotte HLY0503-11MC.

Prof. (cm)	^{210}Pb dpm/g	±	^{231}Pa dpm/g	±	^{230}Th dpm/g	±	^{234}U dpm/g	±	^{238}U dpm/g	±	^{232}Th dpm/g	±
0,25	22,42	0,58	1,30	0,01	23,19	0,33	1,44	0,03	1,48	0,04	1,97	0,06
0,75	9,96	0,28										
1,25	8,68	0,28	1,16	0,02	24,66	0,24	1,38	0,03	1,49	0,05	1,45	0,04
1,75	8,24	0,27										
2,25	9,66	0,31	1,15	0,01	29,36	0,28	1,41	0,03	1,55	0,05	2,57	0,08
2,75	9,46	0,30										
3,25	9,71	0,18	0,89	0,01	29,25	0,28	1,24	0,03	1,28	0,04	2,19	0,07
3,75	10,36	0,19										
4,25	11,94	0,24	0,67	0,01	27,42	0,26	1,46	0,03	1,61	0,05	2,49	0,08
4,75	11,40	0,20										
5,25	11,17	0,18	0,55	0,04	19,19	0,19	1,44	0,03	1,58	0,05	2,25	0,07
5,75	12,52	0,24										
6,25	13,95	0,42	0,72	0,06	13,62	0,50	1,39	0,03	1,49	0,05	2,19	0,07
6,75	14,61	0,48										
7,25	14,03	0,45	0,25	0,03	11,09	0,11	1,50	0,03	1,65	0,05	2,20	0,07
7,75	12,04	0,44										
8,25	10,53	0,35	0,25	0,00	5,76	0,06	1,45	0,03	1,65	0,05	2,24	0,07
8,75	7,72	0,24										
9,25	5,99	0,20	0,26	0,03	2,34	0,12	1,40	0,03	1,62	0,05	1,95	0,06
9,75	5,25	0,18										
10,25	4,49	0,20	1,60	0,06	2,37	0,08	1,32	0,03	1,54	0,05	1,93	0,06
10,75	4,09	0,16										

Prof. (cm)	^{210}Pb dpm/g	±	^{231}Pa dpm/g	±	^{230}Th dpm/g	±	^{234}U dpm/g	±	^{238}U dpm/g	±	^{232}Th dpm/g	±
11,25	3,93	0,16	0,00	0,00	3,37	0,03	1,35	0,03	1,59	0,05	2,07	0,06
11,75	3,78	0,17										
12,25	4,06	0,12	1,06	0,08	2,40	0,10	1,20	0,02	1,37	0,04	1,88	0,06
12,75	4,12	0,15										
13,25	4,00	0,16	0,12	0,00	2,16	0,05	1,32	0,03	1,53	0,05	2,01	0,06
14,25	3,11	0,12	1,73	0,07	2,18	0,02	1,25	0,03	1,45	0,04	2,20	0,07
15,25	3,17	0,12	0,59	0,08	2,08	0,08	1,34	0,03	1,52	0,05	2,07	0,06
16,25	4,73	0,19	0,17	0,00	6,50	0,24	1,36	0,03	1,54	0,05	2,39	0,07
17,25	5,62	0,15	0,18	0,00	9,09	0,09	1,31	0,03	1,52	0,05	2,64	0,08
18,25	3,42	0,11	0,13	0,00	3,95	0,08	1,10	0,02	1,23	0,04	2,32	0,07
19,25	2,73	0,09	0,70	0,04	1,77	0,02	1,31	0,03	1,52	0,05	2,17	0,07
20,25	2,28	0,07	0,61	0,04	1,40	0,06	1,16	0,02	1,33	0,04	1,96	0,06
21,25	2,13	0,69	0,06	0,00	1,40	0,01	1,21	0,02	1,45	0,04	2,11	0,06
22,25	1,90	0,08	0,05	0,00	1,10	0,03	1,08	0,02	1,24	0,04	2,06	0,06
23,25	1,68	0,07	0,05	0,00	1,05	0,01	1,06	0,02	1,23	0,04	1,95	0,06
24,25	1,89	0,07	0,06	0,00	1,03	0,03	1,04	0,02	1,19	0,04	1,95	0,06
25,25	1,93	0,07	0,05	0,00	1,10	0,04	1,09	0,02	1,27	0,04	1,98	0,06
26,25	3,44	0,11	0,07	0,00	3,54	0,10	0,88	0,02	0,99	0,03	1,15	0,04
27,25	5,07	0,15	0,09	0,00	5,76	0,06	1,28	0,03	1,49	0,05	2,52	0,08
28,25	5,29	0,18	0,08	0,00	5,12	0,19	1,36	0,03	1,51	0,05	2,45	0,07
29,25	5,52	0,15	0,07	0,00	4,99	0,11	1,33	0,03	1,55	0,05	2,49	0,08
30,25	5,87	0,16	0,07	0,00	4,61	0,13	1,35	0,03	1,51	0,05	2,58	0,08
31,25	5,82	0,17	0,07	0,00	4,05	0,04	1,34	0,03	1,52	0,05	2,55	0,08
32,25	4,86	0,13	0,07	0,00	3,05	0,09	1,31	0,03	1,49	0,05	2,35	0,07

Prof. (cm)	^{210}Pb dpm/g	±	^{231}Pa dpm/g	±	^{230}Th dpm/g	±	^{234}U dpm/g	±	^{238}U dpm/g	±	^{232}Th dpm/g	±
33,25	4,97	0,12	0,07	0,00	2,78	0,03	1,35	0,03	1,53	0,05	2,45	0,07
34,25			0,06	0,00	2,46	0,07	1,29	0,03	1,44	0,04	2,30	0,07
35,25	3,90	0,11	0,06	0,00	2,05	0,02	1,23	0,03	1,39	0,04	2,27	0,07
36,25	3,06	0,10	0,05	0,00	1,58	0,04	1,14	0,02	1,29	0,04	2,09	0,06
37,25	2,68	0,11	0,05	0,00	1,34	0,01	1,12	0,02	1,27	0,04	2,08	0,06

Tableau A.3 : Données isotopiques sur les foraminifères planctoniques (*Neogloboquadrina pachyderma*) de la carotte HLY050-11MC.

Profondeur (cm)	$\delta^{13}C$	±	$\delta^{18}O$	±
0,25	0,98	0,05	1,43	0,05
1,25	0,93	0,05	1,45	0,05
2,25	0,50	0,05	1,28	0,05
3,25	0,66	0,05	1,15	0,05
4,25	0,88	0,05	1,88	0,05
5,25	0,72	0,05	1,33	0,05
6,25	0,90	0,05	1,50	0,05
7,25	0,98	0,05	1,93	0,05
8,25	0,77	0,05	0,87	0,05
11,25		0,05		0,05
12,25		0,05		0,05
17,25	0,88	0,05	0,99	0,05
18,25	0,95	0,05	1,79	0,05
27,25	0,83	0,05	2,61	0,05
28,25	1,02	0,05	2,12	0,05
29,25	1,11	0,05	1,93	0,05
30,25	1,06	0,05	2,04	0,05
36,25	1,27	0,05	2,48	0,05

Tableau A.4 : Données sédimentologiques et géochimiques de la carotte HLY0503-11TWC.

Profondeur (cm)	% C inorg	±	^{210}Pb dpm/g	±	^{230}Th dpm/g	±
0,50	1,63	0,06	3,45	0,26	12,20	0,15
1,50	1,14	0,06	2,13	0,16		
2,50	0,28	0,06	1,48	0,11		
3,50	0,37	0,06	1,50	0,11		
4,50	0,46	0,06	1,49	0,11		
5,50	0,15	0,06				
6,50	1,34	0,06	3,09	0,24		
7,50	2,11	0,06				
8,50	2,21	0,06	3,88	0,30		
9,50	2,15	0,06				
10,50	2,06	0,06	3,25	0,25		
11,50	2,04	0,06				
12,50	2,37	0,06				
13,50	1,71	0,06				
14,50	1,46	0,06	1,76	0,13		
15,50	1,26	0,06				
16,50	1,16	0,06	1,46	0,11		
17,50	1,11	0,06				
18,50	0,81	0,06	1,08	0,08		
19,50	0,81	0,06				
20,50	0,40	0,06	0,82	0,06		
21,50	0,06	0,06				
22,50	0,07	0,06				

Profondeur (cm)	% C inorg	±	^{210}Pb dpm/g	±	^{230}Th dpm/g	±
23,50	0,09	0,06				
24,50	0,12	0,06	0,84	0,06		
25,50	1,03	0,06				
26,50	1,53	0,06	1,47	0,11		
27,50	1,55	0,06	1,41	0,11	1,20	0,01
28,50	1,60	0,06	1,39	0,11		
29,50	1,26	0,06				
30,50	1,38	0,06	1,19	0,09		
31,50	1,41	0,06				
32,50	1,21	0,06	1,07	0,08		
33,50	1,33	0,06				
34,50	1,08	0,06	0,94	0,07		
35,50	0,81	0,06				
36,50	0,47	0,06	0,99	0,08		
37,50	0,43	0,06				
38,50	0,25	0,06				
39,50	0,23	0,06				
40,50	0,34	0,06	0,98	0,08		
41,50	0,41	0,06				
42,50	0,65	0,06	1,15	0,09		
43,50	1,06	0,06				
44,50	1,42	0,06	0,95	0,07	1,14	0,01
45,50	1,46	0,06				
46,50	0,52	0,06	1,05	0,08		

Profondeur (cm)	% C inorg	±	^{210}Pb dpm/g	±	^{230}Th dpm/g	±
47,50	0,39	0,06				
48,50	0,17	0,06				
49,50	0,11	0,06				
50,50	0,07	0,06	0,99	0,08		
51,50	0,06	0,06				
52,50	0,28	0,06				
53,50	0,05	0,06				
54,50	0,05	0,06				
55,50	0,07	0,06				
56,50	0,45	0,06				
57,50	2,16	0,06				
58,50	2,95	0,06	0,84	0,06	1,07	0,01
59,50	2,95	0,06				

Tableau A.5 : Données sédimentologique de la carotte HLY0503-12MC.

Profondeur (cm)	Granulométrie (μm)	%C inorg	±	%Argile	% Silt
0,25	3,86	3,56	0,06	27,14	72,86
1,25	3,86	2,13	0,06	27,88	72,12
2,25	3,43	2,13	0,06	30,37	69,63
3,25	3,43	2,27	0,06	29,16	70,84
4,25	3,44	3,41	0,06	31,49	68,51
5,25	3,22	4,47	0,06	33,59	66,41
6,25	3,38	5,41	0,06	31,73	68,27
7,25	3,69	4,31	0,06	28,77	71,23
8,25	5,04	2,58	0,06	22,98	77,02
9,25	5,64	0,88	0,06	21,47	78,53
10,25	5,92	0,30	0,06	20,31	79,69
11,25	6,57	0,07	0,06	19,03	80,97
12,25	6,39	0,08	0,06	19,47	80,53
13,25	6,63	0,05	0,06	19,17	80,83
14,25	5,71	0,19	0,06	20,20	79,80
15,25	6,24	0,26	0,06	19,62	80,38
16,25	4,60	0,21	0,06	23,67	76,33
17,25	4,10	0,55	0,06	27,29	72,71
18,25	5,60	0,54	0,06	21,07	78,93
19,25	6,37	0,09	0,06	18,54	81,46
20,25	6,23	0,77	0,06	19,30	80,70
21,25	5,97	0,45	0,06	19,73	80,27
22,25	5,38	0,08	0,06	21,55	78,45
23,25	6,23	0,00	0,06	19,77	80,23

Profondeur (cm)	Granulométrie (μm)	%C inorg	±	%Argile	% Silt
24,25	5,75	0,01	0,06	20,84	79,16
25,25		0,00	0,06		
26,25		0,02	0,06		
27,25		0,64	0,06		
28,25		1,43	0,06		
29,25		1,60	0,06		
30,25		1,63	0,06		
31,25		1,47	0,06		
32,25		1,47	0,06		
33,25		1,85	0,06		
34,25		1,48	0,06		

Tableau A.6 : Données géochimiques des isotopes des séries de l'uranium de la carotte HLY0503-12MC.

Prof. (cm)	^{210}Pb dpm/g	±	^{230}Th dpm/g	±	^{234}U dpm/g	±	^{238}U dpm/g	±	^{232}Th dpm/g	±
0,25	26,69	0,72	16,87	0,22	1,21	0,02	1,28	0,04	1,68	0,05
0,75	9,46	0,27								
1,25	8,02	0,25	19,92	0,19	1,52	0,03	1,67	0,05	2,57	0,08
1,75	9,08	0,30								
2,25	9,57	0,31	29,85	0,28	1,62	0,03	1,82	0,06	3,05	0,09
2,75	9,96	0,33								
3,25	9,42	0,29	23,91	0,67	1,48	0,03	1,60	0,05	4,25	0,13
3,75	10,32	0,31								
4,25	12,87	0,59	18,27	0,18	1,36	0,03	1,49	0,05	2,37	0,07
4,75	11,18	0,30								
5,25	12,33	0,31	13,58	0,13	1,31	0,03	1,41	0,04	2,07	0,06
5,75	12,95	0,38								
6,25	13,68	0,46	10,11	0,54	1,14	0,02	1,21	0,04	1,66	0,05
6,75	12,89	0,40								
7,25	12,86	0,39	9,18	0,09	1,33	0,03	1,42	0,04	1,86	0,06
7,75	12,20	0,38								
8,25	9,84	0,31	6,06	0,06	1,40	0,03	1,51	0,05	2,02	0,06
8,75	7,68	0,27								
9,25	5,56	0,17	2,65	0,09	1,23	0,03	1,39	0,04	1,93	0,06
9,75	4,11	0,15								
10,25	3,12	0,12	1,79	0,06	1,33	0,03	1,56	0,05	2,12	0,06
10,75	2,89	0,11								
11,25	2,49	0,10	1,41	0,01	1,25	0,03	1,44	0,04	2,05	0,06

Prof. (cm)	^{210}Pb dpm/g	±	^{230}Th dpm/g	±	^{234}U dpm/g	±	^{238}U dpm/g	±	^{232}Th dpm/g	±
11,75	2,41	0,09								
12,25	2,35	0,11	1,56	0,06	1,40	0,03	1,56	0,05	1,98	0,06
12,75	2,61	0,14								
13,25	2,20	0,09	1,48	0,04	1,28	0,03	1,48	0,04	1,93	0,06
14,25	2,08	0,09	1,78	0,02	1,40	0,03	1,61	0,05	2,32	0,07
15,25	2,34	0,09	1,41	0,04	0,94	0,02	0,94	0,03	1,56	0,05
16,25	2,54	0,10	1,58	0,05	1,21	0,02	1,36	0,04	2,04	0,06
17,25	5,46	0,09	4,79	0,05	1,25	0,03	1,43	0,04	2,50	0,08
18,25	5,92	0,11	7,17	0,21	1,22	0,02	1,38	0,04	2,60	0,08
19,25	2,62	0,07	1,72	0,02	1,09	0,02	1,25	0,04	2,05	0,06
20,25	2,44	0,07	1,31	0,01	1,20	0,02	1,38	0,04	1,87	0,06
21,25	2,15	0,08	1,05	0,01	1,06	0,02	1,23	0,04	1,94	0,06
22,25	1,99	0,05	1,18	0,02	1,11	0,02	1,27	0,04	1,86	0,06
23,25	1,90	0,07	1,37	0,01	1,26	0,03	1,45	0,04	2,90	0,09
24,25	1,93	0,07	1,13	0,03	1,10	0,02	1,24	0,04	1,91	0,06
25,25	1,84	0,11	1,02	0,03	1,00	0,02	1,14	0,03	1,83	0,06
26,25	2,07	0,08	0,83	0,02	0,81	0,02	0,84	0,03	1,44	0,04
27,25	2,72	0,07	3,72	0,04	1,14	0,02	1,27	0,04	2,04	0,06
28,25	5,64	0,10	4,92	0,09	1,21	0,02	1,37	0,04	2,46	0,07
29,25	6,11	0,16	4,33	0,09	0,96	0,02	0,94	0,03	2,09	0,06
30,25	4,73	0,12	4,06	0,10	1,33	0,03	1,48	0,04	2,61	0,08
31,25	5,30	0,16	3,98	0,04	1,37	0,03	1,57	0,05	2,69	0,08
32,25	5,56	0,16	3,99	0,11	0,92	0,02	0,86	0,03	2,04	0,06
33,25	5,66	0,16	4,40	0,04	1,37	0,03	1,51	0,05	2,56	0,08

Prof. (cm)	^{210}Pb dpm/g	±	^{230}Th dpm/g	±	^{234}U dpm/g	±	^{238}U dpm/g	±	^{232}Th dpm/g	±
34,25	4,77	0,14	3,07	0,08	0,97	0,02	0,89	0,03	1,95	0,06

APPENDICE B

TABLEAUX DE DONNÉES DU CHAPITRE 3

Tableau B.1: Données sédimentologiques de la carotte HLY0503-18MC.

Prof. (cm)	Calcite (%)	Dolomite (%)	Calcite (%)	Dolomite (%)	Calcite (%)	Dolomite (%)	Granulo. (μm)	% C_{org}	±
	>63μm		20-63 μm		<20 μm				
0,25	57,10	0,40	1,60	2,70	3,79	2,67	4,08	1,23	0,07
1,25	69,60	0,20	3,40	1,70	0,90	1,07	3,82	0,92	0,07
2,25	63,40	0,50	0,70	2,00	1,00	1,15	4,00	0,80	0,07
3,25	71,60	0,60	0,50	1,30	0,83	0,98	3,41	0,74	0,07
4,25	58,50	0,60	1,40	0,70	1,04	0,79	3,67	0,76	0,07
5,25	62,80	0,10	3,70	1,90	0,75	0,98	3,56	0,73	0,07
6,25	59,40	0,60	0,20	1,30	1,50	1,06	3,40	0,64	0,07
7,25	73,10	0,40	4,90	2,80	0,95	0,94	3,11	0,64	0,07
8,25	55,30	0,30	18,70	1,40	0,86	0,95	3,46	0,59	0,07
9,25	41,10	0,80	18,30	0,30	0,63	2,03	3,00	0,56	0,07
10,25	42,30	0,40	22,30	0,50	1,09	1,14	2,90	0,54	0,07
11,25	50,80	0,40	9,00	1,90	0,54	1,27	3,29	0,51	0,07
12,25	39,60	0,30	18,70	0,80	0,71	1,04	2,98	0,49	0,07
13,25	36,20	0,20	10,30	1,30	0,85	1,58	3,32	0,47	0,07
14,25	36,30	0,30	6,60	0,80	0,48	1,05	3,16	0,45	0,07
15,25	34,00	0,60	6,10	0,90	1,55	2,31	3,11	0,42	0,07
16,25	14,60	0,20	6,20	3,20	0,70	0,75	3,10	0,40	0,07
17,25	20,90	0,40	3,50	2,70	0,65	1,21	2,74	0,37	0,07
18,25	12,00	1,60	2,20	2,70	0,86	1,17	2,73	0,35	0,07
19,25	8,20	0,80	1,80	1,40	1,30	1,42	2,92	0,35	0,07
20,25	6,60	0,90	2,70	3,40	0,64	1,10	3,03	0,35	0,07

Prof. (cm)	Calcite (%)	Dolomite (%)	Calcite (%)	Dolomite (%)	Calcite (%)	Dolomite (%)	Granulo. (μm)	% C_{org}	±
	>63μm		20-63 μm		<20 μm				
21,25	5,30	1,10	2,20	1,60	1,05	1,27	2,80	0,33	0,07
22,25	12,10	22,00	4,20	8,00	0,98	1,12	2,83	0,35	0,07
23,25	17,60	1,70	5,60	6,20	1,12	1,75	3,11	0,33	0,07
24,25	13,60	14,60	6,80	14,70	0,82	2,21	2,64	0,32	0,07
25,25	6,90	2,10	4,20	5,20	1,53	1,37	2,53	0,28	0,07
26,25	14,50	5,70	1,30	5,80	3,40	1,54	2,43	0,29	0,07
27,25	4,20	10,50	2,00	12,90	2,45	2,13	2,45	0,27	0,07
28,25	3,80	9,50	0,70	7,90	1,42	1,16	2,54	0,25	0,07
29,25	4,10	16,40	1,70	7,80	1,00	1,60	2,47	0,25	0,07
30,25	9,30	23,10	2,20	10,70	1,14	2,85	2,54	0,26	0,07
31,25	10,70	9,60	1,80	12,30	0,70	2,28	2,61	0,26	0,07
32,25	4,10	10,30	1,40	12,70	0,84	1,59	2,60	0,24	0,07
33,25	3,30	7,00	0,80	5,30	1,00	1,24	2,70	0,22	0,07
34,25	1,60	1,20	2,20	3,70	1,36	0,71	3,24	0,18	0,07
35,25	4,90	0,90	1,20	1,40	1,53	1,91	3,29	0,21	0,07
36,25	8,00	0,80	2,30	3,10	0,55	1,36	2,82	0,23	0,07
37,25	6,80	0,60	1,00	0,90	0,66	1,48	2,68	0,21	0,07
38,25	5,20	1,20	1,50	6,00	0,97	2,73	3,78	0,19	0,07
39,25	3,50	1,10	2,80	2,20	0,64	6,69	4,16	0,20	0,07
40,25	7,10	1,50	1,50	10,10	0,90	3,22	4,03	0,20	0,07
41,25	2,30	2,60	1,50	3,90	0,63	2,25	3,61	0,22	0,07
42,25	9,20	0,40	2,10	3,90	0,80	1,60	3,51	0,22	0,07

Prof. (cm)	Calcite (%)	Dolomite (%)	Calcite (%)	Dolomite (%)	Calcite (%)	Dolomite (%)	Granulo. (μm)	% C_{org}	±
	>63μm		20-63 μm		<20 μm				
43,25	32,80	0,90	3,50	2,10	1,49	1,48	3,77	0,22	0,07
44,25	14,10	0,50	4,90	2,60	0,99	1,65	3,14	0,21	0,07
45,25	31,80	0,40	6,90	0,50	0,82	1,04	3,02	0,22	0,07
46,25	29,20	0,30	17,20	0,90	0,94	0,69	3,02	0,21	0,07

Tableau B.2 : Données isotopiques de la carotte HLY0503-18MC.

Profondeur (cm)	^{210}Pb dpm/g	±	^{234}U dpm/g	±	^{230}Th dpm/g	±	^{232}Th dpm/g	±	^{234}U/^{238}U	±
0,25	72,63	1,43	1,33	0,01	14,05	0,14	2,22	0,01	1,01	0,01
0,75	25,86	0,52								
1,25	9,04	0,25	1,67	0,01	14,61	0,15	2,67	0,01	0,96	0,01
1,75	7,35	0,19								
2,25	6,85	0,19	1,65	0,01	14,08	0,14	2,61	0,01	0,97	0,01
2,75	7,45	0,22								
3,25	6,46	0,28	1,69	0,01	14,09	0,14	2,69	0,01	0,97	0,01
3,75	7,70	0,31								
4,25	7,69	0,19	1,73	0,01	14,12	0,14	2,77	0,01	0,96	0,01
4,75	8,03	0,29								
5,25	8,17	0,31	1,68	0,01	13,53	0,14	2,68	0,01	0,97	0,01
5,75	8,38	0,34								
6,25	9,83	0,34	1,67	0,01	13,21	0,13	2,79	0,01	0,95	0,01
6,75	10,82	0,42								
7,25	10,34	0,43	1,70	0,01	13,04	0,13	2,79	0,01	0,96	0,01
7,75	10,51	0,40								
8,25	10,33	0,39	1,65	0,01	12,61	0,12	2,75	0,01	0,97	0,01
8,75	11,11	0,35								
9,25	11,57	0,35	1,67	0,01	12,45	0,12	2,87	0,01	0,97	0,01
9,75	12,33	0,40								
10,25	11,61	0,41	1,74	0,01	12,65	0,13	2,90	0,01	0,97	0,01
10,75	12,43	0,45								
11,25	12,73	0,42	1,64	0,01	12,52	0,12	2,87	0,01	0,93	0,01

Profondeur (cm)	^{210}Pb dpm/g	±	^{234}U dpm/g	±	^{230}Th dpm/g	±	^{232}Th dpm/g	±	^{234}U/^{238}U	±
11,75	13,23	0,22								
12,25	13,09	0,24	1,74	0,01	13,31	0,13	2,97	0,01	0,98	0,01
13,25	13,75	0,25	1,66	0,01	12,51	0,12	2,84	0,01	0,97	0,01
14,25	13,14	0,24	1,71	0,01	12,78	0,12	2,98	0,01	0,97	0,01
15,25	13,23	0,29	1,58	0,01	11,75	0,11	2,78	0,01	0,98	0,01
16,25	13,20	0,23	1,65	0,01	9,67	0,09	2,93	0,01	0,96	0,00
17,25	14,12	0,29	1,74	0,01	9,38	0,09	3,10	0,01	0,95	0,00
18,25	13,80	0,28	1,61	0,00	8,23	0,08	2,94	0,01	0,97	0,00
19,25	13,73	0,29	1,62	0,01	7,51	0,07	2,90	0,00	0,94	0,00
20,25	13,47	0,28	1,52	0,01	7,44	0,07	2,80	0,01	0,97	0,01
21,25	13,27	0,32	1,57	0,01	8,57	0,08	2,93	0,01	0,95	0,01
22,25	14,31	0,32	1,56	0,01	9,60	0,09	2,92	0,01	0,96	0,01
23,25	14,59	0,39	1,38	0,01	10,92	0,11	2,64	0,01	1,03	0,01
24,25	19,75	0,48	1,38	0,01	12,71	0,13	2,65	0,01	1,04	0,01
25,25	20,47	0,36	1,54	0,01	17,46	0,17	2,95	0,01	1,03	0,01
26,25	27,16	0,47	1,76	0,01	22,52	0,22	3,36	0,02	1,05	0,01
27,25	26,65	0,43	1,86	0,01	26,40	0,25	3,43	0,01	1,02	0,01
28,25	21,78	0,38	1,59	0,00	23,06	0,22	2,98	0,01	1,04	0,00
29,25	18,75	0,36	1,53	0,01	18,73	0,19	2,91	0,01	0,99	0,01
30,25	16,89	0,38								
31,25	13,86	0,15	1,42	0,01	11,83	0,11	2,70	0,01	1,02	0,01
32,25	13,66	0,16	1,43	0,01	10,53	0,10	2,69	0,01	1,02	0,01
33,25	11,45	0,17	1,45	0,01	12,13	0,12	2,77	0,01	0,99	0,01

Profondeur (cm)	^{210}Pb dpm/g	±	^{234}U dpm/g	±	^{230}Th dpm/g	±	^{232}Th dpm/g	±	^{234}U/^{238}U	±
34,25	9,87	0,16	1,28	0,01	14,68	0,15	2,50	0,01	1,01	0,01
35,25	10,25	0,17	1,22	0,01	12,00	0,12	2,36	0,01	1,01	0,01
36,25	9,89	0,16	1,22	0,01	8,44	0,09	2,40	0,01	1,02	0,01
37,25	9,18	0,15	1,22	0,01	5,41	0,06	2,37	0,01	1,01	0,01
38,25	8,55	0,15	1,21	0,01	11,23	0,12	2,29	0,01	1,03	0,01
39,25	8,83	0,15	1,36	0,01	9,66	0,10	2,55	0,01	0,99	0,01
40,25	8,63	0,14	1,35	0,01	8,18	0,09	2,52	0,02	0,99	0,01
41,25	12,57	0,31	1,32	0,01	7,62	0,08	2,45	0,01	1,01	0,01
42,25	21,20	0,83	1,60	0,01	8,86	0,09	2,39	0,01	0,97	0,01
43,25	10,80	0,16	1,27	0,01	10,52	0,11	2,33	0,01	1,03	0,01
44,25	12,28	0,18	1,34	0,01	9,20	0,09	2,32	0,01	1,04	0,01
45,25	12,08	0,22	1,41	0,01	7,35	0,07	2,40	0,01	1,00	0,01
46,25	12,93	0,23	1,32	0,00	5,83	0,06	2,24	0,01	1,02	0,01

REFERENCES

Backman, J., Jakobsson, M., Frank, M., Sangiorgi, F., Brinkhuis, H., Stickley, C., O'Regan, M., Lovlie, R., Palike, H., Spofforth, D., Gattacecca, J., Moran, K., King, J., and Heil, C. (2008). Age model and core-seismic integration for the Cenozoic Arctic Coring Expedition sediments from the Lomonosov Ridge. Paleoceanography 23.

Bauch, D., Carstens, J., and Wefer, G. (1997). Oxygen isotope composition of living Neogloboquadrina pachyderma (sin.) in the Arctic Ocean. Earth and Planetary Science Letters 146, 47-58.

Bourdon, B., Turner, S., Henderson, G. M., and Lundstrom, C. C. (2003). Introduction to U-series geochemistry. Uranium-Series Geochemistry 52, 1-21.

Carmack, E. C. (2000). The Arctic Ocean's freshwater budget: Sources, Storage and Export. In "The Freshwater Budget of the Arctic Ocean." (E. L. Lewis, E. P. Jones, P. Lemke, T. D. Prowse, and P. Wadhams, Eds.), pp. 623. NATO Sciences Series, Dordrecht/ Boston/London.

Clark, D. L., Whitman, R. R., Morgan, K. A., and Mackay, S. D. (1980). Stratigraphy and glacial-marine sediments of the America Basin, central Arctic Ocean. Geological Society of America Special Paper 181, 1-57.

Darby, D. A., Jakobsson, M., and Polyak, L. (2005). Ice breaker Expedition collects key Arctic Seafloor and Ice data. EOS 86, 549-552.

Donk, J. v., and Mathieu, G. (1969). Oxygen Isotope Compositions of Foraminifera and Water Samples from the Arctic Ocean. Journal of Geophysical Research 74, 3396-3407.

Futterer, D. K. (1992). ARCTIC'91: The expedition ARK-VIII/3 of RV 'Polarstern' in 1991. In "Report on Polar Research." pp. 244.

Grantz, A., Clark, D. L., Phillips, R. L., Srivastava, S. P., Blome, C. D., Gray, L. B., Haga, H., Mamet, B. L., McIntyre, D. J., McNeil, D. H., Mickey, M. B., Mullen, M. W., Murchey, B. I., Ross, C. A., Stevens, C. H., Silberling, N. J., Wall, J. H., and Willard, D. A. (1998). Phanerozoic stratigraphy of Northwind Ridge, magnetic anomalies in the Canada Basin, and the geometry and timing of rifting in the Amerasia Basin, Arctic Ocean. Bulletin of the Geological Society of America 110, 801-820.

Henderson, G. M., and Anderson, R. F. (2003). The U-series toolbox for paleoceanography. Uranium-Series Geochemistry 52, 493-531.

Hillaire-Marcel, C., and de Vernal, A. (2008). Stable isotope clue to episodic sea ice formation in the glacial North Atlantic. Earth and Planetary Science Letters 268, 143-150.

Ivanovich, M., and Harmon, R. S. (1992). Uranium-series disequilibrium: applications to earth, marine, and environmental sciences, 2nd edition. Uranium-series disequilibrium: applications to earth, marine, and environmental sciences, 2nd edition.

Jackson, H. R., Mudie, P. J., and Blasco, S. M. (1985). Initial Geological Report on CESAR-the Canadian Expedition to Study the Alpha Ridge, Arctic Ocean. Paper, Geological Survey of Canada 84-22.

Kaufman, D. S., Polyak, L., Adler, R., Channell, J. E. T., and Xuan, C. (2008). Dating late Quaternary planktonic foraminifer Neogloboquadrina pachyderma from the Arctic Ocean using amino acid racemization. Paleoceanography 23.

McNeely, R., Dyke, A. S., and Southon, J. R. (2006). Canadian margine reservoirs age, preliminary data assessment. Geological Survey Canada Open File 5049.

Murton, J. B., Bateman, M. D., Dallimore, S. R., Teller, J. T., and Yang, Z. 2010. Identification of Younger Dryas outburst flood path from Lake Agassiz to the Arctic Ocean. *Nature* **464**, 740-743.

Ostlund, H. G., Possnert, G., and Swift, J. H. (1987). Ventilation rate of the deep Arctic ocean from carbon 14 data. Journal of Geophysical Research 92, 3769-3777.

Peterson, B. J., McClelland, J., Curry, R., Holmes, R. M., Walsh, J. E., and Aagaard, K. (2006). Trajectory shifts in the arctic and subarctic freshwater cycle. Science 313, 1061-1066.

Poirier, A., and Hillaire-Marcel, C. (2009). Os-isotope insights into major environmental changes of the Arctic Ocean during the Cenozoic. Geophys. Res. Lett. 36.

Polyak, L., Bischof, J., Ortiz, J. D., Darby, D. A., Channell, J. E. T., Xuan, C., Kaufman, D. S., Lovlie, R., Schneider, D. A., Eberl, D. D., Adler, R. E., and Council, E. A. (2009). Late Quaternary stratigraphy and sedimentation patterns in the western Arctic Ocean. Global and Planetary Change 68, 5-17.

Saenko, O. A., Wiebe, E. C., and Weaver, A. J. (2003). North Atlantic response to the above-normal export of sea ice from the Arctic. Journal of Geophysical Research C: Oceans 108, 17-1.

Sellèn, E., Jakobsson, M., Frank, M., and Kubik, P. W. (2009). Pleistocene variations of beryllium isotopes in central Arctic Ocean sediment cores. Global and Planetary Change 68, 38-47.

Serreze, M. C., and Francis, J. A. (2006). The arctic amplification debate. Climatic Change 76, 241-264.

Serreze, M. C., Barrett, A. P., Slater, A. G., Woodgate, R. A., Aagaard, K., Lammers, R. B., Steele, M., Moritz, R., Meredith, M., and Lee, C. M. (2006). The large-scale freshwater cycle of the Arctic. Journal of Geophysical Research C: Oceans 111.

Spielhagen, R. F., and Erlenkeuser, H. (1994). Stable oxygen and carbon isotopes in planktic foraminifers from Arctic Ocean surface sediments: Reflection of the low salinity surface water layer. Marine Geology 119, 227-250.

Stein, R. (2008). Introduction to the Arctic: Significance and History. In "Developments in Marine Geology." pp. 3-34. Elsevier.

White, D., Hinzman, L., Alessa, L., Cassano, J., Chambers, M., Falkner, K., Francis, J., Gutowski, W. J., Jr., Holland, M., Holmes, R. M., Huntington, H., Kane, D., Kliskey, A., Lee, C., McClelland, J., Peterson, B., Rupp, T. S., Straneo, F., Steele, M., Woodgate, R., Yang, D., Yoshikawa, K., and Zhang, T. (2007). The arctic freshwater system: Changes and impacts. J. Geophys. Res. 112.

Winton, M. (2006). Does the Arctic sea ice have a tipping point? Geophysical Research Letters 33.